Theoretical Study on the Degeneracy Space between the Electronic States in Organic Molecules

Masato Sumita

Doctoral Program in Frontier Science

Submitted to
the Graduate School of Pure and Applied Sciences
in Partial Fulfillment of the Requirements
for the Degree of Doctor of Philosophy
in Science

at the University of Tsukuba

Doctoral Committee

Professor Kazuya Saito

Professor Tatsuo Arai

Professor Kenji Morihashi

Professor Unpei Nagashima

To the persons who supported me.

Contents

Chapter 1

Introduction

1.1 Light and Molecules

On the earth, there are materials which have various recognizable color for human. Human recognize the materials having the color which is reflected by the complementary light of the light absorbed by molecules. The molecules absorb the light whose wave length lie between 700 nm and 300 nm, i.e.,visible and ultra violet radiations. Generally, the color of light gradually changs from purple to red with elongating wavelength. Figure 1.1 shows the relation of complementary colors. That is to say, perception of the color is attributed to the molecule absorbing light.[1] The energy of

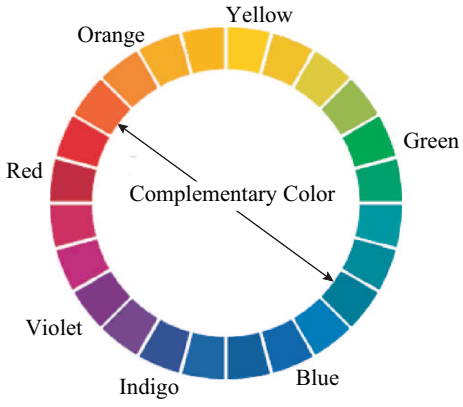

Figure 1.1: The relation of complementary color. Colors at opposite ends of a lines passing through the center form complementary pairs.

these light is 170-470 kJ mol^{-1}. Represented by a thermal unit, i.e., Kelvin, these

energy corresponds to 20000-50000 K. Table 1.1 shows averaged bond-energies for typical chemical bonds in organic molecules.[2] The energy of light is large enough to break chemical bonding in organic molecules though the strength of chemical bond depends on each molecule. Surprisingly, though materials on the earth absorb so

Table 1.1: Averaged bond-energies in kJ mol^{-1}

	H	C	N	O
H	436			
C	412	348(Single bond)		
		612(Double bond)		
		518(Triple bond)		
N	388	305(Single bond)	163(Single bond)	
		613(Double bond)	409(Double bond)	
		890(Triple bond)	945(Triple bond)	
O	463	360(Single bond)	157	146(Single bond)
		743(Double bond)		497(Double bond)

enormous energy, they exist stably. Naively, the following questions arise. Why the materials exactly exist without break? Where is the absorbed energies gone? Recent development of quantum chemical calculation make it possible to answer these questions partially: Molecule itself has the mechanism that the energy of light is efficiently converted into the energy of molecular vibration. This mechanism seems to involve the deformation of molecules and worked in molecules which construct lives.

The lives on the earth is also stable to the sunray including visible and ultra violet radiation. Deoxyribonucleic acid (DNA) carries the genetic information of all cellular forms of life. To protect the genetic information, nucleoside bases and these pair (Figure 1.2) is likely to have a high photostability.[3] Furthermore, lives do not dismiss the energy of light. If you read this thesis using your own eyes, you already use the energy of light because visual transduction process is induced by ultrafast photoreaction of a Schiff base molecule (Figure 1.3).[1,4] Moreover, considering the fact that plants lie on the lowest area in the food pyramid, the sunray is the origin of lives because plants form their bodies through photosynthesis. In the photosynthesis,

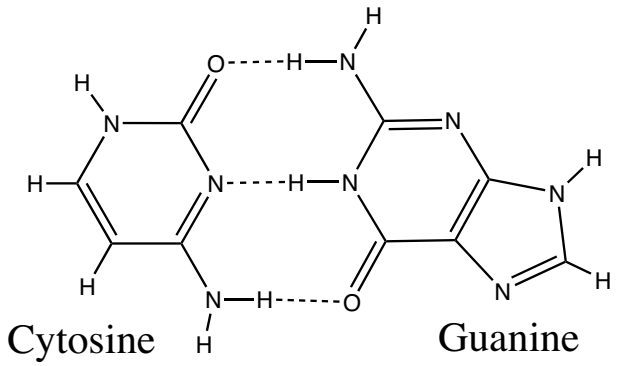

Figure 1.2: According to the recent quantum chemical calculation, the photostability of Cytosine-Guanine pair is induced by the central proton transformation.

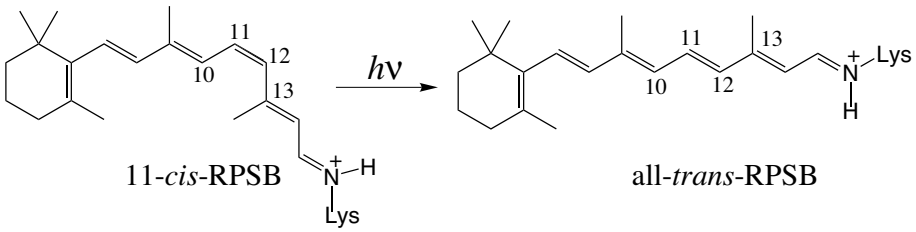

Figure 1.3: 11-cis to all-trans photoisomerization of Retinal protonated Schiff base is the trigger of vision.

a light absorbing molecule (chlorophyll) plays an important role.

On the other hand, in manufacturing chemicals, light is beneficial but sometimes harmful. The reactions which are thermally impossible are often achieved by light radiation but these reaction is sometimes undesirable. As one of the benefical examples, 2+2 additional reaction where two ethylene involved is well-known.[5] The 2+2 additional reaction is thermally forbidden, which is easily deduced by Woodward-Hoffmann rule. However, this 2+2 additional reaction is achieved by light irraddiation (Figure 1.4). Therefore the knowledge of the response of chemicals to the light

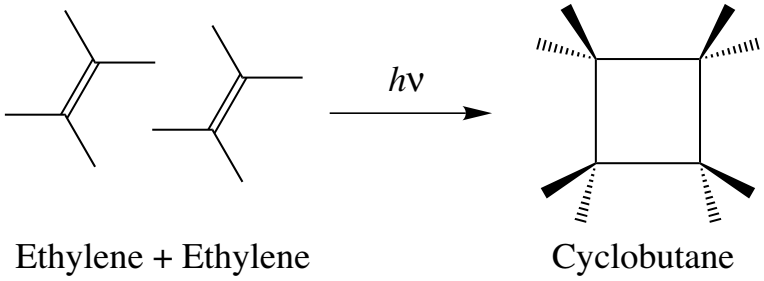

Figure 1.4: 2+2 additional reaction is achieved by light irradiation.

is important in manufacturing chemicals.

The deformation of molecules after light absorption induces various photoproduct or exhibits the photostability as mentioned above. Therefore, the behavior of these molecules under the light is important for designing or synthesizing the molecule. To know the behavior of molecule, the method based on the quantum mechanical treatment is necessary. It is very convenient for analyzing the reaction and physical property to introduce the concept of potential energy surface (PES).

The purpose of this work is very simple. That is just only to elucidate the photochemical processes using PES. The elucidation of chemical reaction processes will give a useful information on designing chemicals. Unlike the previous work, however we try to elucidate the chemical reaction by replacing a singular "point" on PES with a singular "space". We should force readers to travel up to our detailed purpose of this work. In this chapter, we introduce the concept of the PES based on the Born-Oppenheimer approximation.[6] Though this valuable approximation is reviewed and interpreted elsewhere,[7,8] the following concise review will rerealize the value of the study which will be described later. The Born-Oppenhimer adiabatic

approximation is introduced by neglecting the coupled term between nuclei and electrons, i.e. derivative coupling which characterizes the singularity on the PES.

1.2 Derivative Coupling

To treat molecules in quantum mechanical approach, it is necessary to define the total Schrödinger equation of a molecule. Assuming the molecule is in a stationary state, the equation should be written by the total degree of freedom of the molecule, i.e., translations, rotations, vibrations (the internal degrees of freedom of the molecule) and electron motion. These degrees of freedom can be treated separately by applying some approximations to the molecule. The separation of internal degrees of freedom from translations is a trivial task.[9] The rotations and vibrations of molecules can be separated assuming that the displacement of nuclei which construct the molecule is infinitesimal.[9,10] On the other hand, the electron distribution surely depend on the nuclear motion. Hence, it seems to be impossible to treat the electronic and nuclear motion separately. However, well known approximation, Born-Oppenheimer approximation, makes it possible to treat the electrons and atoms motions separately.

Born-Oppenheimer approximation is based on the fact that a nucleus is much heavier than an electron, that is, electrons immediately adjust their state according to the motion of nuclei, the motion of nuclei and electrons are separated. The separation of the motion of nuclei and electrons means to neglect the coupling term, derivative coupling. In this section, the derivative coupling is briefly described.

Common form of molecular Hamiltonian is

$$H_{total} = T_n + T_e + U(\boldsymbol{r}, \boldsymbol{R}), \tag{1.1}$$

where T_n and T_e are the kinetic energy operators of the nuclei and electrons, respectively, and $U(\boldsymbol{r}, \boldsymbol{R})$ is the total potential energy of the nuclei and electrons.

By neglecting T_n, the electronic Hamiltonian can be defined:

$$H_e = T_e + U(\boldsymbol{r}, \boldsymbol{R}). \tag{1.2}$$

H_e is an operator in the electronic space that depends parametrically on $\boldsymbol{R}$. Its eigenvalues $V_i(\boldsymbol{R})$ and eigenfunction $\phi_i(\boldsymbol{r}, \boldsymbol{R})$ fulfill

$$H_e\phi_i(\boldsymbol{r}, \boldsymbol{R}) = V_i(\boldsymbol{R})\phi_i(\boldsymbol{r}, \boldsymbol{R}). \tag{1.3}$$

The set of eigenfunction $\{\phi_i(\boldsymbol{r}, \boldsymbol{R})\}$ is a complete basis in the electronic space at every value of $\boldsymbol{R}$. Hence,

$$\sum_i \phi_i^*(\boldsymbol{r}', \boldsymbol{R})\phi_i(\boldsymbol{r}, \boldsymbol{R}) = \delta(r - r'), \tag{1.4a}$$

and the following orthonormality condition is satisfied,

$$\int \phi_i^*(\boldsymbol{r}, \boldsymbol{R})\phi_j(\boldsymbol{r}, \boldsymbol{R})d\boldsymbol{r} \equiv \langle i(\boldsymbol{R})|j(\boldsymbol{R})\rangle = \delta_{ij}. \tag{1.4b}$$

In the bra and ket notation, only the indices i and j are retained. Here, we are interested in solving the total Schrödinger equation with respect to H_{total}. Thus, the assumption, electrons immediately adjust their state according to the motion of nuclei, is applied. That is, using the eigenfunction in eq. (1.1), total wave function is defined by the following:

$$\Psi = \sum_i \phi_i(\boldsymbol{r}, \boldsymbol{R})\chi_i(\boldsymbol{R}). \tag{1.5}$$

This expansion is known as the Born-Oppenheimer expansion. Here, $\chi_i(\boldsymbol{R})$ is the wavefunction for nuclei. It has been argued that eq. (1.5) may not be justified for describing continuum states.[11] There are sufficient arguments which allow one to take the pragmatic stand point that the Born-Oppenheimer expansion is valid also for continuum states.[12] Substituting eq. (1.5) in the following full Schrödinger equation,

$$H_{total}\Psi(\boldsymbol{r}, \boldsymbol{R}) = E\Psi(\boldsymbol{r}, \boldsymbol{R}), \tag{1.6}$$

Then, we obtain,

$$\sum_i H\phi_i(\boldsymbol{r}, \boldsymbol{R})\chi_i(\boldsymbol{R}) = E\sum_i \phi_i(\boldsymbol{r}, \boldsymbol{R})\chi_i(\boldsymbol{R}). \tag{1.7}$$

Multiply by $\phi_j^*(\boldsymbol{r}, \boldsymbol{R})$ and integrate over the electronic coordinates,

$$\begin{aligned} \sum_i \phi_j^*(\boldsymbol{r}, \boldsymbol{R})H\phi_i(\boldsymbol{r}, \boldsymbol{R})\chi_i(\boldsymbol{R}) &= E\sum_i \phi_j^*(\boldsymbol{r}, \boldsymbol{R})\phi_i(\boldsymbol{r}, \boldsymbol{R})\chi_i(\boldsymbol{R}), \\ \int d\boldsymbol{r}\sum_i \phi_j^*(\boldsymbol{r}, \boldsymbol{R})H\phi_i(\boldsymbol{r}, \boldsymbol{R})\chi_i(\boldsymbol{R}) &= E\int d\boldsymbol{r}\sum_i \phi_j^*(\boldsymbol{r}, \boldsymbol{R})\phi_i(\boldsymbol{r}, \boldsymbol{R})\chi_i(\boldsymbol{R}). \end{aligned} \tag{1.8a}$$

The right hand side of eq. (1.8a)

$$\begin{aligned} &= E\sum_i \int d\boldsymbol{r}\phi_j^*(\boldsymbol{r},\boldsymbol{R})\phi_i(\boldsymbol{r},\boldsymbol{R}) \\ &= E\sum_i \delta_{ij}\chi_i(\boldsymbol{R}) \ (\because \text{eq. (1.4b)}) \\ &= E\chi_j(\boldsymbol{R}), \end{aligned} \tag{1.8b}$$

and the left hand side of eq. (1.8a)

$$\begin{aligned} &= \sum_i \int d\boldsymbol{r}\phi_j^*(\boldsymbol{r},\boldsymbol{R})(T_n + H_e)\phi_i(\boldsymbol{r},\boldsymbol{R})\chi_i(\boldsymbol{R}) \\ &= \sum_i \int d\boldsymbol{r}\phi_j^*(\boldsymbol{r},\boldsymbol{R})T_n\phi_i(\boldsymbol{r},\boldsymbol{R})\chi_i(\boldsymbol{R}) \\ &\quad + \sum_i \int d\boldsymbol{r}\phi_j^*(\boldsymbol{r},\boldsymbol{R})H_e\phi_i(\boldsymbol{r},\boldsymbol{R})\chi_i(\boldsymbol{R}) \\ &= \sum_i \{\langle j(\boldsymbol{R})|T_n i(\boldsymbol{R})\rangle\chi_i(\boldsymbol{R}) + \langle j(\boldsymbol{R})|i(\boldsymbol{R})\rangle T_n\chi_i(\boldsymbol{R})\} \\ &\quad + \sum_i V_i(\boldsymbol{R})\delta_{ji}\chi_i(\boldsymbol{R}) \ (\because \text{eq. (1.4b)}) \\ &= (T_n + V_j(\boldsymbol{R})) + \sum_i \langle j(\boldsymbol{R})|T_n i(\boldsymbol{R})\rangle\chi_i(\boldsymbol{R}) \\ &= (T_n + V_j(\boldsymbol{R}))\chi_i(\boldsymbol{R}) + \sum_i (\delta_{ji}T_n - \langle j(\boldsymbol{R})|T_n|i(\boldsymbol{R})\rangle)\chi_i(\boldsymbol{R}). \end{aligned} \tag{1.8c}$$

Therefore, the following equation is obtained,

$$(T_n + V_j(\boldsymbol{R}))\chi_j(\boldsymbol{R}) - \sum_i \Lambda_{ji}\chi_i(\boldsymbol{R}) = E\chi_j(\boldsymbol{R}), \tag{1.9}$$

where Λ_{ji} is called the nonadiabatic couplings which describe the dynamical interaction between the electronic and nuclear motion. They are given by

$$\Lambda_{ji} = \delta_{ji}T_n - \langle j(\boldsymbol{R})|T_n|i(\boldsymbol{R})\rangle, \tag{1.10}$$

To give more specific discussion, T_n should be replaced by

$$T_n = -\frac{1}{2M}\boldsymbol{\nabla}\cdot\boldsymbol{\nabla}, \tag{1.11}$$

where the gradient $\boldsymbol{\nabla}$ is a vector in nuclear space. M is an averaged nuclear mass. Hence the following explicit form for the nonadiabatic couplings is obtained

$$\begin{aligned}
\Lambda_{ji} &= \delta_{ji}T_n - \langle j|T_n|i\rangle \\
&= \delta_{ji}T_n + \frac{1}{2M}\langle j|\boldsymbol{\nabla}\cdot\boldsymbol{\nabla}|i\rangle \\
&= -\frac{1}{2M}\delta_{ji}\boldsymbol{\nabla}\cdot\boldsymbol{\nabla} + \frac{1}{2M}\{\langle j|\boldsymbol{\nabla}|\boldsymbol{\nabla}i\rangle + \langle j|\boldsymbol{\nabla}|i\rangle\boldsymbol{\nabla}\} \\
&= -\frac{1}{2M}\delta_{ji}\boldsymbol{\nabla}\cdot\boldsymbol{\nabla} + \frac{1}{2M}\{\langle j|\boldsymbol{\nabla}^2 i\rangle + \langle j|\boldsymbol{\nabla}|i\rangle\boldsymbol{\nabla} + \langle j|\boldsymbol{\nabla}i\rangle\boldsymbol{\nabla} + \langle j|i\rangle\boldsymbol{\nabla}^2\} \\
&= -\frac{1}{2M}\delta_{ji}\boldsymbol{\nabla}^2 + \frac{1}{2M}\{\langle j|\boldsymbol{\nabla}^2 i\rangle + 2\langle j|\boldsymbol{\nabla}i\rangle\boldsymbol{\nabla}\} + \frac{1}{2M}\delta_{ji}\boldsymbol{\nabla}^2 \\
&= \frac{1}{2M}\{\langle j|\boldsymbol{\nabla}^2 i\rangle + 2\langle j|\boldsymbol{\nabla}i\rangle\boldsymbol{\nabla}\} \\
&= \frac{1}{2M}\{2\boldsymbol{F}_{ji}\cdot\boldsymbol{\nabla} + G_{ji}\}. \qquad (1.12)
\end{aligned}$$

Where, $\boldsymbol{F}_{ji}$ and G_{ji} are known as nonadiabatic derivative couplings and the nonadiabatic scalar couplings, respectively. They are denoted as the following,

$$\boldsymbol{F}_{ji} = \langle j|\boldsymbol{\nabla}i\rangle, \qquad (1.13)$$

and

$$G_{ji} = \langle j|\boldsymbol{\nabla}^2 i\rangle, \qquad (1.14)$$

By using $\boldsymbol{F}$, eq. (1.9) becomes

$$\begin{aligned}
&\{T_n + V_j(\boldsymbol{R})\}\chi_j(\boldsymbol{R}) + \sum_i \frac{1}{2M}\{2\boldsymbol{F}_{ji}\cdot\boldsymbol{\nabla} + G_{ji}\}\chi_i(\boldsymbol{R}) - E\chi_j(\boldsymbol{R}) \\
= &\ \frac{1}{2M}\nabla\cdot\nabla\chi_j(\boldsymbol{R}) + \sum_i \frac{1}{2M}\{2\boldsymbol{F}_{ji}\cdot\boldsymbol{\nabla} + G_{ji}\}\chi_i(\boldsymbol{R}) + (V_j - E)\chi_j(\boldsymbol{R}) \\
= &\ \frac{1}{2M}\{\boldsymbol{\nabla}\cdot\boldsymbol{\nabla}\chi_j(\boldsymbol{R}) + \sum_i (2\boldsymbol{F}_{ji}\cdot\boldsymbol{\nabla} + G_{ji})\chi_i(\boldsymbol{R})\} + (V_j - E)\chi_j(\boldsymbol{R}) \\
= &\ \frac{1}{2M}\sum_i \{\boldsymbol{\nabla}\cdot\boldsymbol{\nabla}\delta_{ji} + 2\boldsymbol{F}_{ji}\cdot\boldsymbol{\nabla} + G_{ji}\}\chi_i(\boldsymbol{R}) + (V_j - E)\chi_j(\boldsymbol{R}) \\
\therefore &\ \frac{1}{2M}\{(\boldsymbol{\nabla} + \boldsymbol{F})^2 + \boldsymbol{V} - E\}\boldsymbol{\chi} = 0. \qquad (1.15)
\end{aligned}$$

Eq. (1.15) demonstrates that the coupled motion of electrons and nuclei can be reduced to the study of nuclear motion in the matrix potential $\boldsymbol{V}$. Here we used the following relationship between $\boldsymbol{F}$ and $\boldsymbol{G}$:

$$\boldsymbol{G} = (\boldsymbol{\nabla}\cdot\boldsymbol{F}) + \boldsymbol{F}\cdot\boldsymbol{F}. \qquad (1.16)$$

which is derived by applying $\boldsymbol{\Delta}$ to eq. (1.13) and using the following property of $\boldsymbol{F}$. The matrix of derivative coupling $\boldsymbol{F}$ is antihermite from the orthonormalization, eq. (1.4b). That is, applying $\boldsymbol{\nabla}$ to $\boldsymbol{F}$,

$$\begin{aligned} \boldsymbol{\nabla}\langle i(\boldsymbol{R})|j(\boldsymbol{R})\rangle &= \boldsymbol{\nabla}\delta_{ij} \\ \langle \boldsymbol{\nabla} i(\boldsymbol{R})|j(\boldsymbol{R})\rangle + \langle i(\boldsymbol{R})|\boldsymbol{\nabla} j(\boldsymbol{R})\rangle &= 0 \\ \therefore \boldsymbol{F}^{\dagger} &= -\boldsymbol{F}. \end{aligned} \tag{1.17}$$

Because of the antihermite, if $\phi_i(\boldsymbol{r}, \boldsymbol{R})$ and expansion quantities $\chi_i(\boldsymbol{R})$ are chosen to be real, the diagonal of the derivative coupling matrix $\boldsymbol{F}$ vanish. Now, we are ready to describe Born-Oppenheimer adiabatic approximation.

1.3 Born-Oppenheimer Adiabatic Approximation

In this section, we introduce Born-Oppenheimer approximation. As the outcome of the approximation, nuclei move on the only single potential energy surface. As shown in Sec. 1.2, the dynamical interaction between the electronic and nuclear motion is described by the non-adiabatic coupling Λ_{ji}, eq. (1.10). Therefore, applying the Born-Oppenheimer approximation means neglecting all non-diagonal elements of Λ_{ij} in eq. (1.9). That is,

$$\begin{aligned} (T_n + V_j(\boldsymbol{R}))\chi_j(\boldsymbol{R}) - \Lambda_{jj}\chi_j(\boldsymbol{R}) &= E\chi_j(\boldsymbol{R}) \\ \therefore (T_n + \boldsymbol{V} - \boldsymbol{\Lambda})\boldsymbol{\chi}(\boldsymbol{R}) &= E\boldsymbol{\chi}\ (\boldsymbol{R}) \end{aligned} \tag{1.18}$$

This resulting equation is the Born-Oppenheimer approximation. If the electronic wavefunction $\phi_i(\boldsymbol{r}, \boldsymbol{R})$ is taken to be real, the derivative coupling $\boldsymbol{F}$ vanishes, and $\Lambda = G/2M$ as is shown in eq. (1.12). Eq. (1.18) indicates that the nuclear motion is limited within the single electronic potential V_j. As will be shown in the next section, Born-Oppenheimer expansion, eq. (1.5) is accurate for an electronic state which is well separated energetically from all other electronic states. Then, assuming that the electronic states are separated sufficiently, Λ in eq. (1.18) is neglected. The following equation is obtained:

$$\{T_n + \boldsymbol{V}\ (\boldsymbol{R})\}\boldsymbol{\chi}(\boldsymbol{R}) = E\boldsymbol{\chi}\ (\boldsymbol{R}) \tag{1.19}$$

which is commonly called the Born-Oppenheimer adiabatic approximation or briefly the adiabatic approximation. Similar to eq. (1.15), eq. (1.19) demonstrate that the coupled motion of electrons and nuclei can be reduced to the study of nuclear motion in the matrix potential $\boldsymbol{V}$. Therefore, the exploration of the topograph of $\boldsymbol{V}$ in response to the displacement of nuclei (i,e, $\boldsymbol{V}$ as the function of the displacement of nuclei) would be beneficial to know the equilibrium structure of the molecule and the possible chemical reaction. However, as mentioned above, eq. (1.19) is valid only when the derivative coupling, $\boldsymbol{F}$, is negligible.

1.4 The Breakdown of Adiabatic Approximation

The adiabatic approximation would be accurate, when $\boldsymbol{F}_{ji}$ is small. Unfortunately, the unfavorable situation, where the adiabatic approximation is not valid, can be expected. To see this situation, the following expression for the derivative coupling is useful. By applying the gradient $\boldsymbol{\nabla}$ to the electronic Schrödinger equation (1.3) and multiplying $\phi_j(\boldsymbol{r},\boldsymbol{R})$ and integrating over the electronic coordinates,

$$\begin{aligned}
\langle j(\boldsymbol{R})|\boldsymbol{\nabla} H_e|i(\boldsymbol{R})\rangle &= V_i(\boldsymbol{R})\langle j(\boldsymbol{R})|\boldsymbol{\nabla} i(\boldsymbol{R})\rangle \\
\langle j(\boldsymbol{R})|(\boldsymbol{\nabla} H_e)|i(\boldsymbol{R})\rangle + \langle j(\boldsymbol{R})|H_e|\boldsymbol{\nabla} i(\boldsymbol{R})\rangle &= \\
\langle j(\boldsymbol{R})|(\boldsymbol{\nabla} H_e)|i(\boldsymbol{R})\rangle + V_j^*(\boldsymbol{R})\langle j(\boldsymbol{R})|\boldsymbol{\nabla} i(\boldsymbol{R})\rangle &= \\
\therefore \boldsymbol{F}_{ji}(\boldsymbol{R}) = \frac{\langle j(\boldsymbol{R})|\boldsymbol{\nabla} H_e|i(\boldsymbol{R})\rangle}{V_i(\boldsymbol{R}) - V_j(\boldsymbol{R})} & \qquad (1.20)
\end{aligned}$$

Therefore, the denominator does inform us on the situations in which the derivative couplings become large. Namely, in the vicinity of a degeneracy between the potential energies, $\boldsymbol{V}_i(\boldsymbol{R})$ and $\boldsymbol{V}_j(\boldsymbol{R})$, the derivative couplings can be substantial and the adiabatic approximation for the involved electronic states can be expected to break down. Non-adiabatic processes are predicted to occur in the vicinity of the degeneracy. Therefore, non-adiabatic processes should be treated by some methods in these area. To treat the non-adiabatic processes, two major treatments are picked up as the following:

(i) Non-Born-Oppenheimer processes:[13] Electronic and nuclear motion must be treated equally. Namely, the Born-Oppenheimer approximation is abandoned. These processes usually involve very high nuclear kinetic energies.

(ii) Born-Huang approach:[14] Non adiabatic processes are represented by adiabatic state. In this approach, the coupled motion of electrons and nuclei can be reduced to the study of nuclear motion in the potential $\boldsymbol{V}$, that is to say, the concept of PES is maintained.

In this thesis, we used the Born-Hung approach. In this approach, non-radiation transition between the electronic state occurs in the crossing region between two or more PESs. However, to describe the vicinity of the degeneracy using adiabatic state, adiabatic state is transmitted to the diabatic state (the term of the coupled electronic state is not included). Therefore, in the vicinity of the degeneracy, some characteristic property, which is invalid for adiabatic state, is exhibited.

References

[1] K. Nassau, *The Physics And Chemistry Of Color*, John Wiley & Sons, inc. 2001.

[2] P. W. Atkins, *Physical Chemistry 6Rev.* Oxford University Press, 1998.

[3] (a) G. Groenhof, L. V. Schäfer, M. BoggioPasqua, M. Goette, H. Grubmüller, M. A. Robb, *J. Am. Chem. Soc.* **129**, 6812 (2007). (b) P. R. L. Markwich, N. L. Doltsinis, *J. Chem. Phys.* **126**, 175102 (2007).

[4] J. Lugtenburg, R. Mathies, in: D.G. Stavenga, W.J. Grip, E.N. Pugh (Eds.), *Handbook of Biological Physics*, vol. 3, Elsevier, Amsterdam, 2000, p. 55.

[5] (a) F. Bernardi, S. De, M. Olivucci, M. A. Robb, *J. Am. Chem. Soc.* **112**, 1737 (1990). (b) F. Bernardi, M. Olivucci, M. A. Robb, *Acc. Chem. Res.* **23**, 405 (1990).

[6] M. Born, J. R. Oppenhieimer, *Ann. Phys. (Leipzig)*, **84**, 457 (1927).

[7] M. Bear, *Physics Reports*, **358**, 75 (2002).

[8] L. S. Cederbuum, *Born-Oppenheimer approximation and beyond. In Conical Intersections: Electronic Structure, Dynamics & Spectroscopy (Advance Series in Physical Chemistry vol. 15)*, W. Domcke, D. R. Yarkony, H. Köppel, Eds: World Scientific: Singapore, 2004, p 4.

[9] X. Wu, R. E. Wyatt, M. D'Mello, *J. Chem. Phys*, **101**, 2953 (1994). Y.-S. M. Wu, A. Kuppermann, *Chem. Phys. Lett.* **235**, 105 (1995). B. Kendrich, R. T. Pack, *J. Chem. Phys.* **104**, 7475 (1996).

[10] E. B. Wilson, Jr. J. C. Decius, P. C. Cross, *Molecular Vibrations: The Theory of Infrared and Raman Vibrational Spectra*, Dover publicationns, inc. New York, 1955.

[11] R. G. Wooley, B. T. Sutclife, *Chem. Phys. Lett.* **45**, 393 (1976).

[12] N. C. Hundy, A. M. Lee, *Chem. Phys. Lett.* **252**, 425 (1996).

[13] E. Deumens, A. Diz, R. Longo, Y. Öhrn, *Rev. Mod. Phys.* **66**, 917 (1994).

[14] M. Born, K. Huang, *Dynamical Theory of Crystal Lattices* (Oxford University Press), 1954.

Chapter 2

Conical Intersection

In this chapter, we would like to see the shape of the PES in the vicinity of a degeneracy point. Additionally, it will be shown that an isolated degeneracy point cannot exist except for diatomic molecules. At the last of this chapter, we can say the detailed purpose of this work.

2.1 Born-Huang Approach

In the Born-Huang approach,[1] the total wave function for state k in a basis of N^α, single-valued electronic wave functions is written as,

$$\Psi_k = \sum_i^{N^\alpha} \phi_i(\boldsymbol{r},\boldsymbol{R})\chi_i(\boldsymbol{R}). \tag{2.1}$$

If N^α is infinite, this expansion is accurate i.e. equal to the Born-Oppenheimer expansion, eq. (1.5). Practically, this expansion is truncated. The electronic states themselves are expanded as:

$$\phi_i(\boldsymbol{r},\boldsymbol{R}) = \sum_{\alpha=1}^{N^{CSF}} \Theta_\alpha(\boldsymbol{r},\boldsymbol{R})c_\alpha^i(\boldsymbol{R}), \tag{2.2}$$

where Θ_α are configuration state functions (CSFs). N^{CSF} is the number of CSFs. c_α^i is the weight to Θ_α.

The CSFs, Θ_α are constructed from molecular orbital,

$$\Theta_\alpha = \mathcal{A}\varphi(\boldsymbol{r},\boldsymbol{R})X(N^e, S, M; i) \tag{2.3}$$

where φ is the spatial function, $X(N^e, S, M; i)$ is the spin eigenfunctions corresponding to a given number of electrons, N^e, and the total spin quantum number, S, as obtained from the branching diagram method. The detailed explanation about the spin eigenfunctions can be found in Ref. 2. $\mathcal{A}$ is the antisymmetrizer,

$$\mathcal{A} = \frac{1}{\sqrt{N^e!}} \sum_P (-1)^P P, \tag{2.4}$$

which imposes the antisymmetry principle to a many electron wave function.

2.2 Adiabatic Electronic States

The electronic states, ϕ_i, are chosen to be the adiabatic states, i.e., eigenfunction of the electronic Hamiltonian H_e. That is, eq. (1.3) is satisfied;

$$(H_e - V_i(\boldsymbol{R}))\phi_i(\boldsymbol{r}, \boldsymbol{R}) = 0, \tag{2.5}$$

where the eigenvalue V_i is the ith potential energy. Using eq. (2.2), eq. (2.5) becomes

$$(H_e - V_i(\boldsymbol{R}))\{ \sum_{\alpha=1}^{N^{CSF}} \Theta_\alpha(\boldsymbol{r},\boldsymbol{R}) c_\alpha^i(\boldsymbol{R})\} = 0. \tag{2.6}$$

Multiplying $\Theta_\kappa(\boldsymbol{r},\boldsymbol{R})$ from the left hand side and integrating, the following equation can be obtained,

$$\sum_\alpha (\langle \Theta_\kappa | H_e | \Theta_\alpha \rangle - \langle \Theta_\kappa | V_k | \Theta_\alpha) c_\alpha^i = 0$$

$$\therefore \{\boldsymbol{H} - \boldsymbol{V}\}\boldsymbol{c} = 0. \tag{2.7}$$

As already shown in the previous chapter, the nonadiabatic process is predicted to occur at which two electronic states are degenerated. That is, nuclear and electronic motion cannot be treated separately. In this chapter, we will show the shape of PES in the vicinity of the degeneracy.

2.3 Conical Intersection

To see the PES in the vicinity of the degeneracy using Born-Huang approach, The electronic Hamiltonian, eq. (1.2), is expanded with respect to $\boldsymbol{R}$,

$$H_e = H_e^0 + \frac{\partial H_e}{\partial \boldsymbol{R}} d\boldsymbol{R}, \tag{2.8}$$

provided the section to H_e^o is available. For convenience, the system which is constructed by only two CSFs, Θ_1 and Θ_2, is considered. The electronic states are given by

$$\begin{aligned} \phi_1(\boldsymbol{r},\boldsymbol{R}) &= \Theta_1(\boldsymbol{r},\boldsymbol{R})C_1^1 + \Theta_2(\boldsymbol{r},\boldsymbol{R})C_2^1, \\ \phi_2(\boldsymbol{r},\boldsymbol{R}) &= \Theta_1(\boldsymbol{r},\boldsymbol{R})C_1^2 + \Theta_2(\boldsymbol{r},\boldsymbol{R})C_2^2. \end{aligned} \tag{2.9}$$

Θ_1, Θ_2 should satisfy

$$\begin{aligned} (H_e - E_1)\Theta_1 = 0, \\ (H_e - E_2)\Theta_2 = 0. \end{aligned} \tag{2.10}$$

E_1 and E_2 are the potential energies for Θ_1 and Θ_2 respectively. Hence, eq. (2.7) becomes,

$$\begin{pmatrix} H_{11} - V & H_{12} \\ H_{12} & H_{22} - V \end{pmatrix} \boldsymbol{c} = 0. \tag{2.11}$$

Here,

$$H_{ij} = \langle \Theta_i | H_e | \Theta_j \rangle \tag{2.12}$$

Eq. (2.12) can be written by using eq. (2.8),

$$H_{ij} = \langle \Theta_i | H_e^0 | \Theta_j \rangle + \langle \Theta_i | \frac{\partial H_e}{\partial \boldsymbol{R}} | \Theta_j \rangle d\boldsymbol{R}. \tag{2.13}$$

For future convenience, we define the following expression,

$$S = \frac{1}{2}(H_{22} + H_{11}), \tag{2.14a}$$

$$G = \frac{1}{2}(H_{22} - H_{11}), \tag{2.14b}$$

$$W = H_{12}. \tag{2.14c}$$

Using eq. (2.14), eq. (2.11) becomes,

$$\begin{pmatrix} S - G - V & W \\ W & S + G - V \end{pmatrix} \boldsymbol{c} = 0. \tag{2.15}$$

The condition, that $\boldsymbol{c}$ does have the solution except for trivial solutions, is

$$\begin{aligned}\begin{vmatrix} S-G-V & W \\ W & S+G-V \end{vmatrix} &= (S-V-G)(S-V-G)-W^2 \\ &= (S-V)^2-G^2-W^2=0. \\ \therefore V-S &= \pm\sqrt{G^2+W^2}, \\ V &= S\pm\sqrt{G^2+W^2}. \end{aligned} \tag{2.16}$$

and eigenvector $\boldsymbol{c}$

$$\begin{aligned}\begin{pmatrix} S-G-V & W \\ W & S+G-V \end{pmatrix}\begin{pmatrix} c_1 \\ c_2 \end{pmatrix} &= 0. \\ \therefore c_2 &= \frac{-S+G+V}{W}c_1. \end{aligned} \tag{2.17}$$

To satisfy the normalization condition,

$$\begin{aligned} c_1^2+c_2^2 &= \frac{W^2+(-S+G+V)^2}{W^2}=1 \\ \therefore c_1^2 &= \frac{W^2}{W^2+(-S+G+V)^2} \end{aligned} \tag{2.18}$$

Since there are no meaning in the sign of $c_{1,2}$, we select plus solution of eq. (2.18). Hence, the following eigenvector is obtained,

$$\begin{aligned} c_1 &= \frac{W}{\sqrt{W^2+(-S+G+V)^2}} \\ c_2 &= \frac{-S+G+V}{\sqrt{W^2+(-S+G+V)^2}} \end{aligned} \tag{2.19}$$

The relationship between the elements of eigenvector, c_1 and c_2, is reminiscent of that between sine and cosine. This relation become crucial fact to explain the geometric phase effect (phase change rule).

(i) When $V=S+\sqrt{G^2+W^2}$,

$$\begin{aligned} A=V-S &= \sqrt{G^2+W^2} \\ \therefore W^2 &= A^2-G^2 \end{aligned} \tag{2.20}$$

here we selected plus sign of W

$$W = \sqrt{A^2 - G^2} \tag{2.21}$$

substitute this W in eq. (2.19),

$$\begin{aligned} c_1 &= \sqrt{\frac{A^2 - G^2}{W^2 + (A-G)^2}} = \sqrt{\frac{A-G}{2A}} = -\sin\Lambda \\ c_2 &= \sqrt{\frac{(-S+G+V)^2}{A^2 - G^2 + (-S+G+V)^2}} = \sqrt{\frac{A+G}{2A}} = \cos\Lambda \end{aligned} \tag{2.22}$$

Here, we assigned "$-\sin$" to c_1 since setting the wave function of upper state on anti-bonding orbital seems to be reasonable.

(ii) when $V = S - \sqrt{G^2 + W^2}$,

$$\begin{aligned} -A = V - S &= -\sqrt{G^2 + W^2} \\ W &= \sqrt{A^2 - G^2} \end{aligned} \tag{2.23}$$

substitute W to eq. (2.19),

$$\begin{aligned} c_1 &= \sqrt{\frac{A^2 - G^2}{A^2 - G^2 + (G-A)^2}} = \sqrt{\frac{A+G}{2A}} = \cos\Lambda \\ c_2 &= -\sqrt{\frac{(A-G)^2}{2A^2 - 2AG}} = -\sqrt{\frac{A-G}{2A}} = \sin\Lambda \end{aligned} \tag{2.24}$$

Therefore, the eigenfunctions become,

$$\begin{aligned} \phi_1 &= \Theta_1 \cos\Lambda + \Theta_2 \sin\Lambda \\ \phi_2 &= -\Theta_1 \sin\Lambda + \Theta_2 \cos\Lambda \end{aligned} \tag{2.25}$$

If eq.(2.8) is the expansion around the degeneracy point whose nuclear coordinate is $\boldsymbol{R}_0$,

$$\begin{aligned} E_0 &= \langle\Theta_1|H_e^0|\Theta_1\rangle = H_{11}^0(\boldsymbol{R}_0) \\ &= \langle\Theta_2|H_e^0|\Theta_2\rangle = H_{22}^0(\boldsymbol{R}_0), \end{aligned} \tag{2.26a}$$

and

$$\langle\Theta_1|H_e^0|\Theta_2\rangle = H_{12}^0(\boldsymbol{R}_0) = 0. \tag{2.26b}$$

Hence, the following concrete equations are obtained,

$$S = E_0 + \frac{1}{2}\{\langle\Theta_1|\frac{\partial H_e}{\partial \boldsymbol{R}}|\Theta_1\rangle + \langle\Theta_2|\frac{\partial H_e}{\partial \boldsymbol{R}}|\Theta_2\rangle\}d\boldsymbol{R}, \tag{2.27a}$$

$$G = \frac{1}{2}\{\langle\Theta_1|\frac{\partial H_e}{\partial \boldsymbol{R}}|\Theta_1\rangle - \langle\Theta_2|\frac{\partial H_e}{\partial \boldsymbol{R}}|\Theta_2\rangle\}d\boldsymbol{R}, \tag{2.27b}$$

$$W = H_{12} = \langle\Theta_1|\frac{\partial H_e}{\partial \boldsymbol{R}}|\Theta_2\rangle d\boldsymbol{R}. \tag{2.27c}$$

Here, by Hellmann-Feynman theorem, the coefficient of G can be written as

$$\langle\Theta_2|\frac{\partial H_e}{\partial \boldsymbol{R}}|\Theta_2\rangle - \langle\Theta_1|\frac{\partial H_e}{\partial \boldsymbol{R}}|\Theta_1\rangle = \frac{\partial(E_2 - E_1)}{\partial \boldsymbol{R}} = \boldsymbol{g}. \tag{2.28}$$

which is known as a gradient difference vector (GD), the displacement causing the most strong change in the energy difference between E_1 and E_2. On the other hand, the coefficient of W,

$$\langle\Theta_1|\frac{\partial H_e}{\partial \boldsymbol{R}}|\Theta_2\rangle = \boldsymbol{h} \tag{2.29}$$

$\boldsymbol{h}$ is the numerator of eq. (1.20), that is the parallel to the derivative coupling vector. Therefore, $\boldsymbol{h}$ is the deformation of the molecule in which the nonadiabatic process strongly occurs. Since the PES along the derivative coupling becomes uncontinuum at the degeneracy point, it is impossible to estimate the length of derivative coupling but its direction is meaningful. Hereafter, we use the term of the derivative coupling vector as indicating only its direction.

$\boldsymbol{g}$ and $\boldsymbol{h}$ are the degeneracy lifting displacement. The plane, which spanned by $\boldsymbol{g}$ and $\boldsymbol{h}$, is called a branching plane or g-h plane.[3] Provided that $\boldsymbol{g} \neq 0$ and $\boldsymbol{h} \neq 0$, as shown in eq. (2.16), the shape of PES in the vicinity of the degeneracy point becomes two PESs conically intersecting region with respect to the displacement along $\boldsymbol{g}$ and $\boldsymbol{h}$. That is to say, $V = S - \sqrt{G^2 + W^2}$ is the PES of an under state and $V = S + \sqrt{G^2 + W^2}$ is the PES of an upper state. Figure 2.1 shows the shape of the typical conical intersection. If $\boldsymbol{g} = 0$ and $\boldsymbol{h} = 0$, but $\boldsymbol{\nabla g} \neq 0$, $\boldsymbol{\nabla h} \neq 0$, the intersection is in a class that includes the Renner-Teller intersection.[4]

Since our discussion is based on the spin free Hamiltonian, obtained result is limited to the degeneracy between the same spin multiplicity states. Therefore, the intersection between the same spin multiplicity states is called a conical intersection. The conical intersection was suggested by Teller[5] in 1937 for the first time.

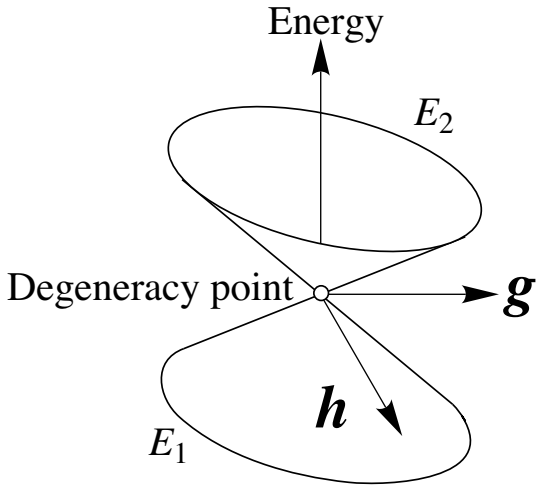

Figure 2.1: Conical intersection whose apex is a degeneracy point. $\boldsymbol{g}$ and $\boldsymbol{h}$ are the gradient difference vector and derivative coupling vector, respectively.

He pointed out the possible existence of the conical intersection even if intersecting states are the same spatial symmetry by drastic discussion and suggested its importance in photochemistry. 60 years later, the ubiquitous exitance of the conical intersection is shown by the unbiased potential energy search[6–9] in some organic molecules. Nowadays, the conical intersection is a crucial concept to discuss the photochemistry and photophysics of the molecule as discussed later in this chapter.

2.4 Classification

Conical intersections can be classified by its topograph and spatial symmetries of intersecting states. Especially, topograph of CIs strongly influence the dynamics of molecules

2.4.1 By Symmetry

According to the noncrossing rule,[10] two potential energy surfaces having the same symmetry are not permitted for diatomic molecules. Only states of different symmetry can cross. However, in more than diatomic molecule, the intersection between potential energy surfaces of the same symmetries can exist.

Symmetry-Required Conical Intersection

Symmetry-required conical intersections correspond to the two electronic states from the components of a degenerate irreducible representation. Symmetry-required conical intersection is sometimes called Jahn-Teller intersection after Jahn-Teller effect. Here, we would like to pick up the ethylene radical like cation or anion as an example. Figure 2.2, shows the schematic PES along the rotation around central C–C. When ethylene cation or anion radical is planar, its structural symmetry is D_{2h}. Thus, electron arrangement in the ground state is $(b_{3u})^1$ for cation and $(b_{3u})^2(b_{2g})^1$ for anion, i.e. the spatial symmetry of the ground state is $^2B_{3u}$ for cation and $^2B_{2g}$ for anion (See Figure 2.3 for ethylene π orbitals). On the other hand, in the $\pi - \pi^*$ excited state, $(b_{2g})^1$ for cation, $(b_{3g})^1(b_{2g})^2$ for anion. Corresponding spatial symmetry of the $\pi - \pi^*$ excited state is $^2B_{2g}$ for cation, $^2B_{3u}$ for anion. When cental C-C double bond is rotated by 90°, the electron arrangements in the ground state and the $\pi - \pi^*$ excited state become $(e)^1$ and $(e)^1$ for cation, and $(e)^2(e)^1$ and $(e)^1(e)^2$ for anion, i.e. the spatial symmetry of the ground state and $\pi - \pi^*$ excited state are ^2E for both cation and anion radical. Namely, when ethylene anion and cation radical becomes D_{2d} symmetry with cental C–C bond rotated by 90°, the ground and $\pi - \pi^*$ excited state is degenerate due to the symmetry.

This is an example of symmetry required conical intersections. However, the symmetry is not the nature of conical intersection. Conical intersections which are not required by symmetry are called accidental intersections.

Accidental Symmetry-Allowed Conical Intersection

Accidental symmetry-allowed conical intersections correspond to the intersection of two states of distinct spatial symmetry. Because these conical intersections does not contradict with the non-crossing rule, readers would easily understand its existence. Interestingly, symmetry required conical intersection is remained as symmetry allowed-conical intersection as we will be shown later. If the hydrogen of ethylene radical is substituted making its symmetry lower, the conical intersection where the central double bond is rotated by ca. 90° is remained (see Fig. 2.4). Namely, the symmetry is not the nature of the electronic state degeneracy.

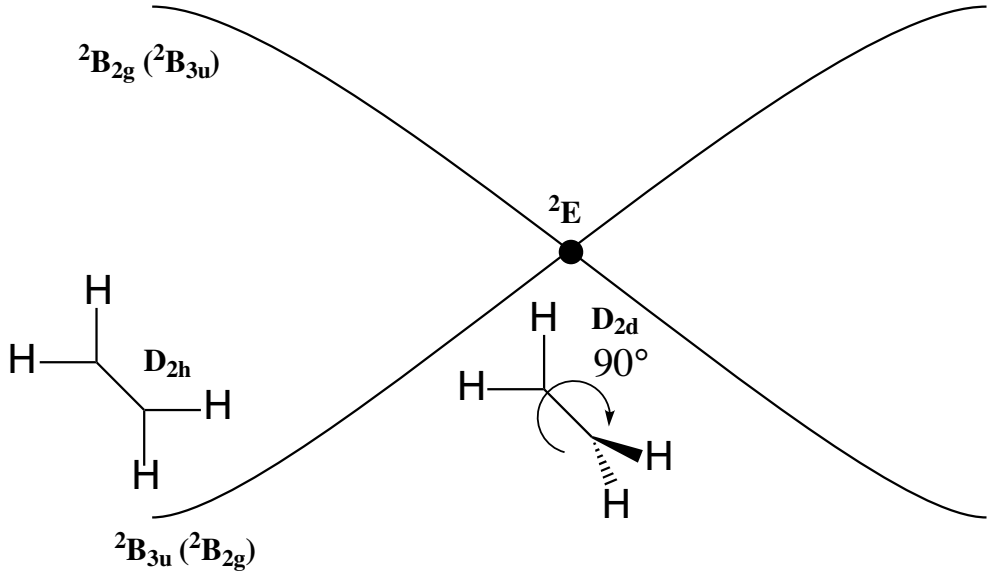

Figure 2.2: Symmetry-required conical intersection in ethylene. The spatial symmetry for electronic state for cation (for anion) is shown.

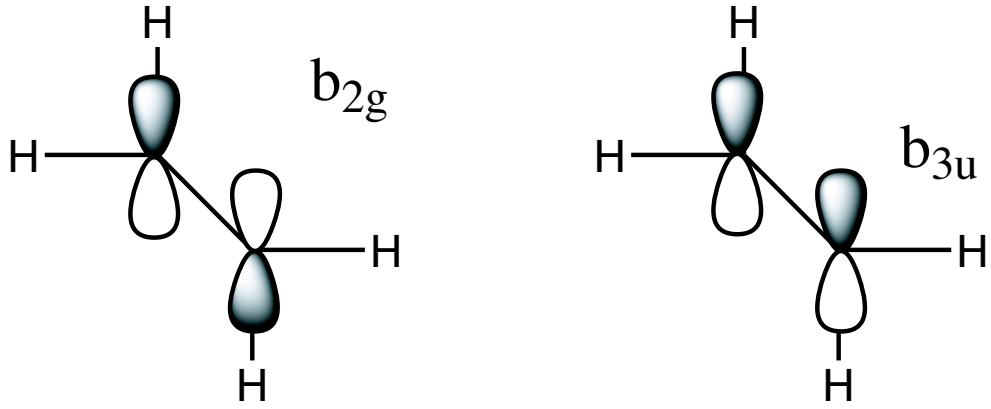

Figure 2.3: The π orbitals of ethylene with D_{2h} symmetry. b_{2g} is the antibonding orbital and b_{3u} is the bonding orbital.

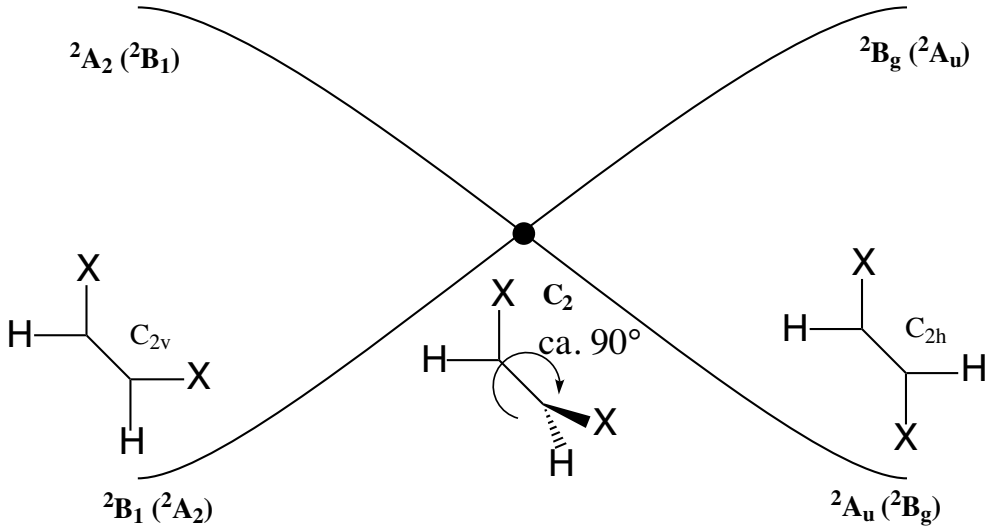

Figure 2.4: Symmetry-allowed conical intersection in substituted ethylene radical. x indicates some substituent. The spatial symmetry for electronic state for cation (for anion) is shown.

Accidental Same-Symmetry Conical Intersection

Accidental same-symmetry conical intersections correspond to the intersection of two states of the same symmetry. Because this type of conical intersection contradicts with the non-crossing rule, these existence was discussed in some detail.[3] However recent computational advances have clarified that the existence of this type of conical intersection is ubiquitous.[11] In this thesis, the conical intersection where the molecule have C_1 symmetry will be also shown.

2.4.2 By Topograph

Conical intersections can be classified by its topograph in the vicinity of degeneracy points. The topograph around conical intersections influence the dynamics of molecules. Thus the exploration of potential energy surface around the conical intersection is very important. Conical intersections are qualitatively classified into peaked, intermediate, and sloped conical intersection by tilt of diabolo, conical intersection. More quantitative classification is carried out by Yarkony.[12] In Fig. 2.5, typical topograph of the conical intersection is shown schematically. It is worthy to

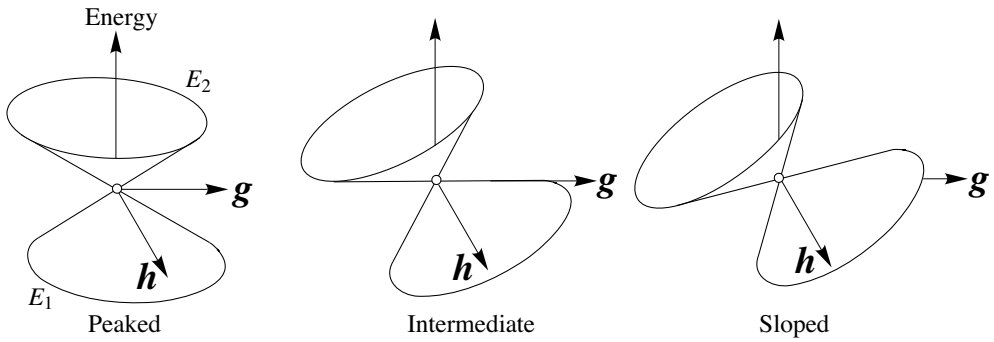

Figure 2.5: Conical intersection classification by the topograph

give simple explanation about its character.

Peaked Conical Intersection

In peaked CI, the two electronic states intersect with gradients of opposite sign to each other. This intersections are well-known since most Jahn-Teller intersections (symmetry-required conical intersections) belong to this type. Because of its topograph, the peaked conical intersection becomes a bifurcation point leading to various products.

Intermediate Conical Intersection

In intermediate CI, one of the electronic states intersects with zero gradient. Intermediate CI was exploited by Rudenberg et al.[13] Though the dynamics in the vicinity of intermediate conical intersection is interesting, its functionality is not known. It is difficult to locate the intermediate conical intersection even if the unbiased conical intersection searching strategy is adapted.

Sloped Conical Intersection

In sloped CI, the two electronic states intersect with gradients of the same sign. Namely, this conical intersection plays the role that a excited molecule goes back to the reactant without reaction. Therefore, the existence of sloped CI can be the main reason for the photostability of the molecule.

2.5 Effect

Conical intersections were thought to be extremely rare or inaccessible (i.e. located too high in energy) in organic compounds and thus were disregarded for many years. However, recent development in computational strategy to locating conical intersections shows the ubiquitous existence of conical intersections[7–9] which lie in energetically accessible region and its influence on chemistry is great as shown in the following.

2.5.1 Ultra Fast Photoreaction

When accessible conical intersections exist, the Landau-Zener model[14] provides a semi-classical model for fast radiationless decay. In this case, photoreaction can take place within a single vibrational oscillation through, or near the surface crossing and radiationless decay occurs on a scale of ps to fs.[15] If surface crossings are not present, or are present but not easily accessible, the process of radiationless decay is better described as the transformation of electronic energy into a manifold of vibronic states associated with the lower electronic state according to the Fermi Golden rule.[14] The Fermi Golden rule type decay occurs at a local minimum on the excited state (may be avoided crossing). This process is much slower than decay at a surface crossing and typical internal conversion rates are found to be $10^{-5} - 10^{-6}$ s. In Fig. 2.6, schematic potential energy surfaces are shown.

2.5.2 Internal Conversion

After irradiation, some excited molecules go back to the ground state without emitting fluorescence, i.e., radiationless decay. That can only occur where the energy gap between excited and ground state is within a few kcal mol^{-1}. The existence of conical intersections explains this internal conversion process. Figure 2.7 schematically shows the internal conversion for potential energy surfaces. Sloped conical intersection seems to be involved in this internal conversion processes. Typical example is azulene,[16] and cytosine-guanine base pair in DNA.[17] Sometimes, peaked conical intersections are involved in the internal conversion. In this cases short life time intermediate can be expected. Fulvene[18] and various nucleic acid bases[19] are

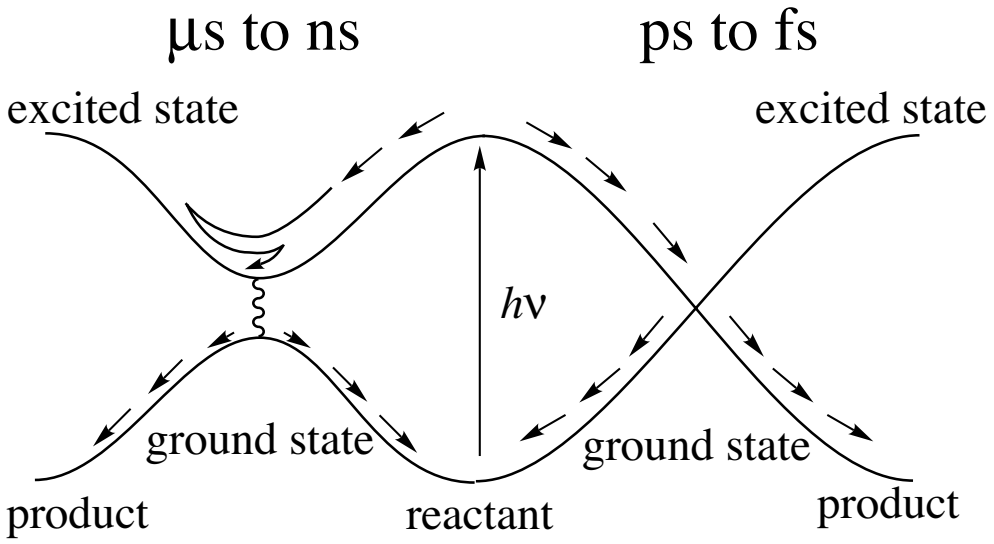

Figure 2.6: Landau-Zener model can explain the ultra fast photoisomerization which occurs on a scale of ps to fs. Fermi Golden rule is impossible for explaining the ultra fast photoisomerization.

examples.

2.5.3 Geometric Phase

The geometric phase effect is concerned with the nuclear motion of the adiabatic electronic wave function. Let's consider the result of transporting ϕ_i around a path that encloses a point of conical intersection. The expected result is that ϕ_i should return to itself because ϕ_i should be single-valued. However, that process applied to the eigenfunctions, (2.25), ϕ_i is not the single-valued. First of all, it is necessary to know the path that encloses a point of conical intersection. To get the closed path on the branching plane, the following unitary matrix is useful.

$$u = \begin{pmatrix} \cos\Lambda & \sin\Lambda \\ -\sin\Lambda & \cos\Lambda \end{pmatrix}. \tag{2.30}$$

By using u, diagonalize H matrix,

$$\begin{pmatrix} H_{11} & H_{12} \\ H_{12} & H_{22} \end{pmatrix} = \boldsymbol{I}S + \begin{pmatrix} -G & W \\ W & G \end{pmatrix}. \tag{2.31}$$

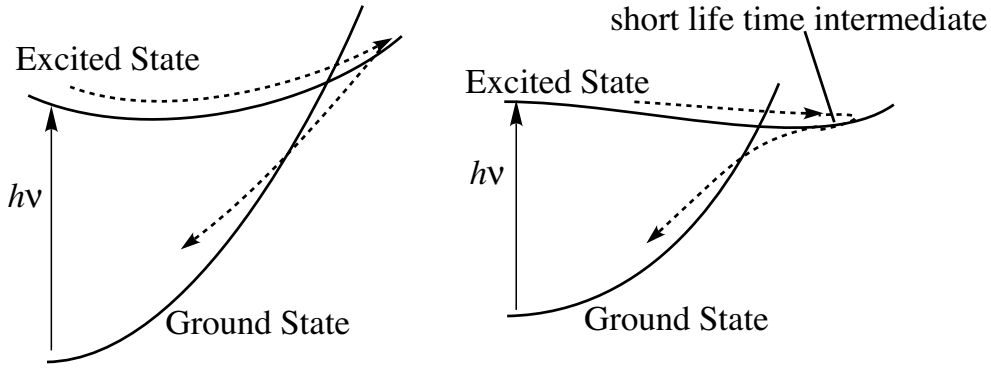

Figure 2.7: Schematic potential energy surfaces exhibiting internal conversion processes. Left is the case of a sloped conical intersection is involved. Right is the case of a peaked conical intersection is involved.

Obviously, the first term of eq. (2.31) is not changed by applying u. Thus, the relevant matrix is the second term.

$$u^{\dagger}\begin{pmatrix} -G & W \\ W & W \end{pmatrix}u = \begin{pmatrix} G\cos 2\Lambda - W\sin 2\Lambda & -G\sin 2\Lambda + W\cos 2\Lambda \\ -G\sin 2\Lambda + W\cos 2\Lambda & G\cos 2\Lambda + W\sin 2\Lambda \end{pmatrix}. \tag{2.32}$$

To make the non-diagonal element zero,

$$\begin{aligned} -G\sin 2\Lambda + W\cos 2\Lambda &= 0 \\ \therefore \tan 2\Lambda &= \frac{W}{G}. \end{aligned} \tag{2.33}$$

Above equation indicates that transporting along the closed path including conical intersection on the branching plane is the change of Λ from 0 to π. Hence, in eq. (2.25),

$$\phi_1(\Lambda + \pi) = -\phi_1(\Lambda). \tag{2.34}$$

That is, the sign of electronic state is changed by result of transporting along the closed path. This geometric phase effect was explored by Longuet-Higgins[20] for the first time. Recently, using this effect, methods to locate the conical intersection have been developed.[21] However, experimentally, geometric phase effect does not observed in contrast to the theoretical prediction.[22] Moreover, trajectory calculation on $H_2 + H \rightarrow H + H_2$ shows that the geometric effect is canceled.[23]

2.5.4 Trapping Effect

This effect is the influence of conical intersections on the ground state reactions. It is commonly asserted that upward transitions from the lower surface to the upper surface should be less likely because there are a peak in the lower surface. However, there are several cases in which conical intersections are relevant in the chemistry of molecules even in the ground state. That is called diabatic trapping effect, which disturbs or slows down the chemical reaction due to upward transitions from the lower surface to the upper surface. Well-known example is the photodissociation of bromoacetyl chloride, where C–Cl bond dissociation is major photoreaction though its transition state is higher than that of C–Br bond dissociation. That paradox is explained by the trapping effect between first two excited state.[24] Other examples, which has been recently reported, are intramolecular charge transfer of bis(methylene)adamantyl radical cation[25] and nitro-nitrite isomerization in nitroamide and nitromethane.[26]

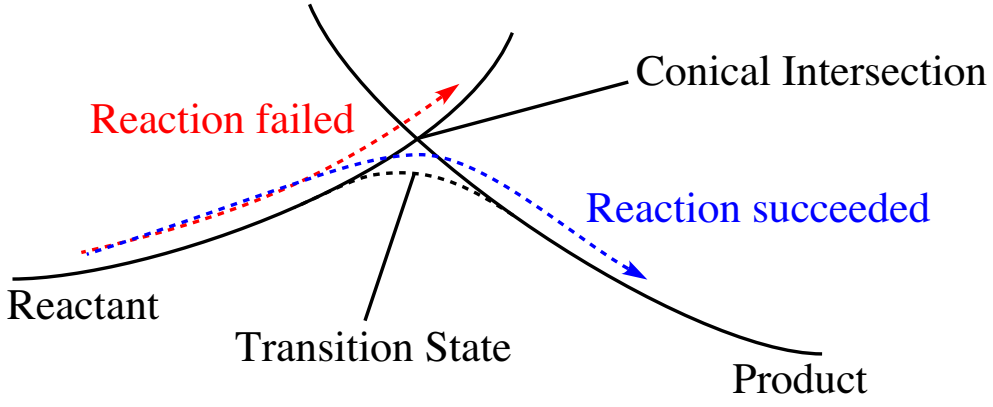

Figure 2.8: Schematic potential energy surfaces exhibiting diabatic trapping effect

2.6 Degeneracy Space

The existence of conical intersections is very important for explaining the above phenomena in both excited and ground states. However, these crucial points are not isolated points.

Consider the displacement from the degeneracy point ($\boldsymbol{R}_0$, which satisfies $H^0_{11}(\boldsymbol{R}_0) = H^0_{22}(\boldsymbol{R}_0)$ and $H^0_{12}(\boldsymbol{R}_0) = 0$. That means

$$\Delta G(\boldsymbol{R}) = \frac{1}{2}\boldsymbol{g} \cdot d\boldsymbol{R},\ \Delta W(\boldsymbol{R}) = \boldsymbol{h} \cdot d\boldsymbol{R} \tag{2.35}$$

If $\Delta G(\boldsymbol{R}) \neq 0$ and $\Delta W(\boldsymbol{R}) \neq 0$, i.e., $d\boldsymbol{R}$ overlaps with $\boldsymbol{g}$ and $\boldsymbol{h}$, the degeneracy is lifted. On the other hand, if $\Delta G(\boldsymbol{R}) = \Delta W(\boldsymbol{R}) = 0$, i.e., $d\boldsymbol{R}$ is orthogonal to $\boldsymbol{g}$ and $\boldsymbol{h}$. the degeneracy conditions, $H_{11} = H_{22}$ and $H_{12} = 0$ are maintained. Therefore, if n is the number of degree of freedom of the molecule, degeneracy is preserved in the $(n-2)$-dimensional complement space to $\boldsymbol{g}$ and $\boldsymbol{h}$. At any points in the $(n-2)$-dimensional complement space, conical intersection can be shown by defining $\boldsymbol{g}$ and $\boldsymbol{h}$. This $(n-2)$-dimensional space is called conical intersection hyperline or seam.[27,28] In this thesis, we call this as degeneracy space (DS).

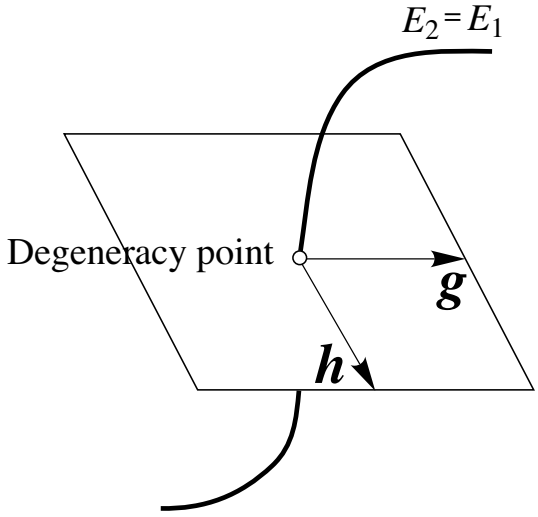

Figure 2.9: Degeneracy is preserved in the $(n-2)$-dimensional complement space to $\boldsymbol{g}$ and $\boldsymbol{h}$.

As already mentioned, the unbiased methods to search the conical intersection were developed. In practical, these methods are to locate the lowest energy degeneracy point (LEDP) in the $(n-2)$-dimensional space. By virtue of these unbiased method, the ubiquitous existence of conical intersections has been clarified. Moreover, these method had also unveiled the importance of DS. In the case of three atom molecule, DS is one-dimensional. Therefore, it is relatively easy to characterize DS. However, in the case of more than three atom molecule, it becomes a

difficult attempt to characterize the DS. The purpose of our study is clarification of the influence of the DS on chemical reactions. That is to say, interpretation of photoreaction processes should change by considering a degeneracy space instead of a degeneracy point. Figure 2.10 shows model PES with a degeneracy point (i.e. conical intersection). On the other hand, Figure 2.11 shows model PES with a degeneracy space. The purpose of this work is to elucidate the effect of DS on the photochemical reaction processes. To this end, it is necessary to characterize the DS. In the next chapter, we show the our original method to characterize the degeneracy space.

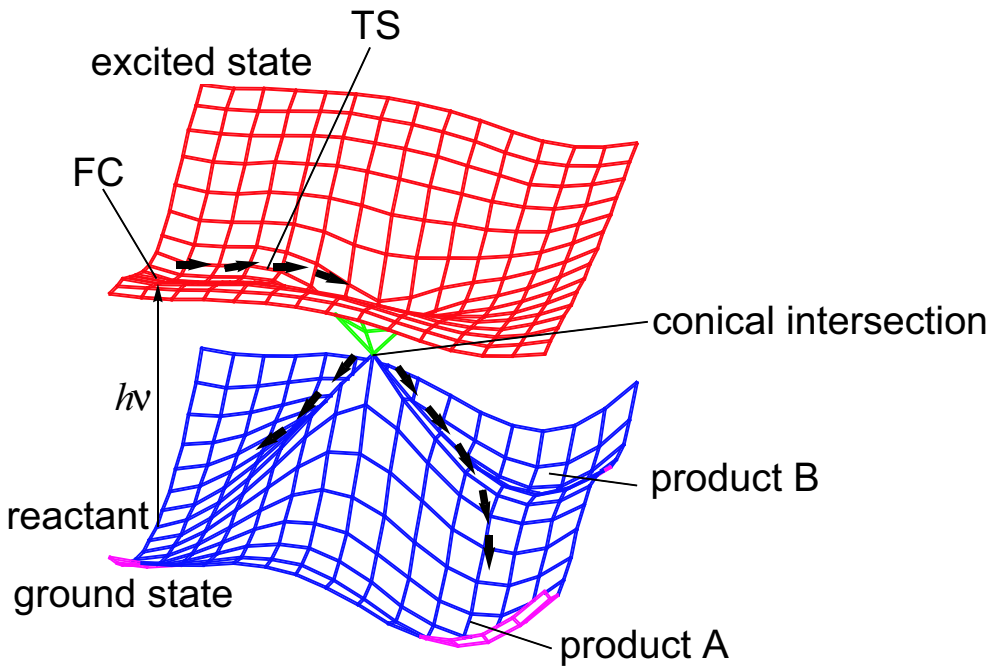

Figure 2.10: Model potential energy surfaces which include a degeneracy point (conical intersection). In this PES, the decay area where excited state to ground state transition occurs is only one point. FC is the abbreviation of Franck-Condon point and TS is the transition state. The existance of TS sometimes enhance quantum yield of fluorescence, i.e., prevents the excited molecule from reaching conical intersection.

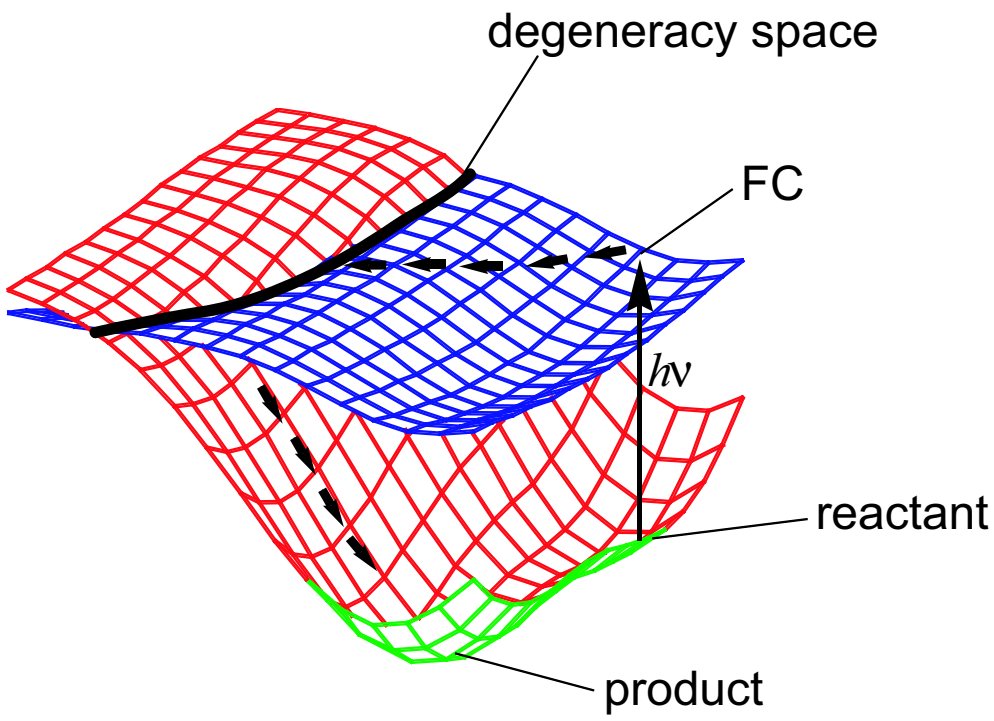

Figure 2.11: Model potential energy surfaces which include a degeneracy space. In this PES, the decay area is a space (line there). Hence, excited molecule can transit to gound state anywhere in the degeneracy space

2.7 Complete Active Space Self-Consistent Field

Though there are several calculation methods in quantum chemistry, the suitable method for our purpose is limited to the method using multi-configuration wave function. To calculate the derivative coupling, eq. (2.29), a wave function expanded by multi-configuration state functions is needed. Therefore, we used mainly complete active space self-consistent field (CASSCF),[29] which is one of the multi-configuration self-consistent field (MCSCF) methods. In MCSCF, to describe the derivative of the molecular orbitals, the coupled perturbed state-averaged MCSCF (CPMCSCF)[30] is necessary. The description about the MCSCF of CPMCSCF is beyond this thesis. Here, we would like to describe the character of CASSCF when one uses.

In CASSCF, orbitals are divided into the following three spaces:

(i) Inactive space

(ii) Active space

(iii) Virtual space

The inactive and active space are occupied by electrons. The inactive space is always described by single configuration. On the other hand, full configuration of electrons is considered in the orbitals included in the active space. You can carry out the calculation including the static electronic correlation within the active space. In this thesis, CASSCF whose active space is constructed from n electrons and m orbitals is denoted as CAS(n,m). Finally, the virtual space is selected as the virtual orbitals for always.

The most characteristic and important aspect of CASSCF concerns with the selection of the active space. One should select the suitable orbitals for describing the potential energy surfaces. Sometimes, you should change the active space to describe entire reaction path. Unsuitable selection of the active space may induce the orbital breaking. If the active space is broken while you exploring the PES, you should abort the calculation immediately because these calculations are meaningless. If the active space you selected is suitable, CASSCF becomes very powerful tool for describing diradical species and excited states of some molecules.

There are some deficiencies in CASSCF. For instance, vertical excited energies calculated by CASSCF are generally higher than that observed in experiments. This

is due to restricting electron configuration within active space. That is, excited space for electrons is artificially limited to the active space. Accordingly, CASSCF sometimes gives wrong qualitative shapes of potential energy surfaces. To compensate these defections of CASSCF, more expensive calculations like multi-reference configuration interaction (MRCI), which includes dynamical electronic correlation, is needed. As will be shown in Chap. 4, the calculation which includes dynamical electronic correlation modifies the potential energy surfaces obtained by CASSCF.

References

[1] M. Born, K. Huang, *Dynamical Theory of Crystal Lattices* (Oxford University Press), 1954.

[2] R. Pauncz, *The Construction of Spin Eigenfunctions: An Exercise Book* (Plenum Pub. Corp.) 2000.

[3] D. R. Yarkony, *Rev. Mod. Phys.* **68**, 985 (1996).

[4] R. Renner, *Z. Phys.* **92**, 172 (1934).

[5] E. Teller, *J. Phys. Chem.* **41**, 109 (1937).

[6] N. Koga, K. Morokuma, *Chem. Phys. Lett.* **119**, 371(1985).

[7] I. N. Ragazos, M. A. Robb, F. Bernardi, M. Olivucci, *Chem. Phys. Lett.* **197**, 217 (1992).

[8] M. R. Manaa, D. R. Yarkony, *J. Am. Chem. Soc.* **116**, 11444 (1994).

[9] M. J. Bearpark, M. A. Robb, H. B. Schlegel, *Chem. Phys. Lett.* **223**, 269 (1994).

[10] J. von. Neumann, E. Wigner, *Physik. Z*, **30**, 467 (1929).

[11] D. R. Yarkony, *Acc. Chem. Res.* **31**, 511(1998).

[12] D. R. Yarkony, *J. Phys. Chem.* **114**, 2601(2001).

[13] G. J. Atchity, S. S. Xantheas, K. Ruedenberg, *J. Phys. Chem.* **95**, 1862(1991).

[14] M. Desouter-Lecomte, J. C. Lorquet, *J. Phys. Chem.* **71**, 4391(1979).

[15] H. Köppel, L. S. Cederbaum, W. Domcke, S. S. Shaik, *Angew. Chem. Int. Ed. Engl.* **22**, 210(1983).

[16] (a) M. A. Bearpark, F. Bernardi, S. Clifford, M. Olivucci, M. A. Robb, B. R. Smith, T. Breven, *J. Am. Chem. Soc.* **118**, 169 (1996). (b) Y. Amatatsu, Y. Komura, *J. Chem. Phys.* **125**, 174311(2006).

[17] (a) G. Groenhof, L. V. Schäfer, M. BoggioPasqua, M. Goette, H. Grubmüller, M. A. Robb, *J. Am. Chem. Soc.* **129**, 6812 (2007). (b) P. R. L. Markwich, N. L. Doltsinis, *J. Chem. Phys.* **126**, 175102 (2007).

[18] M. J. Bearpark, F. Bernardi, M. Olivucci, M. A. Robb, B. R. Smith, *J. Am. Chem. Soc.* **118**, 5254 (1996).

[19] (a) L. Serrano-Andrés, M. Merchán, A. C. Borin, *Cham. Eur, J.* **12**, 6559(2006). (b) L. Serrano-Andrés, M. Merchán, A. C. Borin, *Proc. Natl. Acad. Soc. USA*, **103**, 8691 (2006). (c) M. Merchán, R. Gonazález-Luque, T. Climent, L. Serrano-Andrés, E. Rodríguez, Mar Reguero, D. Peláez, *J. Phys. Chem. B*, **110**, 26471 (2006). (d) F. Santoro, V. Barone, T. Gustavsson, R. Inprota, *J. Am. Chem. Soc.* **128**, 16312 (2006). (e) L. Blancafort, B. Cohen, P. M. Hare, B. Kohler, M. A. Robb, *J. Phys. Chem. A*, **109**, 4431 (2005).

[20] H. C. Longuet-Higgins, *Proc. Roy. Soc. London A*, **334**, 147 (1975).

[21] (a) S. Zilberg, Y. Haas, *J. Phys. Chem. A*, **103**, 2364 (1999). (b) S. Zilberg, Y. Haas, *Chem. Eur. J.* **5**, 1755 (1999). (b) S. Zilberg, Y. Haas, *Chem. Phys.* **259**, 249 (2000). (c) S. Zilberg, Y. Haas, *Photochem. Photobiol. Sci.* **2**, 1256 (2003).

[22] Y.-S. M. Wu, A. Kuppermann, *Chem. Phys. Lett.* **201**, 2953 (1993).

[23] J. C. Juanes-Marcos, S. C. Althorpe, E. Wrede, *Science*, **309**, 1227(2005).

[24] (a) B. Lasorne, M. -C. Bacchus-Montabonel, N. Vaech, M. Desouter-Lecomte, *J. Chem. Phys.* **120**, 1271 (2004). (b) M. -C. Bacchus-Montabonel, N. Vaech, B. Lasorne, M. Desouter-Lecomte, *Chem. Phys. Lett.* **374**, 307 (2003).

[25] L. Blancafort, P. Hunt, M. A. Robb, *J. Am. Chem. Soc.* **127**, 3391(2005).

[26] J. Soto, J.F. Arenas, J. C. Otero, D. Peláez, *J. Phys. Chem. A*, **110**, 8221(2006).

[27] F. Bernardi, M. Olivucci, M. A. Robb, *Chem. Soc. Rev.* **25**, 321(1996).

[28] D. R. Yarkony, *Conical Intersection: Their Description and Consequences. In Conical Intersections: Electronic Structure, Dynamics & Spectroscopy (Advance Series in Physical Chemistry vol. 15)*, W. Domcke, D. R. Yarkony, H. Köppel, Eds: World Scientific: Singapore, 2004, p 41.

[29] B. O. Roos, P. R. Taylor, P. E. M. Siegbahn, *Chem. Phys.* **48**, 157(1980). B. O. Roos, *The Multiconfigurational Self-Consistent Field Theory. In Lecture Notes in Quantum Chemistry (European Summer School in Quantum Chemistry*, B. O. Roos, Ed: Springer-Verlag Berlin Heidelberg 1992, p 177.

[30] D. R. Yarkony, *Determination of Potential Energy Surface Intersections and Derivative Couplings in the Adiabatic Representation, In Conical Intersections: Electronic Structure, Dynamics & Spectroscopy (Advance Series in Physical Chemistry vol. 15)*, W. Domcke, D. R. Yarkony, H. Köppel, Eds: World Scientific: Singapore, 2004, p 129.

Chapter 3

Characterization of the Degeneracy Space

In this chapter, we describe our original method to characterize degeneracy space, a two step procedure and discuss its validity.

3.1 Introduction

Recent theoretical calculation elucidated the importance of the conical intersections which are the real state crossing between the same spin multiplicity states.[1,2] A degeneracy point (DP), which is an apex of a conical intersection, is not an isolated point, but consecutive space (see the next section about the detail). The method to locate stationary DP (e.g., the lowest energy degeneracy point: LEDP) has been already established.[3,4] However, some theoretical calculation indicated the importance of exploring the degeneracy space (DS).[5–7] Hence, the method to explore the DS as a function of an arbitrary internal coordinate of the molecule is desired. Some methods characterizing the DS along an arbitrary internal coordinate of molecules have been reported. In the method based on Lagrange multipliers for optimization in the DS,[3] the determination of the section of the DS along a variable is possible.[8] In the projected gradient method,[4] when one uses the method with a geometric constrain beyond symmetry, the point at which energies are not degenerated is located. This undesirable result is called a "cancellation error" which has been discussed and some methods to circumvent the problem have been proposed.[7,9–12] According to

these discussions, the origin of cancellation error is due to the lost of the orthogonality between a degeneracy lifting space and its complement space. We will however show that it is not the case.

We circumvent the cancellation error by a two-step procedure.[9,10,13] This chapter explain the the two-step procedure in detail, and clarify how well energy is minimized using the procedure and what condition is required for the procedure. To this end, we selected fulvene as a calculation target.

Fulvene is known as one of the isomers of benzene and a product of its photoisomerization.[14–17] The radiationless decay from the first excited (S_1) state in fulvene is observed.[18–21] Theoretically, this radiationless decay can be explained by the existence of some DPs.[12,22–24] These theoretical results suggested the possibility of the exocyclic methylene rotation by 180°. On the other hand, cis–trans photoisomerization is experimentally observed in fulvene derivative. The photoisomerization of E–Z 2-tert-Butyl-9-(2,2,2-triphenylthylidene)fluorene is recently observed experimentally.[25] This means that fulvene is useful as photo switches if suitable substitutions are selected. To select the suitable substitutions, it is necessary to know the condition that makes it possible the exocyclic methylene to rotate by 180°. Bearpark et al. suggested that the 0-0 excitation to S_1 is needed for the rotation.[22] In this chapter, considering the existence of the S_1/S_0 DPs, we additionally discuss the condition of the exocyclic methylene rotation by 180°. Bearpark et al.[12] have already revealed that three S_1/S_0 DPs (DP_{planar}: C_{2v} planar structure, DP_{63}: exocyclic methylene is rotated by about 63° with C_2, and DP_{perp}: exocyclic methylene is perpendicular to five membered ring with C_{2v}) exist in the same S_1/S_0 DS which is predicted to chemically relevant to cis–trans photoisomerization in contradiction to the suggestion by Deeb et al.[26] However, we have some questions about the previous mapping S_1/S_0 DS.[12] Here we will give more reliable results in the geometry with better energy degeneracy.

In Section 3.2, we analyze the origin of the "cancellation error" and suggest the method to assess the validity upon using our computational strategy.[9,10,13] In Section 3.4, picking up the exocyclic methylene rotation of fulvene, we will show the valid condition in applying two-step procedure based on section 3.2. Utilizing the procedure, the possibility of the methylene rotation in a fulvene molecule by 180° is discussed.

3.2 Theoretical Discussion

To describe the conical intersection, an apex of which is a DP, two coordinates are needed.[1,27] One is a gradient difference vector (GD),

$$\boldsymbol{g} = \boldsymbol{\nabla}(E_1 - E_0), \tag{3.1}$$

and the other is a derivative coupling vector (DC),

$$\boldsymbol{h} = \langle \Psi_1 | \boldsymbol{\nabla} \Psi_0 \rangle \ . \tag{3.2}$$

In eqs. (3.1) and (3.2), the gradient $\boldsymbol{\nabla}$ is a vector operator in nuclear coordinates. Ψ_1 and Ψ_0 are wave functions of the upper and lower states, respectively. Their energies are denoted as E_1 and E_0. The pair ($\boldsymbol{g}$, $\boldsymbol{h}$) is usually called a branching plane or g-h plane.[1,27] In the complement orthogonal space to the branching plane, the degeneracy is preserved. In this chapter, we refer to this complement space as a degeneracy space (DS) which is sometimes called a conical intersection hyperline or seam.[1,27] The DS is $(n-2)$-dimensional space for two states, where n is the number of molecular internal degrees of freedom. We denote unit vectors, $\boldsymbol{x}_1$ and $\boldsymbol{x}_2$,

$$\boldsymbol{x}_1 = \frac{\boldsymbol{g}}{|\boldsymbol{g}|}, \ \boldsymbol{x}_2 = \frac{\boldsymbol{h}}{|\boldsymbol{h}|} \tag{3.3}$$

on the branching plane and $(n-2)$-dimension internal coordinate orthogonal to the branching plane as $\boldsymbol{x}_3$, $\boldsymbol{x}_4$ $\ldots \boldsymbol{x}_n$. $\boldsymbol{x}_i$ $(i = 3, 4...n)$ is referred to as intersection adapted coordinate.[27] Intersection adapted coordinate is different from non-redundant internal coordinates because each of $\boldsymbol{x}_i$ $(i = 1, 2...n)$ is represented as a linear combination of some variables like bond lengths, bond angles and/or dihedral angles. To locate the lowest energy degeneracy point (LEDP) in DS, some optimization methods have been developed.[3,4,28] The projected gradient method[4] is extensively used. If this method is used together with a geometric constraint beyond molecular symmetry, however, a point at which the energy of two states are not degenerated is finally reached. We have pointed out that this error is due to constraining the variables that has components in the branching plane.[9] In the following discussion, we show that the error is due to constraining the variables that has components in both the branching plane and the intersection adapted coordinate.

In the projected gradient method, the following gradient is used,

$$\boldsymbol{g}^{\mathrm{CIO}} = P\boldsymbol{\nabla}E_1 + 2(E_1 - E_0)\boldsymbol{\nabla}(E_1 - E_0) \ , \tag{3.4}$$

where P is the projection operator onto the $(n-2)$-dimensional intersection adapted coordinate. That is to say, P deducts DC and GD from $\boldsymbol{\nabla} E_1$. Here, we write the GD in non-normalized form for simplicity though the GD in eq. (3.4) is practically coded in normalized form, $\boldsymbol{x}_1$.

Hereafter, we regard E_1 as a function of internal molecular coordinates, v_i (i=1,2,...,n), and define $\boldsymbol{e}_i$ as unit vector in the direction of displacement of v_i. $\boldsymbol{e}_i$ must be orthogonal to each other. For instance, $\boldsymbol{e}_i$ can be obtained by orthogonalizing the unit vector of physically significant set like bond lengths, bond angles and dihedral angles.[29] Then, $\boldsymbol{\nabla} E_1$ can be represented by derivatives with respect to v_i ($i = 1, 2, ..., n$).

$$\boldsymbol{\nabla} E_1 = \frac{\partial E_1}{\partial v_1}\boldsymbol{e}_1 + \frac{\partial E_1}{\partial v_2}\boldsymbol{e}_2 + \ldots + \frac{\partial E_1}{\partial v_n}\boldsymbol{e}_n \ , \tag{3.5}$$

For convenience, we classify the components of $\boldsymbol{\nabla} E_1$ into four groups.

$$\begin{aligned} \boldsymbol{\nabla} E_1 &= \frac{\partial E_1}{\partial \boldsymbol{v}_L}\boldsymbol{e}_L{}^{\mathrm{T}} + \frac{\partial E_1}{\partial \boldsymbol{v}_M}\boldsymbol{e}_M{}^{\mathrm{T}} + \frac{\partial E_1}{\partial \boldsymbol{v}_S}\boldsymbol{e}_S{}^{\mathrm{T}} + \frac{\partial E_1}{\partial \boldsymbol{v}_P}\boldsymbol{e}_P{}^{\mathrm{T}} \\ &= \sum_h \frac{\partial E_1}{\partial v_{L,h}}\boldsymbol{e}_{L,h} + \sum_i \frac{\partial E_1}{\partial v_{M,i}}\boldsymbol{e}_{M,i} + \sum_j \frac{\partial E_1}{\partial v_{S,j}}\boldsymbol{e}_{S,j} + \sum_k \frac{\partial E_1}{\partial v_{P,k}}\boldsymbol{e}_{P,k} \ , \end{aligned} \tag{3.6}$$

where $\boldsymbol{v}_L$ is the group of the components which has no overlap with the branching plane. Both $\boldsymbol{v}_M$ and $\boldsymbol{v}_S$ are the groups of the components having overlap with branching plane but $\boldsymbol{v}_S$ is the variable that is constrained. On the other hand, $\boldsymbol{v}_P$ is the group of the components that lie within the branching plane. Corresponding unit vectors are denoted by $\boldsymbol{e}_L$, $\boldsymbol{e}_M$, $\boldsymbol{e}_S$ and $\boldsymbol{e}_P$, and distinguished by an additional subscript. After applying P, eq. (3.6) becomes,

$$P\boldsymbol{\nabla} E_1 = \sum_h \frac{\partial E_1}{\partial v_{L,h}}\boldsymbol{e}_{L,h} + \sum_i c_{M,i}\frac{\partial E_1}{\partial v_{M,i}}\boldsymbol{e}_{M,i} + \sum_j c_{S,j}\frac{\partial E_1}{\partial v_{S,j}}\boldsymbol{e}_{S,j} \ , \tag{3.7}$$

where coefficients, $c_{M,i}$ and $c_{S,j}$, satisfies

$$\begin{aligned} c_{M,i} &= 1 - \boldsymbol{x}_1 \cdot \boldsymbol{e}_{M,i} - \boldsymbol{x}_2 \cdot \boldsymbol{e}_{M,i} \\ &= 1 - c_{M,i}^{'} \ , \end{aligned} \tag{3.8a}$$

$$\begin{aligned} c_{S,j} &= 1 - \boldsymbol{x}_1 \cdot \boldsymbol{e}_{S,j} - \boldsymbol{x}_2 \cdot \boldsymbol{e}_{S,j} \\ &= 1 - c_{S,j}^{'} \ . \end{aligned} \tag{3.8b}$$

The branching plane component should be represented by the deducted component. Then we write the component of the second term in eq. (3.4) as

$$\boldsymbol{\nabla}(E_1 - E_0) = \sum_i c_{M,i}^{'} \frac{\partial E_1}{\partial v_{M,i}} \boldsymbol{e}_{M,i} + \sum_j c_{S,j}^{'} \frac{\partial E_1}{\partial v_{S,j}} \boldsymbol{e}_{S,j} + \sum_k \frac{\partial E_1}{\partial v_{P,k}} \boldsymbol{e}_{P,k} \ . \tag{3.9}$$

Equation (3.4) then becomes

$$\begin{aligned} \boldsymbol{g}^{\mathrm{CIO}} = & \sum_h \Big(\frac{\partial E_1}{\partial v_{L,h}} \Big) \boldsymbol{e}_{L,k} + \sum_i \left(c_{M,i} \Big(\frac{\partial E_1}{\partial v_{M,i}} \Big) + 2(E_1 - E_0) c_{M,i}^{'} \Big(\frac{\partial E_1}{\partial v_{M,i}} \Big) \right) \boldsymbol{e}_{M,i} \\ & + \sum_j \left(c_{S,j} \Big(\frac{\partial E_1}{\partial v_{S,j}} \Big) + 2(E_1 - E_0) c_{S,j}^{'} \Big(\frac{\partial E_1}{\partial v_{S,j}} \Big) \right) \boldsymbol{e}_{S,j} + \sum_k 2(E_1 - E_0) \Big(\frac{\partial E_1}{\partial v_{P,k}} \Big) \boldsymbol{e}_{P,k} \ . \end{aligned} \tag{3.10}$$

Although the third summation term is eliminated for geometric constraint, we keep this term for clear discussion. The following condition is also implicitly imposed because of the orthogonality between the intersection adapted coordinates and branching plane:

$$P \boldsymbol{\nabla} E_1 \cdot \boldsymbol{\nabla}(E_1 - E_0) = \sum_i c_{M,i} c_{M,i}^{'} \Big(\frac{\partial E_1}{\partial v_{M,i}} \Big)^2 + \sum_j c_{S,j} c_{S,j}^{'} \Big(\frac{\partial E_1}{\partial v_{S,j}} \Big)^2 = 0 \ . \tag{3.11}$$

According to eq. (3.10), the convergence condition then reads

$$\frac{\partial E_1}{\partial v_{L,h}} = 0 \ , \tag{3.12a}$$

$$c_{M,i} \frac{\partial E_1}{\partial v_{M,i}} + 2(E_1 - E_0) c_{M,i}^{'} \frac{\partial E_1}{\partial v_{M,i}} = 0 \ , \tag{3.12b}$$

$$c_{S,j} \frac{\partial E_1}{\partial v_{S,j}} + 2(E_1 - E_0) c_{S,j}^{'} \frac{\partial E_1}{\partial v_{S,j}} = C_{S,j} \ , \tag{3.12c}$$

$$2(E_1 - E_0) \frac{\partial E_1}{\partial v_{P,k}} = 0 \ . \tag{3.12d}$$

Here, $C_{S,j}$ is finite. Equation (3.12a) shows that optimization will be successful if the variables that has no overlap with branching plane are employed. As for eq. (3.12d), two situations are possible. One is $E_1 - E_0 = 0$ and the other $\partial E_1 / \partial v_{P,k} = 0$. The former condition is, however, ruled out by the following reason: Multiplying eq. (3.12b) by $c_{M,i}^{'}(\partial E_1 / \partial v_{M,i})$ and using eq. (3.11),

$$\sum_j c_{S,j} c_{S,j}^{'} \Big(\frac{\partial E_1}{\partial v_{S,j}} \Big)^2 = 2(E_1 - E_0) \sum_i {c_{M,i}^{'}}^2 \Big(\frac{\partial E_1}{\partial v_{M,i}} \Big)^2 \ , \tag{3.13}$$

is obtained. Apart from special cases (e.g., the value of $v_{S,j}$ corresponds to that of a LEDP), $c_{S,j}c_{S,j}^{\acute{}}(\partial E_1/\partial v_{S,j})^2$ is not zero from eq. (3.12c). The right hand side of eq. (3.13) is not zero, accordingly. Namely, the optimization converges to the point where two states does not degenerate (i.e., $E_1 \neq E_0$). This is really a " cancellation error." If either $c_{S,j}$ or $c_{S,j}^{\acute{}}$ is zero, cancellation error does not occur because there are no dependences between $\partial E_1/\partial v_{M,i}$ and $\partial E_1/\partial v_{S,j}$ by eq. (3.11). If both $c_{S,j}$ and $c_{S,j}^{\acute{}}$ are not zero, the cancellation error occurs. Therefore, in contradiction to the previous suggestion (the orthogonality between the first and second term in eq. (3.4) is lost due to the constraint), to keep the orthogonal condition [eq. (3.11)], the first term offsets the second term in eq. (3.4).

Recently, this cancellation error has been circumvented by several methods.[7,9–12] Migani et al.[7] circumvented it by scaling the second term in eq. (3.4) with a factor of 100. Yamazaki et al.[11] circumvented it by orthogonalizing the internal coordinate of molecules. With the gradient of which the constraint is applied before the projection of $\boldsymbol{\nabla} E_1$ onto the intersection adapted coordinate, Bearpark et al.[12] have succeeded to map the S_1/S_0 DS along the exocyclic methylene rotation of fulvene with a maximum energy gap of 0.4 kcal mol^{-1}. It is, however, noteworthy that the points at which a maximum energy gap is approximately 0.4 kcal mol^{-1} (see Table 3.1) can be located by using the default gradient (our first step). That is, there is no difference in effect between the default gradient[4] and the modified gradient.[12]

On the other hand, in our easy computational strategy, after optimization using eq. (3.4) (i.e., converging to the geometry satisfying eq. (3.12)), we carried out the geometry optimization using only the second term in eq. (3.4).[9,10,13] We have used this computational strategy without estimating how well energy is minimized within the intersection adapted coordinate. Here we try to assess the validity of the strategy. Multiplying eq. (3.12b) by $c_{M,j}(\partial E_1/\partial v_{M,i})$ and using eq. (3.11), we obtain

$$\sum_i {c_{M,i}}^2 \Big(\frac{\partial E_1}{\partial v_{M,i}}\Big)^2 = 2(E_1 - E_0) \sum_j c_{S,j} c_{S,j}^{\acute{}} \Big(\frac{\partial E_1}{\partial v_{S,j}}\Big)^2 . \tag{3.14}$$

This equation indicates the variables which have overlap with both branching plane and intersection adapted coordinate cannot work as an independent variable for optimization due to geometric constraint. In turn, the second step optimization is successfully limited in effect within the intersection adapted coordinates if eq. (3.14) is small enough. The two-step procedure is, in this sense, not for improving

the energy degeneracy but for the better geometry in the DS. Validity (or limitation) of the strategy can be assessed by using eq. (3.14) as will be shown later.

3.3 Computational Details

All calculations in this chapter were carried out using CASSCF method implemented in GAUSSIAN 98[30] with the correlation-consistent polarized valence double-zeta (cc-pVDZ) basis set. An active space of six electrons in six orbitals was used, corresponding to π orbitals. CASSCF were carried out using S_1/S_0 state-averaged orbital, with the two states weighted equally.

To characterize S_1/S_0 DS, we carried out two-step optimizations described in the previous section. In the first step, we used eq. (3.4) as gradient until the square root of eq .(3.14) becomes sufficiently small as will be shown in the next section. In the second step, we used only the second term in eq. (3.4).

Starting from C_{2v} planar structures, the S_1/S_0 DS was scanned in C_2 symmetry along the exocyclic methylene twist motion with a step size of 5° up to C_{2v} twisted structures.

Our calculation is not definitive because the CASSCF does not take into account of effects of dynamical electronic correlation. However, the behavior we have predicted in this chapter would not be affected qualitatively by it.

3.4 Results and Discussion

The atomic numbering is shown in Fig. 3.1. Hereafter, θ denotes the twist angle of the exocyclic methylene. In Fig. 3.2, we show the example of the two-step procedure locating DP at $\theta = 45°$.

In eq. (3.14), we have shown that the variables, $\boldsymbol{v}_M$, that have overlap with both the intersection adapted coordinate and the branching plane, are dependent on the constrained variables that also have overlap with these two spaces. From eq. (3.14), the square root of the gradient for $\boldsymbol{v}_M$ in the intersection adapted coordinate is given by

$$\sqrt{\sum_i {c_{M,i}}^2 \Big(\frac{\partial E_1}{\partial v_{M,i}}\Big)^2} = \sqrt{2(E_1 - E_0) \sum_j c_{S,j} c_{\acute{S},j} \Big(\frac{\partial E_1}{\partial v_{S,j}}\Big)^2}\,. \tag{3.15}$$

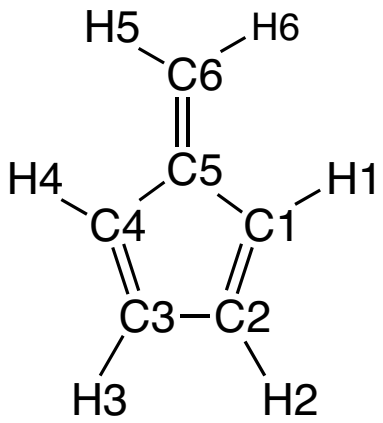

Figure 3.1: Atom numbering using throughout this chapter.

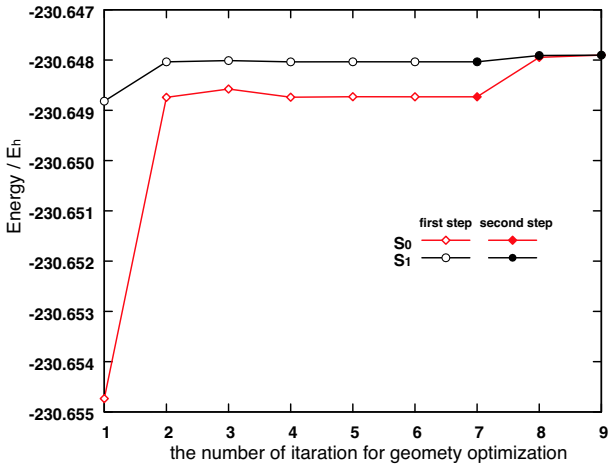

Figure 3.2: Example of the two-step procedure in locating DP at $\theta = 45°$. Starting structure was produced by replacing the value of θ of the DP at $\theta = 40°$ by $45°$. Open symbols (diamond and circle) indicate the first step iteration. Filled symbols (diamond and circle) indicate the second step iteration. At the iteration number 6, the first step (using the default gradient $\mathbf{g}^{\mathrm{CIO}}$ (eq. 3.4)) completed whereas the second step (using the second term of $\mathbf{g}^{\mathrm{CIO}}$ (eq. 3.4)) started from the iteration number 7.

According to eq. (3.15), how geometries are well optimized in intersection adopted coordinate depends on the magnitude of $E_1 - E_0$ and the gradient with respect to constrained variables ($\partial E_1/\partial \boldsymbol{v}_S$) in the first step [using the default gradient, eq. (3.4)]. The value of ($\partial E_1/\partial v_{S,j}$) can roughly be estimated by $C_{S,j}$ in eq. (3.12c). As $C_{S,j}$ includes the normalization factor of the GD, the values of $C_{S,j}$ is larger than ($\partial E_1/\partial v_{S,j}$). In the system we targeted, only one variable, θ, is constrained. It is known that mutual transformation between forces represented by Cartesian coordinates and by non-redundant internal coordinates is possible.[31] Furthermore, the physically significant set can be written by the linear combination of $\boldsymbol{e}_i$. Therefore, the right hand side of eq. (3.15) can be written by using θ.

$$\begin{aligned}\sqrt{\sum_i {c_{M,i}}^2 \Big(\frac{\partial E_1}{\partial v_{M,i}}\Big)^2} &= \sqrt{2(E_1 - E_0) c_{S,\theta} c_{S,\theta}^{\acute{}}}\, \Big|\frac{\partial E_1}{\partial v_{S,\theta}}\Big| \\ &\leq \sqrt{2(E_1 - E_0) c_{S,\theta} c_{S,\theta}^{\acute{}}}\, C_{S,\theta}\ . \end{aligned} \tag{3.16}$$

The values of the $\sqrt{(E_1 - E_0)}$, which is the square root of the difference between energies of the S_1 and S_0 and $C_{S,\theta}$ that is the value of eq. (3.4) as the gradient along θ, are given in Table 3.1. Furthermore, the upper bound of $\sqrt{c_{S,\theta} c_{S,\theta}^{\acute{}}}$ can also be estimated by the inequality between arithmetic and geometric means, i.e., $\sqrt{c_{S,\theta} c_{S,\theta}^{\acute{}}} \leq 0.5$. The degree of optimization in the variables which overlap with both intersection adapted coordinate and the branching plane can therefore be estimated as $0.5\sqrt{2(E_1 - E_0)} C_{S,\theta}$ approximately. From Table 3.1, the gradient of E_1 with respect to the variables which correspond to $\boldsymbol{v}_m$ is approximately 0.0004 (in E_h $\mathrm{\AA}^{-1}$). From our experience, this magnitude is small enough to reoptimize from each point obtained in the first step to locate the S_1/S_0 DP using the second term of eq. (3.4). We show the root mean square (RMS in Cartesian coordinate) of projected gradient on E_1 [the first term in eq.3.4] whose component of exocyclic methylene rotation is given in Table 3.1. According to the values of RMS of Table 3.1, the geometry of the finally obtained DP is optimized within 1.5×10^{-3} E_h $\mathrm{\AA}^{-1}$ at least. These RMS values indicates the structures at DPs obtained by the two step procedure is loosely optimized. There is one more important condition for validity of the two-step procedure. The tendency of change of the value of the RMS indicates a similar change of the value of (3.16) along θ. This means the final geometry may be in the same intersection adapted coordinate of the geometry which is obtained in

the first step. From our experiences, if the tendency of the change of the final RMS is different from that of eq. (3.16), resultant DS would not be meaningful. In Fig. 3.2, we show the example of the two-step procedure locating DP at $\theta = 45°$.

Table 3.1: The values of the difference $(E_1 - E_0)$ (in E_h) and the gradient, eq. (3.4) to θ, and $0.5\sqrt{2(E_1 - E_0)}|C_{S,\theta}|$ (in E_h Å^{-1}) along θ in the first step. The RMS values of the projected gradient which is obtained after the second step is also listed.

θ(degree)	$(E_1 - E_0)$	$C_{S,\theta}$	$0.5\sqrt{2(E_1 - E_0)}\|C_{S,\theta}\|$	RMS
0	0.00000	0.00000	0.00000	0.00000
5	0.00002	−0.01530	0.00005	0.00030
10	0.00008	−0.00890	0.00005	0.00058
15	0.00016	−0.01294	0.00012	0.00085
20	0.00028	−0.01647	0.00019	0.00108
25	0.00041	−0.01928	0.00028	0.00127
30	0.00053	−0.02115	0.00035	0.00140
35	0.00064	−0.02185	0.00039	0.00145
40	0.00070	−0.02119	0.00040	0.00141
45	0.00070	−0.01902	0.00036	0.00127
50	0.00061	−0.01530	0.00027	0.00102
55	0.00042	−0.01018	0.00015	0.00068
60	0.00017	−0.00405	0.00004	0.00027
63.1	0.00000	0.00000	0.00000	0.00000
65	0.00010	0.00235	0.00002	0.00016
70	0.00031	0.00791	0.00010	0.00053
75	0.00038	0.01125	0.00016	0.00074
80	0.00028	0.01103	0.00013	0.00072
85	0.00009	0.00686	0.00005	0.00044
90	0.00000	0.00000	0.00000	0.00000

Now, it is in order to see some details of the characterized DS. The S_1/S_0 DS characterized S_1/S_0 using the above strategy is shown in Fig. 3.3. A recent second order derivative calculation in the S_1/S_0 DS[24] has revealed that DP_{planar} and DP_{perp}

are second- and first-order saddle point, and DP_{63} is almost the global minium on S_1 excited state and S_1/S_0 DS though its energy is slightly lowered by pyramidalization.[32] Our result is favorably compared with the these second derivative calculation. The energies of the two states agreed within 10^{-5} E_h for all the DPs located. Starting from DP_{planar}, we have characterized the S_1/S_0 DS along θ up to DP_{perp}. This result also tells us that θ is the variable which has overlap with both the intersection adapted coordinate and the branching plane. Unless so, the first step optimization should converge to DP.

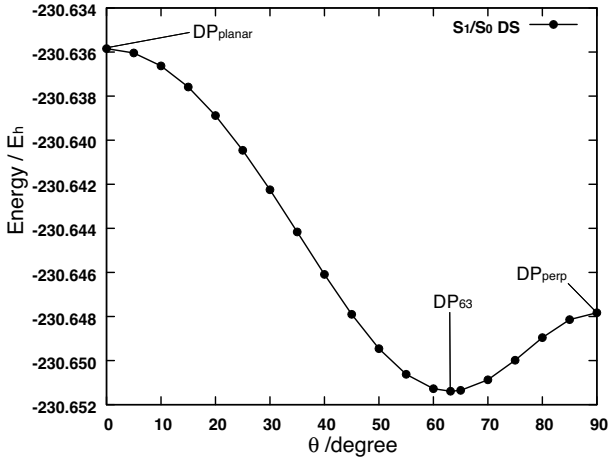

Figure 3.3: The result of the S_1/S_0 DS along θ

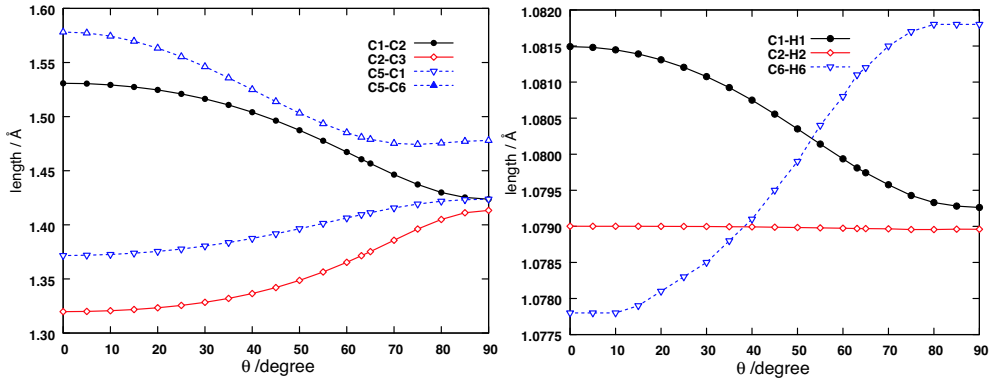

Figure 3.4: Geometric change along S_1/S_0 DS. (a) carbon-carbon bond lengths, (b) carbon-hydrogen bond lengths

The origin of degeneracy of DP_{planar} and DP_{perp} is different. In DP_{planar}, the degeneracy occurs by elongating the exocyclic double bond and enhanced allylic character. On the other hand, in DP_{perp},[22] the degeneracy stems from the D_1/D_0 symmetry required conical intersection of cyclopentadienyl radical:[33,34] The bonds that compose the five-membered ring become more similar to each other. Indeed, the bond lengths of C1–C2, C5–C1, and C2–C3 become about 1.4 Å equally. In spite of the different origin of the DP, Fig. 3.4 shows that the electronic structure is continuously changed from DP_{planar} to DP_{perp}. This demonstrates that DP_{planar} and DP_{perp} are in the common DS.

The behavior of the exocyclic double bond C5–C6 is very interesting. We expected that the tendency of the geometric change of C5–C6 is changed in the vicinity of DP_{63} corresponding to the global minimum on S_1 state. However, around DP_{63} (i.e., around $\theta = 60°$), there are no particular changes. This implies that the electronic structure is not changed around DP_{63}. Instead, the tendency of the geometric change of C5–C6 is changed around DP_{75}. Hence, we can imagine that the DPs between $\theta = 0°$ and $\theta = 75°$ will be photochemically discriminated from the DPs between $\theta = 80°$ and $\theta = 90°$. To clarify the final product via S_1 state, we have performed S_0 geometry optimizations using state-averaged orbital from structures near DP_{63}, DP_{75} and DP_{80}. Starting structures were generated by distorting the DP geometries in direction of GD. These results indicate that the product whose exocyclic methylene is rotated by 180° is available from DP_{80}, but not from DP_{63} and DP_{75}. Therefore, if S_1 excited fulvene can reach the DPs between $\theta = 80°$ and $\theta = 90°$, the exocyclic methylene rotation by 180° is possible. If DPs in this area are stabilized by the proper substitution so that the S_1 excited fulvene can reach this area, cis–trans photoisomerization will become possible. In dibenzofulvene system whose E-Z photoisomerization is observed recently,[25] adding the benzene to fulvene may give rise to the stabilization of the DPs between $\theta = 80°$ and $\theta = 90°$.

3.5 Summary

We have shown that the cancellation error is due to the constraining the variables that has components in both the branching plane and the intersection adapted coordinate. Accordingly, the valid condition for two-step procedure is limited. Taking

into account of the limitation, we have characterized the S_1/S_0 DS along the exocyclic methylene rotation coordinate of fulvene within 1.5×10^{-3} E_h Å^{-1} in energy at worst.

Our calculation we have shown in this chapter is limited to C_2 symmetry. Though systems which have no symmetry like Ref. 25 should be explored, the following conclusion would be worthy to be noted. The photophysical/photochemical behavior changes in the continuous DS. The DPs where the photochemical property changes are not the saddle point on the S_1/S_0 DS within C_2 symmetry. That is, the product obtained via S_1/S_0 DPs in the vicinity of DP_{63} does not change. It is difficult for the exocyclic methylene to rotate by 180°, when S_1 excited fulvene transits to S_0 via DPs between DP_{planar} and DP_{75}. However, in DPs between DP_{80} and DP_{perp}, the exocyclic methylene rotation is expected. Therefore, photochemically, $DP_{80-perp}$ may be discriminated from $DP_{planar-75}$.

References

[1] F. Bernardi, M. Olvucci, M. A. Robb, *Chem Soc. Rev.* **25**, 321(1996).

[2] A. Migani, M. Olivucci, Conical Intersection and Organic Reaction mechanisms. In *Conical Intersections: Electronic Structure, Dynamics and Spectroscopy*, Advance Series in Physical Chemistry, Vol. 15; W. Comcke, D. R. Yarkony, H. Köppel, Eds.; World Scientific: Singapore, 2004; p 271-320.

[3] M. R. Manaa, D. R. Yarkony, *J. Am. Chem. Soc.* **116**, 11444 (1994).

[4] M. J. Bearpark, M. A. Robb, H. B. Schlegel, *Chem. Phys. Lett.* **223**, 269 (1994).

[5] I. J. Palmer, I. N. Ragazos, F. Bernardi, M. Olivucci, M. A. Robb, *J. Am. Chem. Soc.* **115**, 673 (1993).

[6] A. Venturini, T. Vreven, F. Bernardi, M. Olivucci, M. A. Robb, *Organometallics*, **14**, 4953(1995).

[7] A. Migani, M. A. Robb, M. Olivucci, *J. Am. Chem. Soc.* **125**, 2804(2003).

[8] D. R. Yarkony, *J. Phys. Chem. A*, **108**, 3200(2004).

[9] O. Takahashi, M. Sumita, *J. Chem. Phys.* **121**, 7030(2004).

[10] O. Takahashi, M. Sumita, *J. Mol. Struct.:Theochem*, **731**, 173(2005).

[11] S. Yamazaki, S. Kato, *J. Chem Phys.* **123**, 114510 (2005).

[12] M. J. Bearpark, L. Blancafort, M. J. Paterson, *Mol. Phys.* **104**, 1033(2006).

[13] See the next Chapter.

[14] K. Shindo, S. Lipsky, *J. Chem. Phys.* **45**, 2292(1996).

[15] J. K. Foote, M. H. Mallon Jr. J. N. Pitts, *J. Am. Chem. Soc.* **88**, 3698(1966).

[16] K. E. Wilzbach, A. L. Harkness, L. Kaplan, *J. Am. Chem. Soc.* **90**, 1116(1968).

[17] L. Kaplan, K. E. Wilzbach, *J. Am. Chem. Soc.* **90**, 3291 (1968).

[18] J. E. Kent, P. J. Harman, M. F. O'Dwyer, *J. Phys. Chem.* **85**, 2726(1981).

[19] P. J. Harman, J. E. Kent, M. F. O'Dwyer, M. H. Smith, *Aust. J. Chem.* **32**, 2579(1979).

[20] P. J. Domaille, J. E. Kent, M. F. O'Dwyer, *Chem. Phys.* **6**, 66(1974).

[21] R. D. Brown, P. J. Domaille, J. E. Kent, *Aust. J. Chem.* **23**, 1707(1970).

[22] M. J. Bearpark, F. Bernardi, M. Olivucci, M. A. Robb, B. R. Smith, *J. Am. Chem. Soc.* **118**, 5254(1996).

[23] J. Dreyer, M. Klessinger, *J. Chem. Phys.* **101**, 10655(1994).

[24] M. J. Paterson, M. J. Bearpark, M. A. Robb, L. Blancafort, *J. Chem. Phys.* **121**, 11562(2004).

[25] J. W. Barr, T. W. Bell, V. J. Catalano, J. I. Cline, D. J. Phillips, and R. Procupez, *J. Phys. Chem. A*, **109**, 11650(2005).

[26] O. Deeb, S. Cogan, S. Zilberg, *Chem. Phys.* **325**, 251(2006).

[27] D. R. Yarkony, Conical Intersection and Organic Reaction mechanisms. In *Conical Intersections: Electronic Structure, Dynamics and Spectroscopy*, Advance Series in Physical Chemistry, Vol. 15; W. Comcke, D. R. Yarkony, H. Köppel, Eds.; World Scientific: Singapore, 2004; p 41-127.

[28] M. Dallos, H. Lischka, R. Shepard, D. R. Yarkony, P. G. Szalay, *J. Chem. Phys.* **120**, 7330(2004).

[29] D. -H. Lu, M. Zhao, D. G. Truhlar, *J. Comp. Chem.* **12**, 376(1991).

[30] M. J. Frisch, G. W. Trucks, H. B. Schlegel, G. E. Scuseria, M. A. Robb, J. R. Cheeseman, V. G. Zakrzewski, J. A. Montgomery, Jr., R. E. Stratmann,

J. C. Burant, S. Dapprich, J. M. Millam, A. D. Daniels, K. N. Kudin, M. C. Strain, O. Farkas, J. Tomasi, V. Barone, M. Cossi, R. Cammi, B. Mennucci, C. Pomelli, C. Adamo, S. Clifford, J. Ochterski, G. A. Petersson, P. Y. Ayala, Q. Cui, K. Morokuma, N. Rega, P. Salvador, J. J. Dannenberg, D. K. Malick, A. D. Rabuck, K. Raghavachari, J. B. Foresman, J. Cioslowski, J. V. Ortiz, A. G. Baboul, B. B. Stefanov, G. Liu, A. Liashenko, P. Piskorz, I. Komaromi, R. Gomperts, R. L. Martin, D. J. Fox, T. Keith, M. A. Al-Laham, C. Y. Peng, A. Nanayakkara, M. Challacombe, P. M. W. Gill, B. Johnson, W. Chen, M. W. Wong, J. L. Andres, C. Gonzalez, M. Head-Gordon, E. S. Replogle, and J. A. Pople, Gaussian 98 (Revision A.11.3); Gaussian, Inc.: Pittsburgh, PA, 1998.

[31] H. B. Schlegel, *Theor. Chim. Acta*, **66**, 333(1984).

[32] F. Sicilia, M. J. Bearpark, L. Blancafort, M. A. Robb, *Theor. Chem. Acc.* **118**, 241(2007).

[33] W. T. Borden, E. R. Davidson, *J. Am. Chem. Soc.* **101**, 3771(1979).

[34] L. Yu, D. W. Cullin, J. M. Williamson, T. A. Miller, *J. Chem. Phys.* **98**, 2682(1993).

Chapter 4

Numerical Example and Application

In this chapter, two examples will be shown. Both are the photoisomerization around a carbon-carbon double bond. One is the maleic acid and fumaric acid anion radical which exhibits one-way photoisomerization. We show that the origin of "one-way" is due to the ground state not to excited state. The other is penta-2,4-dieniminium which is the model molecule of the retinal protonated Schiff base (RPSB). The 11-cis to all-trans photoisomerization of RPSB is extensively studied on its isomerization process. Some model processes, bicycle pedal motion, hula-twist motion, and hydrogen out-of-plane motion etc, are suggested. We focused on hula-twist motion and hydrogen out-of-plane motion.

4.1 Maleic Acid and Fumaric Acid Anion Radical

4.1.1 Introduction

In recent years, theoretical chemistry has shown the ubiquitous existence of conical intersections (real crossings between the same spin multiplicity states) where the radiationless decay of electronically excited state occurs.[1] The conical intersection provides an efficient decay from the excited state to the ground state in a barrierless, ultrafast manner. Many ultrafast photochemical and photophysical phenomena have been understood by considering the existence of conical intersections. However, the

role of conical intersection is not limited to these ultrafast processes. The decay via conical intersection produces vibrationally hot molecules in the ground state.[1,2] In other words, conical intersection plays a role to transform photoenergy to vibrational energy. This vibrational energy can contribute to thermal reaction in ground states. The reachable conical intersection that is close to the Franck-Condon (FC) energy may consequently enhance the "thermal" reaction.

A degeneracy point (DP), which is an apex of conical intersection, is not an isolated point on the n-dimensional potential energy surface (n is the number of vibrational degrees of freedom of the molecule). DPs make a $(n-2)$-dimensional space called a conical intersection hyperline or seam.,[3,4] Methods have been developed to compute structures of the lowest energy DP (LEDP) in the degeneracy space (DS).[5–7] The LEDP on the DS has often been interpreted as a photochemical funnel. However, recent calculations demonstrate that excited molecules can reach a DS before reaching a LEDP.[8] Furthermore, available product via excited state depends on where the excited molecules transit to the ground state in the DS.[9] This suggests the importance of exploring the DS, which has the possibility to expand the variety of photochemistry and its processes. We also have succeeded in exploring one-dimensional section of the DS in some systems that lies at lower energy than the FC one and may be involved in photochemistry.[10,11]

Involvement of conical intersection in cis $\leftrightarrow$ trans photoisomerization of some molecules has been pointed out.[12] The influence of the DS for this type of photochemistry has, however, not been fully clarified yet. Torikai et al.[13] detected the cis $\leftrightarrow$ trans photoisomerization for dimethyl maleate (DMM) and dimethyl fumarate (DMF), and their anion radicals. The photoisomerization process of such neutral species is believed to involve a conical intersection similar to that in ethylene.[12] The conical intersection in ethylene is very complicated because decoupling of only two electrons causes an avoided crossing between the ground state (S_0) and first excited state (S_1). To reach a S_1/S_0 conical intersection, two more electrons must be decoupled.[12]

Although cis $\leftrightarrow$ trans photoisomerization in radical species is understood more easily than neutral species from a theoretical viewpoint, experimental results on radical species are rare. The photochemistry of maleate anion radicals and fumarate anion radicals and their ester systems is such a rare example. It has been studied

in 2-methyltetrahydrofuran (MTHF)[13] and in aqueous solutions.[14] The experiment in MTHF was mainly reported on dimethyl maleate anion radical ($DMM^{-\bullet}$). When $DMM^{-\bullet}$, which is produced by γ-lay irradiation absorption in MTHF at 77 K, is illuminated with UV light, the isomerization occurs. Namely, after excitation of $DMM^{-\bullet}$ with 345 nm lights, the absorption band shifts to 335 nm. This new absorption indicates the formation of the dimethyl fumarate anion radical ($DMF^{-\bullet}$). On the other hand, the absorption band of $DMF^{-\bullet}$ does not change before and after illumination. These observations show that the isomerization occurs only in the direction of the cis → trans. The same (cis → trans) selectivity was also observed in the isomerization reaction of other radical anions such as stilbene anion radical.[15] It is noteworthy that a similar cis → trans one-way isomerization was reported for the $DMM^{-\bullet}/DMM^{-\bullet}$ system even without UV light illumination at room temperature.[16,17]

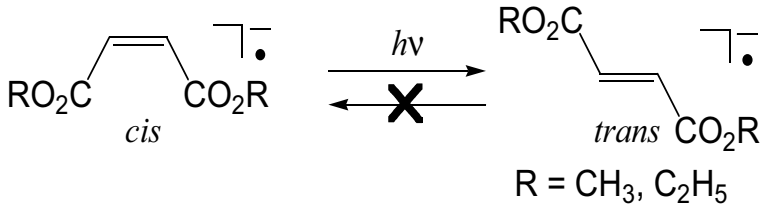

In this work, we have studied the reaction, $MA^{-\bullet} \rightarrow FA^{-\bullet}$ (cis → trans), as a model system of the one-way photoisomerization $DMM^{-\bullet} \rightarrow DMF^{-\bullet}$ by the complete active space self-consisted field (CASSCF) method[18] to elucidate the mechanism of the photoisomerizations.

A few comments are now in order on the potential energy surfaces of the $MA^{-\bullet}/FA^{-\bullet}$ system. The potential energy surfaces of ethylene anion and cation radicals[19] have a symmetry-required conical intersection[3,20] (Jahn-Teller effect) between the ground doublet state (D_0) and the lowest excited state (D_1) at D_{2d} symmetry (90° twist) because both the D_1 and D_0 states belong to degenerate representation (^2E) as shown in Subsec. 2.4.1. Because symmetry-required conical intersections simply change into symmetry-allowed conical intersections[3,20] along appropriate geometrical distortion or substitution, it is naturally expected that olefin ion radicals undergo photochemical double-bond rotation through the corresponding conical intersection near 90° twist. Indeed, as described in this paper, for the case of the model $MA^{-\bullet}/FA^{-\bullet}$

system, the lowest point on the D_1 surface coincides with the D_1/D_0 LEDP at approximately 90° twist. However, this does not explain the one-way character of the $MA^{-\bullet} \rightarrow MF^{-\bullet}$ photoisomerization. The purpose of this work is to elucidate the factor that brings one-way photoisomerization and the influence of the DS. Using the strategy in the previous chapter, we investigated the D_1/D_0 DS along the central C–C bond twisting for this system.[10] Figure 4.1 shows that D_1/D_0 DS whose geometric change is tabulated in Table 4.1.

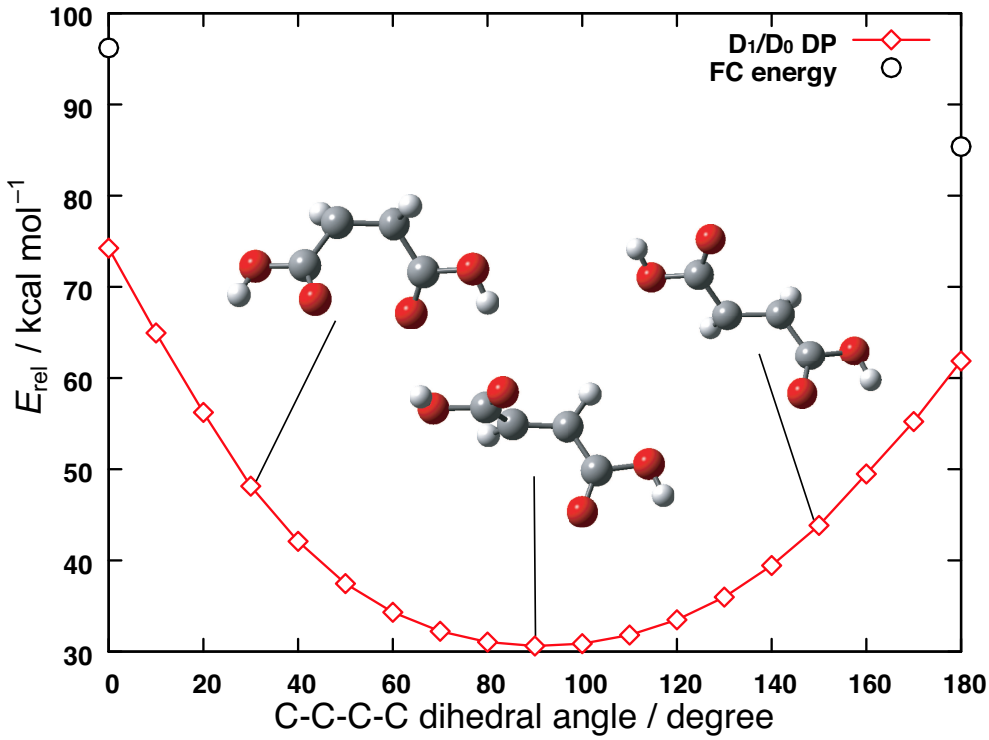

Figure 4.1: One-dimensional D_1/D_0 DS along the central C–C bond twisting, which is characterized by the two step procedure

It had been suggested that the difference in steepness of the D_1/D_0 DS between the cis and trans sides could be responsible for the one-way isomerization. However, exploring the D_1 and D_0 potential energy surfaces (PESs) in detail, we have arrived at a new conclusion. Upon the cis → trans isomerization, two dihedral angles (i.e., C–C–C–C and H–C–C–H) have to change. Although the simultaneous changes of the two dihedral angles are intuitively plausible, separate changes in C–C–C–C and H–C–C–H are also possible. As shown in this paper, we have concluded that large

Table 4.1: Geometrical change along the D_1/D_0 curve in Fig.4.1. See Fig.4.3 about atomic numbering.

C1–C2–C3–C4[a]	H1–C2–C3–H2[a]	C1–C2–C3–H2[a]	Σ[a b]
0	144.3	−107.9	328.6
10	144.7	−102.7	330.9
20	143.4	−98.3	334.6
30	141.1	−94.4	338.7
40	135.9	−92.1	343.9
50	128.9	−90.6	349.1
60	119.5	−90.2	353.9
70	110.4	−89.8	357.2
80	100.5	−89.7	359.3
90	90.5	−89.8	360.0
100	80.7	−89.7	359.4
110	71.6	−89.2	357.5
120	63.5	−88.2	354.5
130	56.5	−86.8	350.6
140	50.3	−84.8	345.7
150	46.5	−81.7	341.0
160	44.5	−77.8	336.4
170	43.1	−73.5	332.0
180	42.0	−69.0	327.2

a) In degrees

b) Sum of the bond angles around C2.

geometrical change on the D_1 potential energy surface is the H–C–C–H dihedral angle distortion whereas the D_0 potential energy surface is responsible for the C–C–C–C dihedral angle rotation. This mechanism is similar to a conclusion in a recent femtosecond-stimulated Raman spectroscopic study of the light-induced 11-cis and all-trans isomerization of retinal in the visual pigment rhodopsin.[21] This report concluded that the decay from the excited state through a conical intersection is largely mediated by fast hydrogen-out-of-plane (HOOP) motion.

4.1.2 Computational Detail

On the neutral species, DMM/DMF and MA/FA, there are some researches about equilibrium structure in ground state through infrared and Raman spectroscopy and theoretical calculation.[22] On anion radical species, however, experimental results are rare. Only a limited method of experiments provides us the information about their equilibrium conformations. The electron spin resonance on $DMM^{-\bullet}$ and $DMF^{-\bullet}$ ruled out the asymmetric conformation with respect to original double bonds.[23] No theoretical studies have been reported concerning the stable conformation of $DMM^{-\bullet}$ and $DMF^{-\bullet}$ in the doublet ground (D_0) state.

First of all, to see the most stable structure of $DMM^{-\bullet}$ and $DMF^{-\bullet}$ in the D_0 state, we carried out the geometry optimization by UB3LYP with the 6-31G* basis set for as many conformations as we can imagine. All calculations in $MA^{-\bullet}$/ $FA^{-\bullet}$ system were performed using GAUSSIAN98.[24] Details of resultant equilibrium geometries are given in Fig. 4.2 and Table 4.2.

All calculated energy and S^2 are summarized in Table 4.2. As shown in the Table 4.2, the resulting S^2 close to 0.75 shows that all calculations by UDFT are reliable. According to these results, the most stable conformations of $DMM^{-\bullet}$ and $DMF^{-\bullet}$ are (g) and (a) respectively. However, ESR experiments[23] ruled out the anti-symmetric conformation with respective to the double bond of $DMM^{-\bullet}$ [(g), (h), (i) and (j)] as mentioned above. Then, we adopted (a) as a model of cis trans photoisomerization. The conformation of $MA^{-\bullet}$/ $FA^{-\bullet}$ as the model molecule is obtained replacing methyl groups by hydrogen atoms.

On the basis of these results, the conformations of $MA^{-\bullet}$/ $FA^{-\bullet}$ shown in Fig. 4.3 are adopted as a model system of $DMM^{-\bullet}$/ $DMF^{-\bullet}$.

The D_0 state and first excited doublet state (D_1;$^1(\pi, \pi^*)$) potential energy sur-

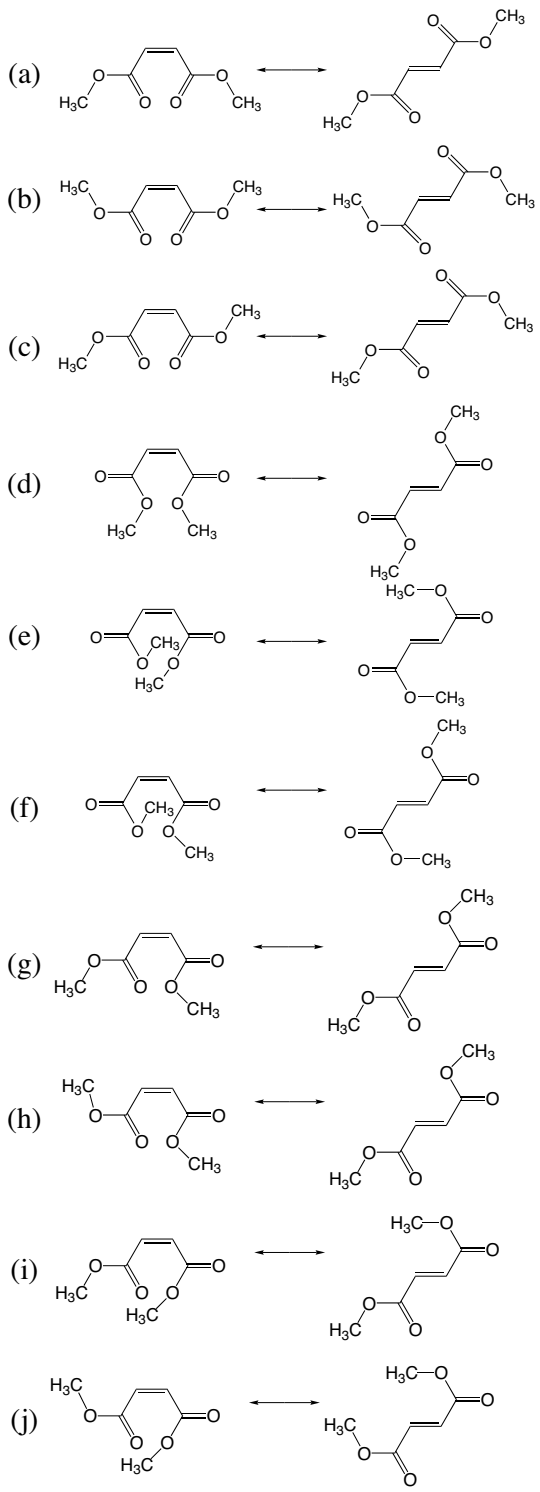

Figure 4.2: Considered conformation of $DMM^{-\bullet}$/ $DMF^{-\bullet}$

faces were computed with the CASSCF method with the cc-pVDZ basis set. To compare energies of stationary points and DPs where the two-root state-averaged orbital is needed (0.5 weights), the energy of the stationary points on the D_1 surface or D_0 surface that were located with the single-state CASSCF were recalculated using the state-averaged orbital. An intuitive choice of active space for describing the D_1 and D_0 states of the investigated system would be eleven electrons in eight π molecular orbitals, which we refer to as CAS(11,8). However, we found that, for the planar D_0 and D_1 states of $MA^{-\bullet}$ and $MF^{-\bullet}$, CAS(11,8) can be truncated to CAS(7,6) because two of the eight π molecular orbitals are almost doubly occupied (> 1.99), corresponding to the OH oxygen lone pairs. Thus, seven electrons in six π molecular orbitals [CAS(7,6)], which corresponds to the π system of the O=C–C=C–C=O moiety, were used as the active space throughout this paper. This active space reduction did not affect to describe the detail of the D_1 and D_0 PESs.

4.1.3 Result and Discussion

The energies of the D_0 and D_1 ($^1(\pi,\pi^*)$) stationary points and the D_1 / D_0 LEDP are listed in Table 4.3, and their geometrical parameters, in Table 4.4. The atomic numbering scheme is shown in Fig. 4.3. The C1–C2–C3–C4 and H1–C2–C3–H2 dihedral angles are denoted by θ_1 and θ_2, respectively. Figure 4.4 shows a schematic representation of the D_0 and D_1 PESs revealed by the present calculations.

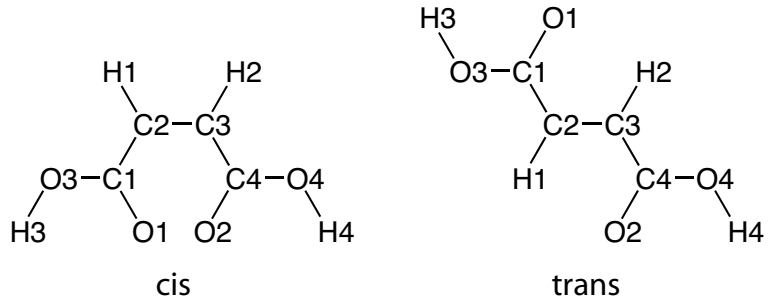

Figure 4.3: Conformation of $MA^{-\bullet}/FA^{-\bullet}$ (with atomic numbering) as a model system of $DMM^{-\bullet}/DMF^{-\bullet}$

Table 4.2: Energy (in atomic unit) and the value of S^2 obtained by UDFT/B3LYP/6-31G*

	cis		trans	
species	symmetry	$E(S^2)$	symmetry	$E(S^2)$
(a)	C_{2v}	−534.35122(0.753)	C_{2h}	−534.36793(0.753)
(b)	C_2	−534.33125(0.754)	C_{2h}	−534.35277(0.754)
(c)	C_1	−534.34107(0.754)	C_s	−534.36026(0.753)
(d)	C_2	−534.35109(0.754)	C_{2h}	−534.36644(0.754)
(e)	C_2	−534.33405(0.756)	C_{2h}	−534.36647(0.754)
(f)	C_1	−534.34251(0.755)	C_s	−534.36646(0.754)
(g)	C_s	−534.35197(0.754)	C_s	−534.36718(0.753)
(h)	C_1	−534.34229(0.754)	C_s	−534.35914(0.754)
(i)	C_1	−534.34327(0.755)	C_1	−534.36718(0.753)
(j)	C_1	−534.33349(0.755)	C_1	−534.35913(0.754)

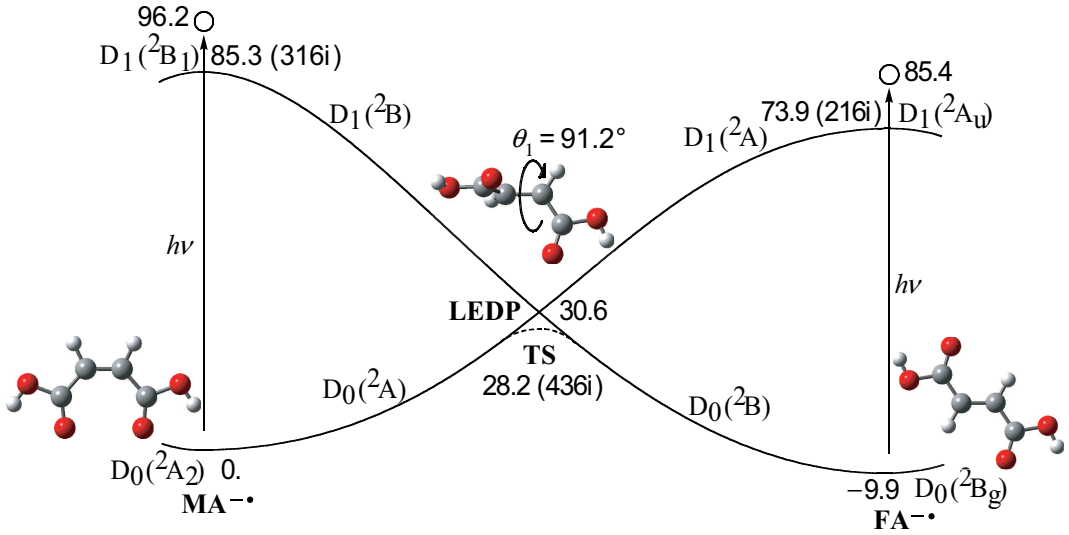

Figure 4.4: Schematic representation of the D_0 and D_1 potential energy surfaces for the $MA^{-\bullet}/FA^{-\bullet}$ system with energies in kcal mol^{-1}. Open circles indicate Franck-Condon points. The imaginary frequencies are given in parentheses (in cm^{-1}).

Table 4.3: CASSCF/cc-pVDZ Energies for the D_0 and D_1 Stationary Points and LEDP

species	symmetry	state	E^{a}	${E_0}^{b}$	${E_1}^{c}$	${E_{rel}}^{d}$
$MA^{-\bullet}$	C_{2v}	$D_0(^2A_2)$	−453.34113	−453.33869	−453.18538	0
$FA^{-\bullet}$	C_{2h}	$D_0(^2B_g)$	−453.35691	−453.35450	−453.20262	−9.9
$MA^{-\bullet}$	C_{2v}	$D_1(^2B_1)$	−453.20480	−453.32230	−453.20282	85.2
$FA^{-\bullet}$	C_{2h}	$D_1(^2A_u)$	−453.22292	−453.33702	−453.22087	73.9
LEDP	C_2	$D_1/D_0(^2A/^2B)$		−453.28991	−453.28991	30.5
TS	C_1	$D_0(^2A)$	−453.3116	−453.2938	−453.2773	28.2

a) Single-state energy in au.

b) State-averaged energy (au) of the D_0 state.

c) State-averaged energy (au) of the D_1 state.

d) Relative energy with respect to $MA^{-\bullet}$ in kcal mol^{-1}.

D_0 and D_1 Stationary Points and LEDP

We optimized the D_0 geometries of $MA^{-\bullet}$ and $FA^{-\bullet}$ within C_{2v} and C_{2h} symmetries, respectively. Their stability was confirmed by vibrational analysis. The D_0 states of these geometries are dominated by a single configuration, which is $(3b_1)^2(3a_2)^1$ for $MA^{-\bullet}$ (94.8 %) and $(3a_u)^2(3b_g)^1$ for $FA^{-\bullet}$ (95.3 %). The central C–C bond (C2–C3) is slightly longer in $MA^{-\bullet}$ (1.410 Å) than in $FA^{-\bullet}$ (1.403 Å). The very large C1–C2–C3 and C2–C3–C4 bond angles of $MA^{-\bullet}$ (131.6°) are ascribed to the repulsion between carbonyl oxygen lone pairs.

Before seeing the excited state of $MA^{-\bullet}$ and $FA^{-\bullet}$ through CAS(7,6), we have checked the relative ordering of states by single-point time-dependent DFT (TDDFT) using B3LYP on the optimized CAS(7,6)/cc-pVDZ D_0 minimum structure of $MA^{-\bullet}$ and $FA^{-\bullet}$. From the TDDFT/cc-pVDZ result in $MA^{-\bullet}$, the first valence excited state of $MA^{-\bullet}$ is not the $^1(\pi,\pi^*)$ (corresponding to $3b_1 \rightarrow 3a_2$) but $^1(n,\pi^*)$ ($12b_2 \rightarrow 3a_2$). These energies of $^1(n,\pi^*)$ and $^1(\pi,\pi^*)$ from the D_0 state were computed to be 361 and 339 nm, in terms of wavelength, respectively (energy difference between them is only 3.4 kcal mol^{-1}). By slight distortion of θ_1 or θ_2, the state corresponding to $^1(\pi,\pi^*)$ excitation becomes the first excited state (D_1). The intersection between $^1(\pi,\pi^*)$ and $^1(n,\pi^*)$ is thus expected at small values of θ_1 and θ_2, though it was not located in this work. On the other hand, the first valence excited state of $FA^{-\bullet}$ is $^1(\pi,\pi^*)$ (corresponding to $3a_u \rightarrow 3b_g$) whose transition energy is computed to be 341 nm from the D_0 state. On the other hand, according to the result of TDDFT/aug-cc-pVDZ, the first valence excited state became $^1(\pi,\pi^*)$ in both $MA^{-\bullet}$ and $FA^{-\bullet}$. These suggest that the $^1(\pi,\pi^*)$ is relevant to the photochemistry of this system.

Four low-lying Rydberg states were also exhibited between D_0 state and the first valence excited state in TDDFT/aug-cc-pVDZ. The energies of transition to the four low-lying Rydberg states are computed to be in the region 772-489 nm for both $MA^{-\bullet}$ and $FA^{-\bullet}$. The UV spectrum in MTHF and aqueous solution[13,14] does not exhibit distinct peaks or shoulders in the region 500-300 nm except for 400 (shoulder) nm, 350 nm (peak), and 335 nm (peak), which would be ascribed to $^1(n,\pi^*)$, $^1(\pi,\pi^*)$ of $MA^{-\bullet}$, and $^1(\pi,\pi^*)$ of $FA^{-\bullet}$, respectively. In the model $MA^{-\bullet}/FA^{-\bullet}$ system, therefore, we ignored the effect by these Rydberg states and considered valence excited-state only.

Going back to the result of CAS(7,6), the vertical (Franck-Condon; FC) D_1

states are also dominated by a single configuration, which is $(3b_1)^1(3a_2)^2$ (89.4%) for $MA^{-\bullet}$ and $(3a_u)^1(3b_g)^2$ for $FA^{-\bullet}$ (90.9%), corresponding to the single excitation from the highest doubly occupied molecular orbital to the singly occupied molecular orbital (SOMO). The vertical excitation energies of $MA^{-\bullet}$ and $FA^{-\bullet}$ were calculated to be 96.2 and 95.3 kcal mol^{-1}, respectively (state-averaged calculation). These are overestimated compared to the experimental values in aqueous solution (82.2 and 86.6 kcal mol^{-1}, respectively[14]). This is anticipated because the CASSCF method is known to emphasize the character of the originally unoccupied orbitals.[25] The lack of dynamic electron correlation (especially $\sigma - \pi$ correlation in the present case) in the CASSCF calculation can also be responsible for this discrepancy. The blue shift on going from $MA^{-\bullet}$ to $FA^{-\bullet}$ was not reproduced by the present calculation, too. However, these discrepancies do not alter our conclusion on the cause of the $MA^{-\bullet}$ $\rightarrow$ $FA^{-\bullet}$ one-way isomerization.

The antibonding orbital between the two central carbons, C2 and C3, is doubly occupied and is the main configuration in the D_1 FC state. This means the effect of the antibonding character is strong on the D_1 PES. Indeed, the D_1 PES already has a negative curvature at the FC geometries in the direction of the rotation around the C2–C3 bond. This is in contrast to the case of the lowest excited singlet (S_1) state of retinal protonated Schiff base (RPSB) models,[26] where the negative curvature for double-bond rotation is encountered only after bond-length relaxation. In the case of $MA^{-\bullet}$ and $FA^{-\bullet}$, if there is no constraint, the rotation around the C2–C3 bond would start just after the excitation to the D_1 state.

The D_1 geometry optimizations in C_{2v} and C_{2h} symmetries resulted in elongation of the C2–C3 bond (Table 4.4). The optimized D_1 geometries of $MA^{-\bullet}$ and $FA^{-\bullet}$ are lower in energy than the corresponding FC geometries by 10.9 and 11.5 kcal mol^{-1}, respectively. Although free molecules does not pass these optimized D_1 geometries, the property of these optimized D_1 geometries will be reflected in the dynamics of excited molecules in the limited space as in MTHF glass.

Vibrational analyses showed that both the optimized planar D_1 geometries also have an imaginary frequency (316i cm^{-1} for $MA^{-\bullet}$ and 216i cm^{-1} for $FA^{-\bullet}$) corresponding to the C2–C3 rotation. The eigenvector of these imaginary vibrational frequencies are shown in Fig. 4.5. Both the D_1 states of $MA^{-\bullet}$ ($^2B_1$ in C_{2v}) and $FA^{-\bullet}$ (^2A_u in C_{2h}) are then stabilized by rotation around the C2–C3 bond. This

Table 4.4: Geometrical Parameters of the Optimized Structures

	$MA^{-\bullet}(D_0)$	$FA^{-\bullet}(D_0)$	$MA^{-\bullet}(D_1)$	$MA^{-\bullet}(D_1)$	LEDP	TS
			Bond lengths (Å)			
C2–C3	1.410	1.403	1.544	1.536	1.449	1.466
C1–C2	1.425	1.419	1.386	1.380	1.422	1.385
C3–C4	1.425	1.419	1.386	1.380	1.422	1.462
C1–O1	1.212	1.219	1.240	1.248	1.216	1.232
C4–O2	1.212	1.219	1.240	1.248	1.216	1.202
C1–O3	1.386	1.376	1.397	1.385	1.378	1.389
C4–O4	1.386	1.376	1.397	1.385	1.378	1.365
C2–H1	1.083	1.080	1.082	1.077	1.087	1.083
C3–H2	1.083	1.080	1.082	1.077	1.087	1.091
O3–H3	0.946	0.947	0.946	0.946	0.947	0.946
O4–H4	0.946	0.947	0.946	0.946	0.947	0.947
			Bond angles (°)			
C3–C2–C1	131.6	122.8	131.6	120.8	123.5	120.8
C2–C3–C4	131.6	122.8	131.6	120.8	123.5	124.8
C2–C1–O1	131.9	129.1	130.8	126.6	129.5	130.1
C3–C4–O2	131.9	129.1	130.8	126.6	129.5	128.3
C2–C1–O3	111.4	113.6	113.2	116.5	113.3	114.2
C3–C4–O4	111.4	113.6	113.2	116.5	113.3	112.8
O1–C1–O3	116.8	117.3	116.0	116.9	117.2	115.7
O2–C4–O4	116.8	117.3	116.0	116.9	117.2	118.9
C3–C2–H1	115.4	119.9	113.4	118.6	121.6	119.6
C2–C3–H2	115.4	119.9	113.4	118.6	121.6	123.1
C1–C2–H1	113.0	117.3	115.0	120.6	114.9	119.6
C4–C3–H2	113.0	117.3	115.0	120.6	114.9	112.1
C1–O3–H3	104.1	104.5	103.8	104.3	104.5	103.0
C4–O4–H4	104.1	104.5	103.8	104.3	104.5	105.8
			Dihedral angles (°)			
C1–C2–C3–C4	0.0	180.0	0.0	180.0	91.23	88.274
H1–C2–C3–H2	0.0	180.0	0.0	180.0	89.27	88.64
C3–C2–C1–O1	0.0	0.0	0.0	0.0	0.448	0.775
C2–C3–C4–O2	0.0	0.0	0.0	0.0	0.448	3.941
C3–C2–C1–O3	180.0	180.0	180.0	180.0	179.7	179.4
C2–C3–C4–O4	180.0	180.0	180.0	180.0	179.7	−177.2
C1–C2–C3–H2	180.0	0.0	180.0	0.0	−89.75	−91.18
H1–C2–C3–C4	180.0	0.0	180.0	0.0	−89.75	−91.91
H1–C2–C1–O1	180.0	180.0	180.0	180.0	−178.6	−179.1
H2–C3–C4–O2	180.0	−180.0	180.0	−180.0	−178.6	−176.5
H1–C2–C1–O3	0.0	0.0	0.0	0.0	0.706	−0.448
H2–C3–C4–O4	0.0	0.0	0.0	0.0	0.706	2.305
C2–C1–O3–H3	180.0	180.0	180.0	180.0	179.5	180.0
C3–C4–O4–H4	180.0	−180.0	180.0	−180.0	179.5	179.4
O1–C1–O3–H3	0.0	0.0	0.0	0.0	−1.184	−1.450
O2–C4–O4–H4	0.0	0.0	0.0	0.0	−1.184	−1.705

lowers the molecular symmetry to C_2, in which the D_1 states of $MA^{-\bullet}$ and $FA^{-\bullet}$ become ^2B and ^2A, respectively. As shown in Fig. 4.5, H1–C2–C3–H2 dihedral angle distortion is the most dominant component in the imaginary modes. Namely, the rotation around the C2–C3 bond while H1–C2–C1–C3 (H2–C3–C4–C2) plane is maintained does not occur. Therefore, it is necessary to explore the D_1 PES along not only the C1–C2–C3–C4 dihedral angle (θ_1) but also the H1–C2–C3–H2 dihedral angle (θ_2) under C_2 symmetry. We show the D_1 and D_0 PESs along θ_2 later.

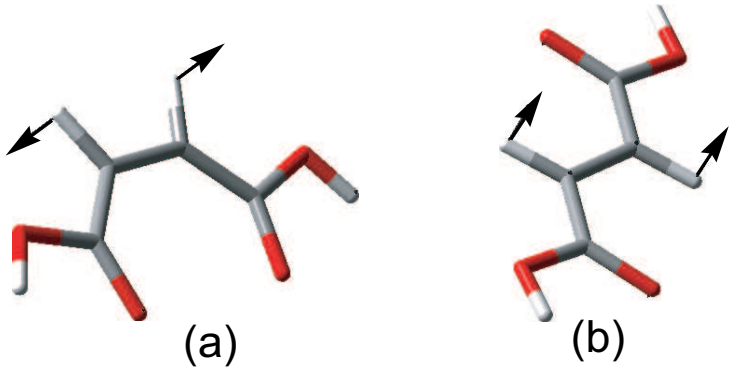

Figure 4.5: Three-dimensional description of vibration modes having imaginary frequencies [(a) 316i cm^{-1} and (b) 216i cm^{-1}] of the planar optimized structures on the D_1 PES.

Geometry optimizations in C_2 symmetry (switching to optimization using state-averaged orbitals and then to DP optimization was necessary) ultimately led to a DP between the D_1 and D_0 (^2B and ^2A) states in which the C2–C3 bond is twisted by ca. 91.2° (Table 4.4 and Fig. 4.4). An optimization in C_1 symmetry resulted in the same DP, which confirms that the DP of C_2 symmetry near the 90° twist is indeed the LEDP (i.e., a true minimum on the D_1/D_0 DS). This perpendicular DP simply originates from the fact that, in C_2 symmetry, the $3b_1$ (bonding) and $3a_2$ (antibonding) orbitals of $MA^{-\bullet}$ exchange with the $3b_g$ (antibonding) and $3a_u$ (bonding) orbitals of $FA^{-\bullet}$, respectively (see Ref. 27 for similar situations in olefin cation radicals). The LEDP is to be the lowest point on the D_1 surface. A similar perpendicular LEDP has been located for penta-2,4-dieniminium (PDI), which is the model molecule of RPSB.[26]

The gradient difference (GD) vector of the present LEDP, which must be to-

tally symmetric, corresponds to the C2–C3 rotation whereas the derivative coupling (DC) vector, which is symmetry-lowering, has an effect of separating the negative charge and the unpaired spins into the two molecular halves. In the direction of the DC vector, we have located the D_0 transition state (TS) of cis-trans adiabatic isomerization with an imaginary frequency of 456i cm^{-1}. Note that there are two TSs on the D_0 surface that are symmetrically located near the LEDP (Fig. 4.6) and have opposite charge-spin separation (i.e., "minus-dot" and "dot-minus"). In the TS geometry shown in Table 4.4, the half containing the C2 atom carries a negative charge of -0.8035 (state-averaged calculation): in the D_1 state at the same geometry, the negative charge is localized in the other half (-0.9497). Thus, in the section along the DC vector, the minus-dot and dot-minus states cross each other at the LEDP of C_2 symmetry where the two halves have equivalent structures. These TSs are 28.2 kcal mol^{-1} higher for the D_0 stable C_{2v} structure of $MA^{-\bullet}$, but 38.1 kcal mol^{-1} higher for the D_0 stable [C_{2h} structure of $FA^{-\bullet}$. This barrier is very low in comparison with the similar perpendicular TSs of PDI, which have been located on the S_0 PES near the S_1/S_0 LEDP [more than 50 kcal mol^{-1} (CASSCF) for both Z- and E-PDI as will be shown in Sec. 4.3]. Then, vibrationally excited $MA^{-\bullet}$ and $FA^{-\bullet}$ on the D_0 PES would be able to reach the transition states. The difference in barrier height of about 10 kcal mol^{-1} between $MA^{-\bullet}$ and $FA^{-\bullet}$ should play an important role after deactivation from the D_1 state. Detailed discussion about this point is in the next section.

From Fig. 4.4, one might expect that $FA^{-\bullet}$ undergoes photoisomerization as well as $MA^{-\bullet}$ does, because the LEDP with a $\theta_1 = 91.2°$ could be equally reached from both the $MA^{-\bullet}$ and $FA^{-\bullet}$ FC regions. However, this is not the case: $DMF^{-\bullet}$ $\rightarrow$ $DMM^{-\bullet}$ photoisomerization has not been observed either in MTHF glass[13] or in aqueous solution.[14] The D_1-state geometry optimization shows that the D_1/D_0 degeneracy begins before approaching $\theta_1 = 91.2°$. When C2–C3 rotation occurs, the θ_2 distortion has to precede the θ_1 distortion because the imaginary frequency of the relaxed structure on the D_1 PES has large components on H1 and H2, as shown in Fig. 4.5.

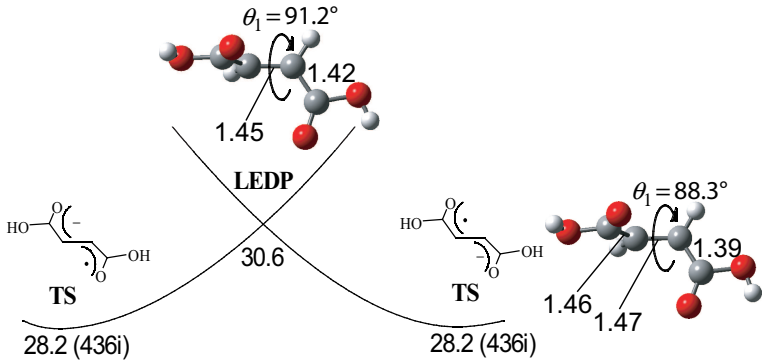

Figure 4.6: Transition states (TSs) of the cis T trans isomerization are symmetrically located near the LEDP with different charge-spin separation (i.e., "minus-dot" and "dot-minus"). Relative energies are given in kcal mol^{-1}. The imaginary frequencies (cm^{-1}) are shown in parentheses.

Two-Dimensional Analysis of D_1-PES

The results of the two-dimensional PES calculation are shown in Fig. 4.7 along θ_1 and θ_2, which we regard as the cis-trans reaction coordinate and the HOOP motion coordinate, respectively. This relaxed scan was performed in C_2 symmetry using the two-root state-averaged orbital while the two dihedral angles were constrained. The ^{2}B state was optimized in the area of $0° \leq \theta_1 \leq 80° \cap 0° \leq \theta_2 \leq 180°$ (as $MA^{-\bullet}$ side in Fig. 4.7a), and the ^{2}A state in the area of $100° \leq \theta \leq 180° \cap 0° \leq \theta \leq 180°$ (as $FA^{-\bullet}$ side in Figure 4.7b). The line where the ^{2}B and ^{2}A PESs intersect corresponds to the D_1/D_0 DS that we have characterized in Fig. 4.1. This intersection lines of Figure 4.7a,b are sequentially connected through the DP at $\theta_1 = 90°$ and $\theta_2 = 90°$ that has also been already located.[10] This D_1/D_0 DS lies well below the Franck-Condon energy.[10] Figure 4.7 shows that even if θ_1 is not distorted by 91.2°, excited $MA^{-\bullet}$ and $MA^{-\bullet}$ can reach the D_1/D_0 DS by θ_2 distortion without barriers. In other words, the deactivation from D_1 to D_0 can be achieved by the θ_2 distortion, i.e., the HOOP motion. This HOOP motion makes it possible for the D_1 excited $MA^{-\bullet}$ and $MA^{-\bullet}$ to transit to D_0 at far points from the LEDP without a large θ_1 distortion. Furthermore, electronic structure becomes its counter isomer upon this deactivation through the HOOP motion though its skeletal structure still remains as the reactant. Besides, the motion along θ_1 and θ_2 does not preserve degeneracy

(as shown in Fig. 4.7). This means that the branching plane, which is spanned by GD and DC vectors along the D_1/D_0 DS, involves these distortion motions (θ_1 and θ_2). Hence, isomerization is easy via this D_1/D_0 DS.

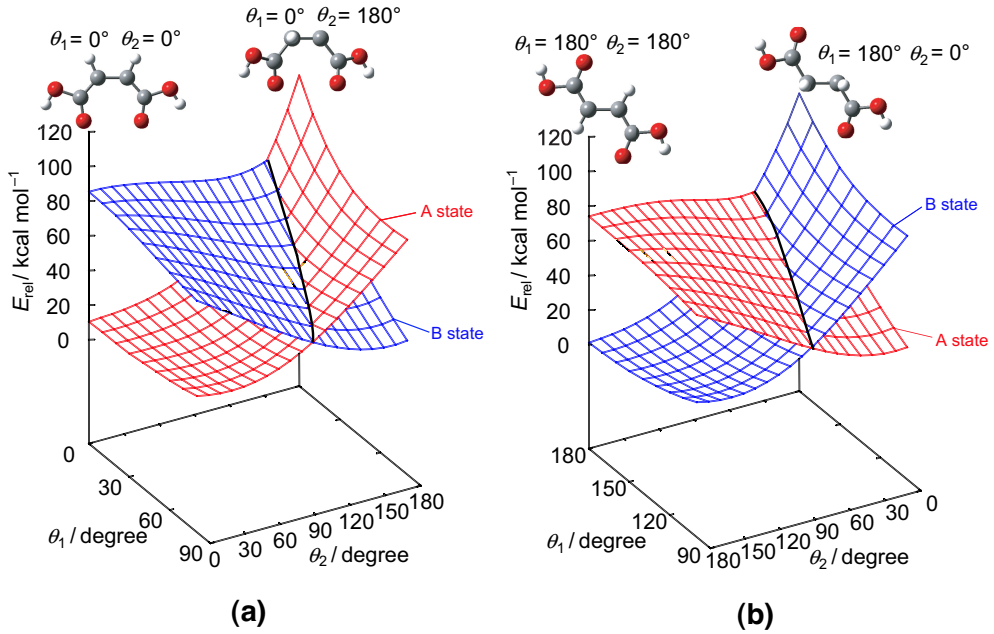

Figure 4.7: ^{2}A and ^{2}B PES scanned along θ_1 and θ_2 within $0° \leq \theta_1 \leq 80° \cap 0° \leq \theta_2 \leq 180°$ (a) (the result of ^{2}B-state optimization) and within $100° \leq \theta_1 \leq 180° \cap 0° \leq \theta_2 \leq 180°$ (b) (^{2}A-state optimization). Two PESs cross along the D_1/D_0 DS which has been already characterized in Ref. 10.

Experimental results[13] show that reactions other than one-way cis $\rightarrow$ trans photoisomerization were not involved. In contrast, the present PES suggests that mutual cis $\leftrightarrow$ trans photoisomerization is possible and that the reverse reaction is not detected experimentally owing to some purely experimental reason(s). The deactivated $MA^{-\bullet}$ and $FA^{-\bullet}$ from the D_1 state via the D_1/D_0 DS, however, would have excess energy, i.e., vibrationally hot. According to the present two-dimensional analysis, the D_1 excited $MA^{-\bullet}$ and $FA^{-\bullet}$ can reach the D_1/D_0 DS at approximately $\theta_1 = 30°$ and $\theta_1 = 170°$, respectively. This is governed by the topography of conical intersection; i.e., the crossing point where sloped conical intersection becomes intermediate conical intersection or peaked conical intersection[28] along the crossing line between ^{2}A and ^{2}B states is regarded as reachable conical intersection. The relative ener-

gies of crossing points at $\theta_1 = 30°$ to the D_0 stable $MA^{-\bullet}$ and at $\theta_1 = 170°$ to the D_0 stable $FA^{-\bullet}$ are 47 and 65 kcal mol^{-1}, respectively. Then, at least, these energies can be used in the D_0 state. After the decay from the D_1 to the D_0 state, $FA^{-\bullet}$ can obtain a larger excess energy than $MA^{-\bullet}$ whereas $FA^{-\bullet}$ is forced to travel longer than $MA^{-\bullet}$ on D_0 to their counter isomers because the D_1 excited $FA^{-\bullet}$ can reach the D_1/D_0 DS with smaller θ_1 distortion from planar conformation than the D_1 excited $MA^{-\bullet}$. Larger excess energy of $FA^{-\bullet}$ is an offset against the small θ_1 distortion. Similarly, smaller excess energy of $MA^{-\bullet}$ is an offset against the large θ_1 distortion. This situation implies that the difference in available excess energy in the D_0 state would not be a determining factor of one-way reaction. Available excess energy, however, should be an important factor.

To isomerize using the excess energy, it is necessary to overcome the energy barrier at the TS (see Figs 4.4 and 4.6) that is the barrier in cis $\leftrightarrow$ trans isomerization in the D_0 state. From the present CASSCF result, this barrier, which marks the boundary between cis and trans forms, is significantly low in comparison with that between Z and E forms of PDI as will be shown in the later section. Then, the following scenario can be suggested for the one-way photoisomerization: The hot $MA^{-\bullet}$ can overcome the barrier, which is 28 kcal mol^{-1} with respect to the D_0 minimum $MA^{-\bullet}$, whereas the hot $FA^{-\bullet}$ cannot because the barrier height is 37 $kcalmol^{-1}$ with respect to the D_0 minimum $FA^{-\bullet}$. The difference of barrier height stems from the steric repulsion that we have already mentioned. That is to say, in $MA^{-\bullet}$, there is a strong repulsive interaction between the two carbonyl oxygens, as is reflected in the large C1–C2–C3 and C2–C3–C4 bond angles. In contrast, there is no steric repulsion in $FA^{-\bullet}$. Consequently, this steric repulsion makes $MA^{-\bullet}$ more unstable than $FA^{-\bullet}$ on the D_0 PES, resulting in the energetic difference in the activation energy seen by cis and trans forms. Indeed, that difference has been experimentally detected that a rapid electrochemically induced $DMM^{-\bullet}$ (cis form) $\rightarrow$ $DMF^{-\bullet}$ (trans from) one-way isomerization process takes place at room temperature.[16,17] Namely, this system of $MA^{-\bullet}/FA^{-\bullet}$ undergoes the one-way isomerization without UV illumination. If D_1 excited molecules can reach the D_1 minimum corresponding to the D_1/D_0 LEDP, mutual cis $\leftrightarrow$ trans photoisomerization should be detected. However, D_1 excited molecules can transit to D_0 at the far points from the LEDP by the HOOP motion. Hence, the $MA^{-\bullet}/FA^{-\bullet}$ deactivated by HOOP motion is forced to

travel up to its isomer in the D_0 state. UV light illumination produces vibrationally hot $MA^{-\bullet}/FA^{-\bullet}$ by the transition via the D_1/D_0 DS. In most photoreaction systems, available products usually depend on the initial conditions and excited-state PES topography.[29] In contrast, in the present system, the initial conditions on the excited state are blurred out and the final product only depends on the ground-state PES topography because the photoenergy is once transferred to vibrational energy.

4.1.4 Summary

We have found that, even if the molecular skeleton that decides the cis or trans form, i.e., the C1–C2–C3–C4 dihedral angle in this paper, does not largely distort, the photoisomerization occurs by the distortion of the H1–C2–C3–H2 dihedral angle (corresponding to the HOOP motion). Moreover, we suggested the following two-step isomerization mechanism. First, H1–C2–C3–H2 dihedral angle distortion occurs on the D_1 PES. Second, C1–C2–C3–C4 dihedral angle distortion occurs on the D_0 PES. Therefore, D_0, not D_1, is responsible for the one-way photoisomerization. This result well corresponds to the recent experiment about the photoisomerization of 11-cis to all-trans RPSB where HOOP is detected at an early stage after light illumination.[21]

Recent theoretical calculation about the model molecule of RPSB have shown the large possibility that a perpendicular S_1/S_0 DP is involved in the photoisomerization.[26] Considering that both olefin ion radicals such as $MA^{-\bullet}/FA^{-\bullet}$ in this paper and highly polar double-bond systems such as RPSB have the analogous perpendicular DP corresponding to the minimum of the first excited state, the PES of $MA^{-\bullet}/FA^{-\bullet}$ is expected to be similar to that of RPSB. Therefore, in these systems, the two-step isomerization suggested in this paper would be general: first HOOP (H–C–C–H dihedral angle distortion) on excited-state surface occurs, and then the large fraction of the net motion along the isomerization coordinate on the ground-state surface.

The C1–C2–C3–C4 dihedral angle usually decides the cis or tans form. The distortion of this dihedral angle occurs on the D_0 PES. We predicted that the D_0 state is responsible for the one-way isomerization. The experimental results can be interpreted by assuming there is the TS on the D_0 state that the cis form can overcome whereas the trans form cannot.[16,17] The suggested mechanism for the

one-way photoisomerization of $DMM^{-\bullet}/DMF^{-\bullet}$ is summarized in Fig. 4.8.

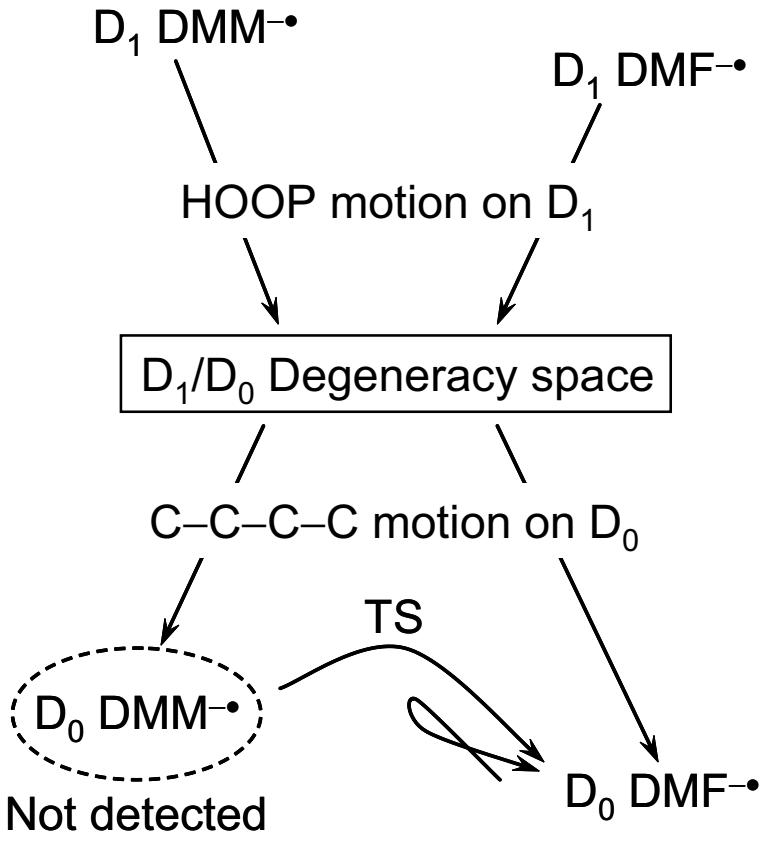

Figure 4.8: Schematic diagram showing the mechanism of the one- way photoisomerization of $DMM^{-\bullet}/DMF^{-\bullet}$ deduced from the present CASSCF calculation on $MA^{-\bullet}/FA^{-\bullet}$.

4.2 Penta-2,4-dieniminium: Hula-Twist Motion

In this section, we explore the funny photoisomerization processes, i.e. hula-twist motion suggested as volume-conserving isomerization process.

4.2.1 Introduction

The primary event in vision is the photochemical 11-cis to all-trans isomerization of the retinal protonated Schiff base (RPSB) chromophore in the visual pigment rhodopsin. This isomerization is one of the fastest photochemical reactions observed so far the primary ground-state transient called photorhodopsin is formed within 200 fs.[30] Recently, there are some experimental and theoretical studies which discuss or support hula-twit (HT) process about the mechanism of this cis → trans photoisomerization.[31,32]

The HT mechanism was proposed as a volume-conserving mechanism of photoisomerization around the double bonds in the limited space.[33] The HT mechanism differs from the conventional one-bond flip (OBF) mechanism, a simple rotation around the double bond. In the HT process, the double-bond and its neighboring single-bond rotate concertedly (Fig. 4.9). Products are different between the OBF and HT processes accordingly. Although no concrete evidence of the HT mechanism is available, a result of a time resolved study, though without the expected product, is possibly interpreted as a symptom of the HT motion.[31]

From the theoretical side, on the other hand, it is generally assumed on the basis of some theoretical calculation[26] that the photoisomerization process is of OBF for highly polar double-bond systems such as RPSB. Some calculation have also been done on the minimal model of RPSB, tZt-penta-2,4-dieniminium (PDI, Scheme 1).[8,34–36] These studies revealed that the minimum energy in the first excited state (S_1) corresponds to the S_1/S_0 lowest energy degeneracy point (LEDP) (see Fig. 4.10). The structure of the S_1/S_0 LEDP shows a diallyl-like structure rotated perpendicularly around the C2–C3 (labeling of the skeletal atoms is shown in Scheme 1). Clearly, this S_1/S_0 LEDP is related not to HT but to OBF process. Recent calculations on photo-excitation/relaxation considering environment effect (QM/MM calculation of RPSB based on CASSCF/ 6-31G* using AMBER force field in protein)[32] suggest little contribution of the HT mechanism.

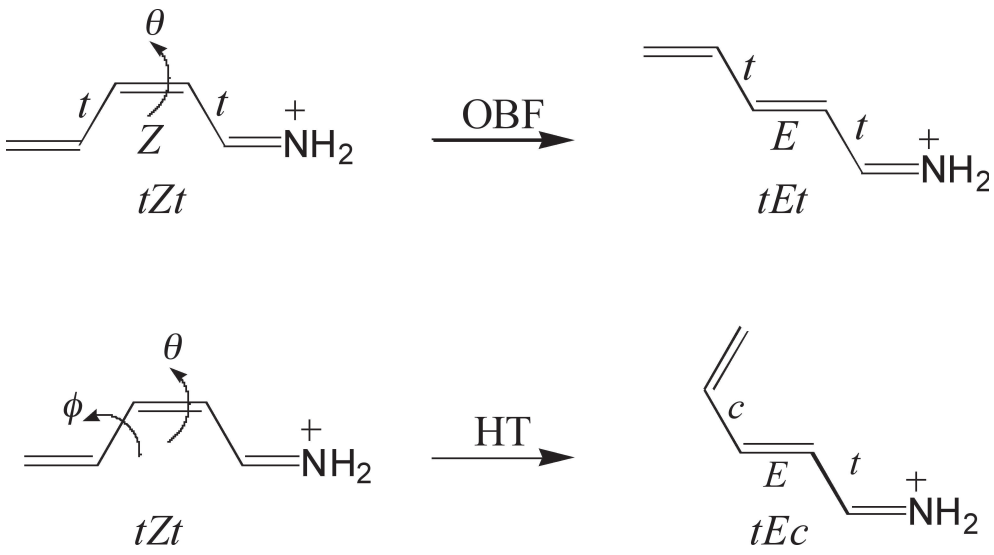

Figure 4.9: Isomerization of tZt-PDI. OBF process, isomerization through the rotation about C2-C3 double bond only; HT process, isomerization through the rotations about both C2-C3 double bond and C3-C4 single bond.

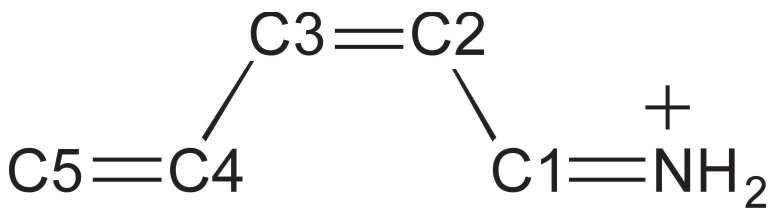

Scheme 1

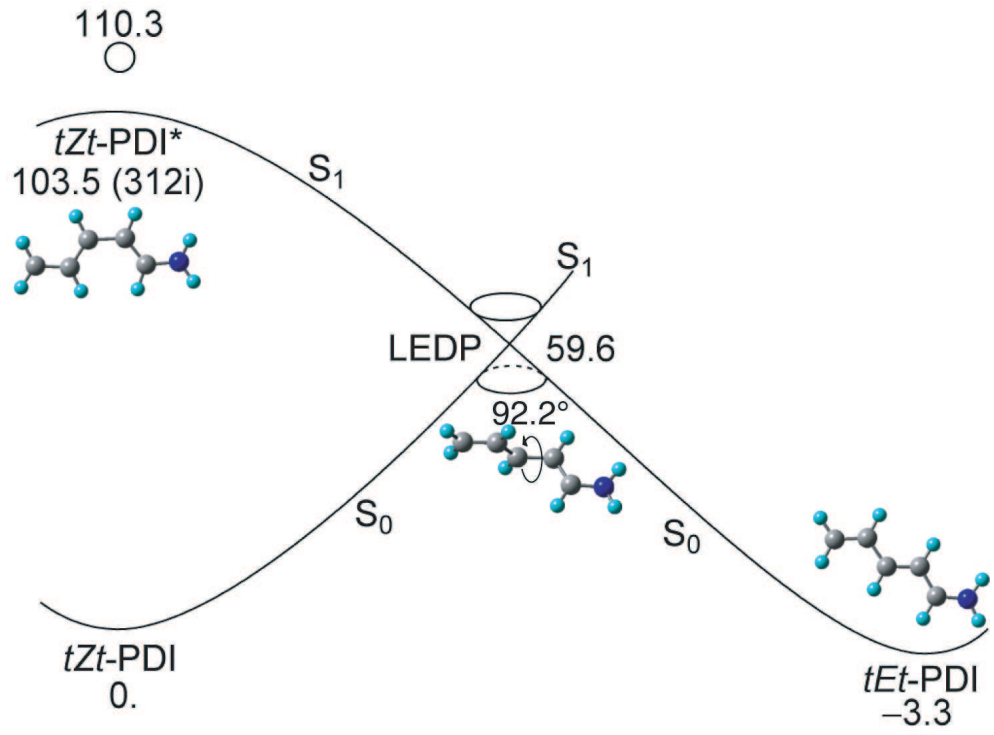

Figure 4.10: Schematic energy diagram of the OBF photoisomerization of tZt-PDI to tEt-PDI by CASSCF/6-31G*. Values are the relative energies (in kcal mol^{-1}) with respect to the S_0 equilibrium structure of tZt-PDI. tZt-PDI* is the S_1 relaxed structure with C_s symmetry, of which imaginary frequency (cm^{-1}) is indicated in parentheses. This imaginary frequency describes the rotational instability around C2-C3. Open circle indicates the $S_0 \rightarrow S_1$ vertical excitation energy of tZt-PDI.

Although existing results of theoretical studies do not suggest the importance of the HT motion in the photo- chemical process, no results have been reported for the potential energy surface around the HT coordinate. This situation prompted the authors to explore the trial HT-3 motion of PDI (i.e. simultaneous rotation of both C2=C3 and C3–C4) on the S_1 state including S_1/S_0 degeneracy space.

4.2.2 Computational Details

The S_1/S_0 degeneracy points (DPs) and S_1 relaxed scan along the HT coordinate were calculated using the complete active space self-consistent eld (CASSCF) theory and 6-31G* basis set implemented in the GAUSSIAN 98 programs.[24] An active space of six electrons in six orbitals was used, corresponding to the π orbitals. All calculations were carried out using state-averaged orbital, with the two states weighted equally. The search for the S_1 relaxed scan was started from the C_s S_1 relaxed structure, tZt-PDI* (Fig. 4.10). As will be seen, this relaxed scan corresponds to the S_1/S_0 degeneracy space on the route to the S_1 minimum.

Recent calculations indicated the ubiquitous existence of DPs, which are very important in photochemical processes since non-adiabatic events occur in the DP regions.[1] Although a DP is often treated as an isolated point on the potential energy surface, this is not the case. Two-state degeneracy persists along an $(n-2)$-dimensional space (Degeneracy space; DS), where n is the number of molecular internal degrees of freedom.[3,4] The projected gradient method by Bearpark et al.[6] is available for locating DPs. This algorithm is, however, only suitable for stationary DPs such as LEDPs on the DS. In fact, an S_1/S_0 DP obtained by the projected gradient method for PDI in C_1 symmetry is only the S_1/S_0 LEDP having a perpendicular structure (Fig. 4.10). Thus, if this algorithm is used with a geometric constraint imposed (beyond the molecular symmetry), the resulting geometry may not be of a DP. To address this shortcoming, we carried out two-step optimization introduced in previous chapter. Using two-step optimization, we performed the relaxed scan of S_1/S_0 DS while constraining two dihedral angles (as will be shown in Figs.4.11 and 4.12).

4.2.3 Results and Discussion

Since HT isomerization under consideration is a diabatic process, it is necessary to find a degeneracy point (DP) related to the HT motion. DPs are very important on discussing the reaction rate because the most efficient transition occurs from an excited state to the ground state at DPs. In non-polar double-bond systems, breaking of only one p bond can give rise to an S_1/S_0 avoided crossing (S_1 minimum). To reach a DP one more bond must be broken. As a consequence, the structures of DPs are of kink-type or hydrogen bridging. The kink-type or hydrogen bridging structures where S_1 and S_0 states are degenerate were indeed found through detailed calculations.[37–39] Isomerization via the HT process is thus considered to be possible in non-polar double-bond systems. Experimentally, all-s-trans-1,3,5,7-octatetraene was reported to undergo reversible conformational change to its 2-s-cis conformer via HT process in an n-octane matrix at 4.2 K.[40] In contrast, in highly polar double-bond systems like PDI, breaking of one π bond is already sufficient to give a S_1/S_0 DP. Increased nuclear charge at nitrogen lowers S_1 by stabilizing one electron pair at nitrogen while rotation of the C–C bond in the ground state destabilizes S_0 but not S_1. This results in the intersection between the two states. In more detail, Riuz et al.[41] discussed the difference between degeneracy points in non-polar and polar conjugated polyenes.

An isolated DP cannot exist mathematically[3] except for diatomic molecule. Indeed, the S_1/S_0 DS extends to the direction of changes in the C1-C2-C3-C4 and C2-C3–C4–C5 dihedral angles. To explore the DS, θ and ϕ are defined as the C1–C2–C3–C4 dihedral angle and the C2–C3–C4–C5 dihedral angle, respectively (Fig. 4.9). The result of two-dimensional relaxed scan of the DS along θ and ϕ is shown in Fig. 4.11. The surface shown is an aggregation of S_1/S_0 DPs, i.e., a segment of the S_1/S_0 DS along θ and ϕ. Due to a convergence problem (the section of $\Delta\theta = 0°$ was not successfully scanned), the scan was performed only within the region of $\Delta\theta = 10 - 180°$ and $\Delta\phi = 0 - 90°$ (Δ indicates the displacement from the initial value of tZt-PDI, i.e., $\theta = 0°$ and $\phi = 180°$). The energy and structure of the DP at the point of $\Delta\theta = 90°$ and $\Delta\phi = 0°$ correspond approximately to those of the LEDP. Clearly, the S_1/S_0 DS extends not only to the direction of θ but also to that of ϕ. The S_1/S_0 DS lies below the vertically excited energy of tZt-PDI (Table 4.5). The DP at $\Delta\theta = 90°$ and $\Delta\phi = 90°$ lies 24.3 kcal mol^{-1} below the vertically excited

energy of tZt-PDI. This implies that S_1 excited tZt-PDI can reach not only to the LEDP of the OBF type, but also to the kink-type (HT type).

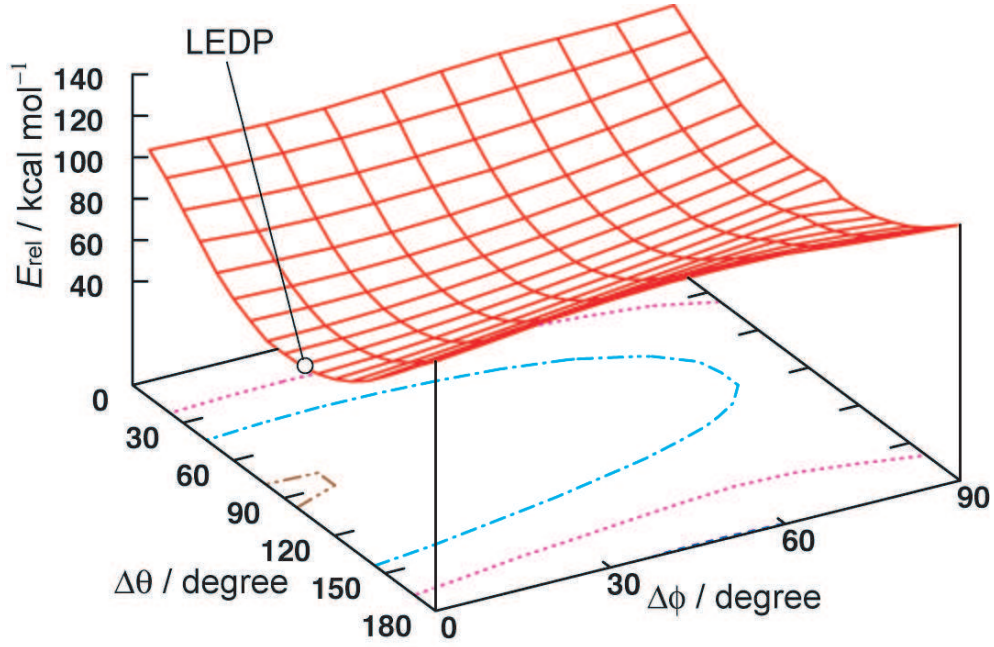

Figure 4.11: S_1/S_0 DS along θ and ϕ. $\Delta\theta$ and $\Delta\phi$ indicate the displacement from the initial value of $\theta = 0°$ and $\phi = 180°$ respectively. E_{rel} is the energy relative to that of the S_0 equilibrium structure of tZt-PDI.

It is very interesting to see whether HT DPs can be reached from tZt-PDI*. Then, we calculated the S_1 relaxed scan along simultaneous change of both θ and ϕ (i.e. $\Delta\theta = \Delta\phi = \Delta$). The result of the relaxed scan calculation for this HT coordinate is shown in Fig. 4.12. Geometry optimization using the state-averaged orbital worked well as far as the two states are significantly separated energetically. However, geometry optimization in the DS is impossible by the method. It was therefore necessary, in the relaxed scan calculation, to switch from the single state geometry optimization using state-averaged orbital to the DP optimization at the $\Delta = 40°$ (DP40) that lies 21.9 kcal mol^{-1} below tZt-PDI* (Table 4.5). From $\Delta = 40°$, the relaxed scan coincides with the S_1/S_0 DS as seen in Fig. 4.12. Remarkably, there is no energy barrier preventing tZt-PDI* accessing to the HT S_1/S_0 crossing structures though the true (i.e., unconstrained) relaxed scan correspond to the OBF mechanism. This implies that the HT motion in highly polar double-bond systems

Table 4.5: CASSCF/6-31G* energies for the S_0 and S_1 stationary points and S_1/S_0 DPs of PDI

Species	State	Symmetry	E_0 [a]	E_1 [b]	E_{rel} [c]
tZt-PDI	S_0	C_s	−248.24954	−248.07371	0.
tZt-PDI*	S_1	C_s	−248.11371	−248.08457	103.5
DP40	S_1/S_0	C_1	−248.11958	−248.11958	81.6
DP60	S_1/S_0	C_1	−248.12958	−248.12958	75.3
LEDP	S_1/S_0	C_1	−248.15452	−248.15452	59.6
tEt-PDI	S_0	C_1	−248.25481	−248.07289	−3.3

a) State-averaged energy for S_0 in atomic unit.

b) State-averaged energy for S_1 in atomic unit.

c) Relative energy with respect to the S_0 equilibrium structure of tZt-PDI in kcal mol^{-1}.

could take place if environmental effects disfavor the OBF motion. It is noted that Fuβ et al. suggested for non-polar double-bond systems, stilbene, that the HT motion is possible without any constraint.[42]

In the section of the S_1/S_0 DS shown in Fig. 4.12, there is a minimum (not a real minimum in the isolated condition) around $\Delta = 60°$ (DP60) that lies 28.2 kcal mol^{-1} below tZt-PDI* (Table 4.5) and 15.7 kcal mol^{-1} above the S_1/S_0 LEDP. According to the recent dynamics study of photoisomerization of tZt-PDI,[36] most of the S_1 trajectories decayed to S_0 before reaching the S_1/S_0 LEDP that has a nearly perpendicular structure ($\theta = 92°$, see Fig. 4.10) as the S_1/S_0 degeneracy extends to smaller angles. If the relaxed scan along Δ corresponds to the reaction coordinate due to some environmental effects, the S_1 excited PDI may decay to S_0 before reaching the DP60 ($\Delta\theta = 60°$ and $\Delta\phi = 60°$). Thus, the concomitant rotation of the adjacent single bond could cause the transition to S_0 at a smaller rotation angle of the double bond than in the OBF process.

To see possible final products from the HT motion on the S_1 surface, tEc-PDI we have performed S_0 geometry optimizations using state-averaged orbital from the structures near DP60 and DP40. Starting structures were generated by distorting

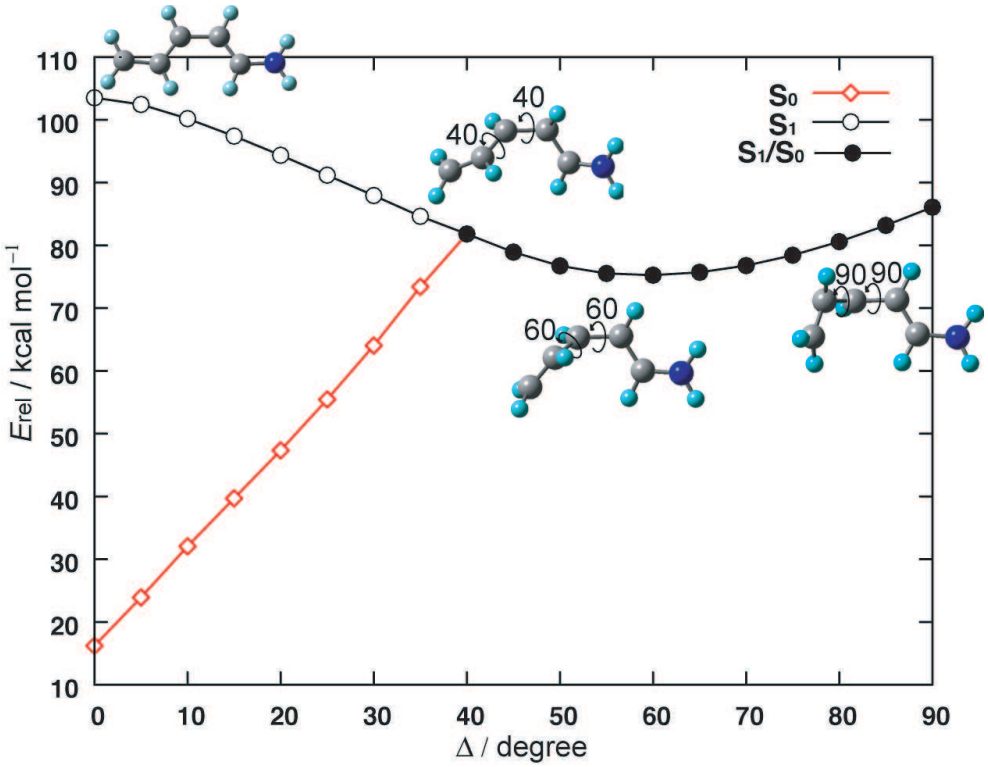

Figure 4.12: S_1 relaxed scan along the HT coordinate ($\Delta\theta = \Delta\phi = \Delta$). E_{rel} is the relative energy with respect to the S_0 equilibrium structure of tZt-PDI.

the DP geometries in the two-dimensional degeneracy-lifting space. All these calculations resulted in either tZt-PDI (reactant) or tEt-PDI (OBF product), the initial twist of the single C3-C4 bond being turned back. The overall process is thus characterized as aborted or attempted HT motion.[41] Therefore, at least in an isolated condition, a complete HT process is not expected to occur even if HT S_1/S_0 DP geometry such as DP40 and DP60 has been reached. This, however, does not mean that the complete HT process is impossible in constrained states.

In Fig. 4.13, changes in skeletal geometry along the HT relaxed scan are shown. At $\Delta = 40°$, where the S_1/S_0 degeneracy begins, there is an abrupt change in tendencies of geometrical changes. Those shown by the N–C1 and C1–C2 bond lengths are remarkable (Fig. 4.13a). While N–C1 is contracted up to $\Delta = 40°$, it is elongated beyond $\Delta = 40°$. On the contrary, C1–C2 bond is elongated up to $\Delta = 40°$, and then, contracted. Similar abrupt changes were also observed in the bond angles (Fig. 4.13b). Those in angles C1–C2–C3 and C2–C3–C4 are remarkable. These indicate that the electronic structure changes rather abruptly around $\Delta = 40°$. A similar abrupt change in electronic state upon reaching a S_1/S_0 DS was also reported in Ref. 8 which is the result of theoretical calculation on tZt-PDI OBF photoisomerization in an isolated condition. The tendency of geometric changes abruptly turns into the other upon the encounter of the S_1 relaxed scan with the S_1/S_0 DS. The abrupt change observed in the present result is reasonable because S_1 and S_0 states mix after passing $\Delta = 40°$. In contrast, N–C1–C2–C3 dihedral angle shows smooth change at $\Delta = 40°$ as seen in Fig. 4.13c. However, from $\Delta = 40°$, the increasing tendency is also changed into decrease.

4.2.4 Summary

The S_1/S_0 DS of PDI is characterized along the HT coordinate (simultaneous change of both C1–C2–C3–C4 dihedral angle and C2–C3–C4–C5 dihedral angle) within the CASSCF theory. It is found that the S_1/S_0 DS extends not only to the direction of C1–C2–C3–C4 dihedral angle but also to that of C2–C3–C4–C5 dihedral angle and that the HT crossing region lies well below the Franck-Condon region. The S_1 relaxed scan of PDI along the HT coordinate exhibited no energy barrier preventing tZt-PDI* from accessing the HT S_1/S_0 crossing region. These results suggest the possible involvement of the HT process in a fast photochemical reaction of retinal

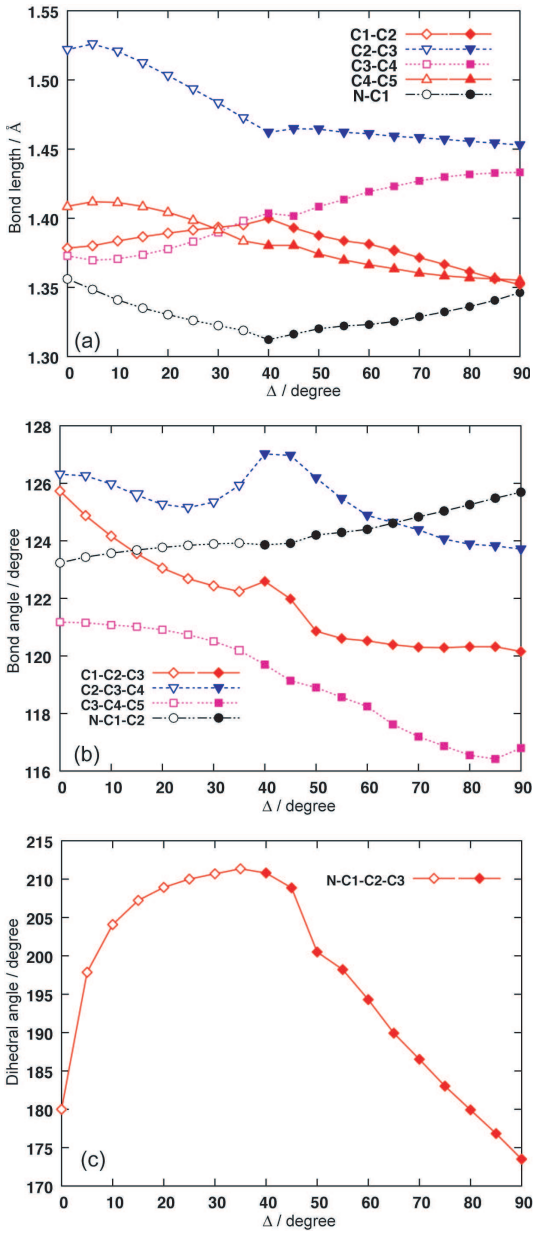

Figure 4.13: Change in skeletal geometry along the HT relaxed scan (Fig. 4.12). (a) bond lengths, (b) bond angles, and (c) dihedral angles. Open symbols, from S_1 geometry optimizations using state-averaged orbitals; filled symbols, from S_1/S_0 DP optimization.

protonated Schiff base chromophore in constrained states. Although our calculations (CASSCF) do not include dynamical electron correlation, the conclusion we have reached in this work would not be affected qualitatively by it. In the next section, we show the Z $\rightarrow$ E photoisomerization of PDI initiated by hydrogen out-of-plane motion on the first excited state.

4.3 Penta-2,4-dieniminium: HOOP Motion

In this section, we show the Z → E photoisomerization of PDI initiated by hydrogen out-of-plane motion on the first excited state. This photoisomerization process resembles to maleic and fumaric acid anion radical system as discussed in Sec. 4.1

4.3.1 Introduction

Retinal protonated Schiff base (RPSB) is a visible prosthetic group, i.e., chromophore of rhodopsin or bacteriorhodopsin whose biological functions as photoreceptors are triggered by their photo-induced isomerization.[31,43,44] In bacteriorhodopsin, the photoisomerization from all-trans to 13-cis RPSB induces the function as proton pump.[43] In rhodopsin, on the other hand, the 11-cis to all-trans photoisomerization of the RPSB (Scheme 1) triggers the conformational changes underlying the activity of rhodopsin that starts the visual transduction process.[31,44] Interestingly,

Scheme 1

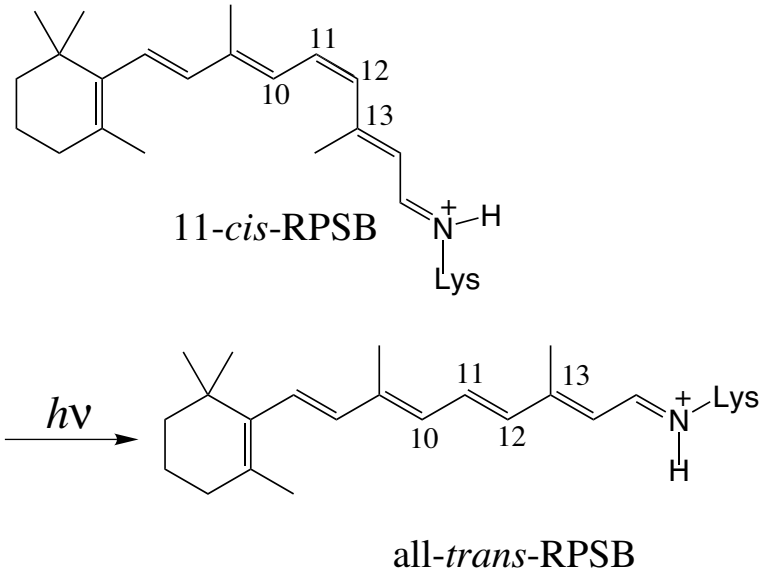

the 11-cis to all-trans photoisomerization of the RPSB in rhodopsin is very efficient (quantum yield is approximately 0.65) and very fast [primary ground-state transient (photorhodopsin) is produced within 200 fs][31,44] though its photoisomerization in solution is not so efficient (quantum yield is approximately 0.15).[45] This fact indi-

cates the protein portion (opsin) catalyzes the 11-cis to all-trans photoisomerization of RPSB by some interactions. RPSB in rhodopsin is bonded to the protein part of rhodopsin (opsin) via a specific lysine residue. Probing the structure of the RPSB in rhodopsin is crucial for understanding its chemical properties because the rate and efficiency of the photochemical reaction are related to its ground state structure.[31] The structure in rhodopsin is substantially detailed by means of NMR, resonance Raman (RR) spectroscopy and X-ray diffraction.[31,46,47] Theoretical calculation has also succeeded in reproducing the experimentally informed structure of RPSB in rhodopsin through quantum mechanics / molecular mechanics (QM/MM) hybrid strategy.[32,48] These results clearly show that RPSB has a helical structure and central C10–C11–C12–C13 dihedral angle is distorted by approximately 8° in contrast to the theoretical prospect of a model RPSB in isolated condition (no twisting about the C11–C12 double bond[49]).

The structural comparison of the RPSB in rhodopsin and in solution is also crucial. These studies provided the information about the nature of the interaction between the protein and the RPSB and clues to clarify the origin of the large difference in photoreactivity between the RPSB in solution and in rhodopsin. The experimental comparison in ^{13}C NMR and RR spectrum were performed.[31,47,50] The large difference in ^{13}C NMR chemical shift of the RPSB between in rhodopsin and in solution was documented.[31,47] The origin of these differences was explained to be due to glutamate counterion (Glu113) influencing on C11, C12, and C13 in rhodopsin.[31,47] This interaction of Glu113 with the RPSB seems to play a role to store the energy in bathorhodopsin (the thermodynamically stable product).[31,47] RR spectroscopy also clarified the difference between in rhodopsin and in solution.[50] The result implies the importance of a hydrogen out-of-plane (HOOP) motion in the excited state. The RR spectrum with frequency between 600 and 2000 cm^{-1} exhibits one prominent sharp peak and two finger print regions in both rhodopsin and solution.[31,50,51] The sharp peak appears around 1550 cm^{-1} that is assigned to C=C stretching vibration. The higher one of the two finger print regions appears from 1200 to 1300 cm^{-1}, which is due to C–C stretching and C–H rocking. The lower one appears from 920 to 1020 cm^{-1}, corresponding to C–CH_3 rocking and C–H wagging (HOOP) motion. Although the frequencies of the peaks of RR in rhodopsin are not so different from those in solution, significant difference can be seen in their inten-

sity. The HOOP mode around 970 cm^{-1} in the protein is more intense than that in solution.[31,50] This HOOP mode is a concerted combination of wagging motions of C11–H and C12–H. Assuming the local structural symmetry is C_{2v}, this HOOP motion is classified to A_2 species. The intensities of the lines in the RR spectrum give additional information on the excited electronic states of the RPSB, since the intensities depend not only on the nature of the ground state vibrations but also on the geometrical distortion of the molecule in the excited electronic state.[31,50] Thus, the protein portion of rhodopsin may have the effect that enforces the H–C11=C12–H HOOP motion. According to the excited state dynamics of the photoisomerization by analyzing deuterium effects for hydrogen atom bonded to C11 and C12 using the method of Fourier transform of optical absorption spectra,[52] the H–C11=C12–H HOOP motion is significantly coupled with the skeletal motion of RPSB in the time range 70-100 fs after light absorption. Therefore, this H–C11=C12–H HOOP motion is expected to have some strong effects on the photoisomerization of the RPSB.

Recent femtosecond-stimulated Raman spectroscopy (FSRS) study[21] on the reaction dynamics of the RPSB documented the interesting results. Kukura et al.[21] represented time-resolved FSRS of rhodopsin from 200 fs to 2 ps. That is to say, the evolution from photorhodopsin (primary ground state product) to the thermodynamically stable product (bathorhodopsin) was probed. According to their result, very intense dispersive lineshapes in the HOOP region between 800 and 950 cm^{-1}, which is reminiscent of that of bathorhodopsin, was observed at early time. This fact indicates that the H–C11–C12–H part of photorhodopsin has already become that of bathorhodopsin. Therefore, they concluded that a large fraction of the atomic rearrangement up to bathorhodopsin possibly occurs in the ground state after the S_1 to S_0 transition mediated mainly by the fast H–C11–C12–H HOOP motion. On the other hand, recent trajectory calculation using the QM/MM strategy with scaled-CASSCF/6-31G* ruled out the fast decay by the HOOP motion strongly coupled with the skeletal structure of the RPSB.[53] However, as will be shown for a model system of the RPSB, it is plausible that the excited RPSB takes the reaction path where the fast decay is mediated by the A_2 HOOP motion strongly coupled with skeletal structure of the RPSB. In this work, we try to elucidate the role of the HOOP motion in the excited state of the RPSB through theoretical calculation. We

have obtained the result compatible with the suggestion by Kukura et al.[21] through the calculation of the potential energy surfaces (PESs) on the penta-2,4-dieniminium (PDI) using the symmetry adapted cluster/configuration interaction (SAC-CI)[54] on optimized structure by the complete active space self-consistent field (CASSCF).[18] We also propose the possible Z to E photoisomerization process of PDI where the S_1 to S_0 decay is mediated by the HOOP motion. PDI (Scheme 2) is known as the minimum model molecule of the RPSB whose Z to E-PDI photoisomerization is assured to mimic the 11-cis to all-trans photoisomerization of RPSB.[8,26,34,36,55,56] It is worthy to document the character about the Z to E photoisomerization of PDI as the model system that was clarified by the previous studies.[8,26,34,36,55,56] First, this photoisomerization is described by two-mode, two-state model. Namely, the isomerization coordinate is described mainly by double and single bond alternation and reactive C=C rotation, and the first excited (S_1) and ground (S_0) states are involved in the photoreaction under the isolated condition. This two-mode and two-state photoisomerization does not change even in the other model systems having longer linkage or the RPSB itself under the isolated condition.[26,34,55,57] Furthermore, recent theoretical calculation elucidated the calculated result in the isolated condition resemble that in protein.[26,48,49,58] Second, PDI has the S_1/S_0 lowest energy degeneracy point (LEDP), at which C2–C3 is twisted by about 90°. This is also similar to the other model system or RPSB itself. The minimum energy path and trajectory calculation in Z-PDI clarified that S_1 excited Z-PDI can reach the S_1/S_0 degeneracy space (DS) before reaching the S_1/S_0 LEDP (C2–C3 is twisted by approximately 73°).[8,36,56] This result is compatible with results of the trajectory calculation by scaled-CASSCF/6-31G* on the RPSB in protein (S_1 to S_0 decay occurs with a high probability when the reactive C=C is twisted by approximately 80°).[49]

Scheme 2

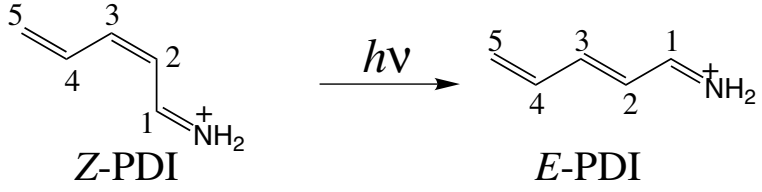

Z-PDI *E*-PDI

As mentioned above, the qualitative shape of PES reflected in the photoisomerization coordinate of PDI is similar to that of systems having longer linkage or RPSB in rhodopsin. Therefore, we concluded that Z to E photoisomerization of PDI is enough system to discuss the qualitative features of the 11-cis to all-trans photoisomerization process of RPSB. A small difference is noteworthy between PDI and other model molecules having longer linkage. As the linked length increased, an energy plateau emerges in the initial part of reaction path way.[26,55,57,58] However, our SAC-CI//CASSCF/6-31G* calculation rather indicates the possible presence of the barrier in the initial part of reaction path way.

4.3.2 Computational Detail

All calculations in this section were performed using GAUSSIAN03.[59] The S_0 and S_1 potential energy surfaces (PESs) were computed with the CASSCF[18] method using 6-31G* basis set. Six π electrons in six π orbitals which correspond to the π system of planar PDI were used as active space. Two-root state-averaged orbital was used (0.5 weights) in the geometry optimization for energy. As will be shown, transition state on S_0 PES (TS_1 and TS_2) was optimized through single-state CASSCF because of convergence failure of state-averaged CASSCF. These energies were recalculated through single point state-averaged CASSCF.

It is well known that CASSCF is not definitive because it does not include the dynamical electronic correlation. Therefore, to confirm the qualitative shape of the S_1 or S_0 PES, we carried out the single point calculation using symmetry adapted cluster/configuration interaction (SAC-CI)[54] with 6-31G* basis set on the geometries optimized by CASSCF/6-31G* (SAC-CI//CAS/6-31G*). Restricted Hartree-Fock (RHF) calculation was used as the reference state of SAC-CI. When we carried out single point calculation using SAC-CI, the energy of the lowest three excited states are calculated. We will report the energies of S_2 state at need in this section. As will be shown, the potential energy surface of SAC-CI//CAS/6-31G* are dramatically different from those of CASSCF/6-31G*. When the geometry optimization using SAC-CI/6-31G* is performed, it is too expensive to calculate the energy of the lowest four states while geometry optimization and vibrational analysis. Hence, only the first excited state is calculated during the geometry optimization using SAC-CI/6-31G* and the energy of the lowest four state are calculated on the obtained geometry.

Conical intersections are very important on discussing the reaction rate because the most efficient transition occurs from an excited state to a ground state at conical intersections[1,4] and shown in previous chapters. A degeneracy point which is an apex of a conical intersection is not an isolated point but a point in an $(n-2)$-dimensional continuous DS (where n is the number of molecular internal degrees of freedom).[3,4] DS is sometimes called a conical intersection hyperline or seam.[3,4] To characterize the S_1/S_0 DS, we used the method introduced in Chapter 3, which enables us to loosely optimize the geometry for energy in the S_1/S_0 DS.[10,11,60]

4.3.3 Result and Discussion

The energies of all stationary points and DP discussed in this section are summarized in Table 4.6. Atomic numbering shown in Scheme 2 is used throughout this section. Hereafter, the C1–C2–C3–C4 dihedral angle and H–C2–C3–H dihedral angle are denoted by θ_1 and θ_2 respectively.

S_1 PES and S_1/S_0 DS as function of θ_1 or θ_2

The results of the relaxed S_1 PES including the S_1/S_0 DS along θ_1 and θ_2 are shown in Fig. 4.14 and 4.15 The geometrical changes corresponding to Figs. 4.14 and 4.15 are shown in Figs. 4.16 and 4.17, respectively. This calculation was started from the S_1 relaxed planar structure (Z-PDI*) where double and single-bond alternation has already taken place. Z-PDI* would correspond to the fluorescent state that was previously reported on model RPSBs.[8,26,36,55–57] Therefore, the topography of PES around Z-PDI* seems to be strongly reflected in the reaction path of S_1 excited Z-PDI. The PESs in Figs. 4.14 and 4.15 show that the number of states involved in the reaction is two (i.e. S_0 and S_1 as shown in the previous study.[8,26,36,55–57] However, some constraint by surroundings (e.g. protein, matrix, etc) where PDI is embedded can be assumed, though our calculation is in isolated condition. Unless the deliberate constraint was brought by surroundings, the possibility for S_1 excited Z-PDI to undergo the reaction path we report here may be low. The reaction path of PDI in isolated condition by more sophisticated strategy with CASSCF/6-31G* was proposed in Ref. 8, 36, 56. The normal vibrational mode of Z-PDI* with an imaginary frequency (312i cm^{-1}) is shown in Fig. 4.18 The A_2 HOOP motion is

Table 4.6: SAC-CI//CASSCF/6-31G* and CASSCF/6-31G* energies for the S_0 and S_1 stationary points and S_1/S_0 DPs of PDI.

Species	State	E_{CAS}[a]	E_{CAS}[b]	$E_{\mathrm{SAC-CI}}$[c]	E_{rel}[d]
Z-PDI (planar)	S_0	–	−248.24954	−248.76375	0.(0.)
	S_1	–	−248.07371	−248.60540	99.4(110.3)
Z-PDI (twist)	S_0	–	−248.24895	−248.73796	16.2(0.4)
	S_1	–	−248.07320	−248.58057	114.9(110.7)
TS_1[e]	S_0	−248.17811	−248.15765	−248.66169	64.0(57.7)
	S_1	–	−248.14588	−248.6547	68.4(65.0)
TS_2[e]	S_0	−248.17845	−248.15582	−248.66689	60.8(58.8)
	S_1	–	−248.14280	−248.63743	79.3(67.0)
Z-PDI*	S_0	–	−248.11371	−248.73462	18.3(85.2)
	S_1	–	−248.08457	−248.61622	92.6(103.5)
RS_{40}	S_0	–	−248.12830	−248.62399	87.7(80.1)
	S_1	–	−248.12185	−248.60766	98.0(80.4)
DP_{C40}	S_0	–	−248.12146	−248.62050	89.9(80.4)
	S_1	–	−248.12145	−248.60346	100.6(80.4)
DC_{H50}	S_0	–	−248.13293	−248.63350	81.7(73.2)
	S_1	–	−248.13292	−248.61777	91.6(73.2)
LEDP	S_0	–	−248.15452	−248.66914	59.4(59.6)
	S_1	–	−248.15452	−248.65290	69.6(59.6)
E-PDI	S_0	–	−248.25481	−248.76866	−3.1(−3.3)
	S_1	–	−248.07289	−248.60620	98.9(110.8)

a) Single-state energy in au.

b) State-averaged CASSCF energy for S_0 and S_1 in atomic unit.

c) SAC-CI energy for S_0 and S_1 on the optimized structure by CASSCF in atomic unit.

d) Relative energy with respect to the S_0 equilibrium structure of Z-PDI in kcal mol^{-1}. Values in parentheses are of state-averaged CASSCF.

e) The geometries are obtained by single-state CASSCF.

one of the main components of this vibration. Therefore, by optimizing the internal coordinates including θ_2 for energy while θ_1 being constrained into an arbitrary value as a scan variable, whether S_1 excited Z-PDI can reach the S_1/S_0 DP mainly by the A_2 HOOP motion or not can be elucidated. As shown in Fig. 4.14, these S_1/S_0 DPs evidently exist. S_1 geometry optimization is succeeded up to $\theta_1 = 40°$, where we switched into S_1/S_0 DP optimization because of the failure in S_1 geometry optimization at $\theta_1 = 50°$. However, the DP at $\theta_1 = 50°$ and S_1 relaxed structure at $\theta_1 = 40°$ (RS_{40}) is not connected geometrically while the DP at $\theta_1 = 40°$ (DP_{C40}) and the S_1 relaxed structure at $\theta_1 = 30°$ is. Therefore, we withdrew the point of the relaxed structure at $\theta_1 = 40°$ from Fig. 4.14.

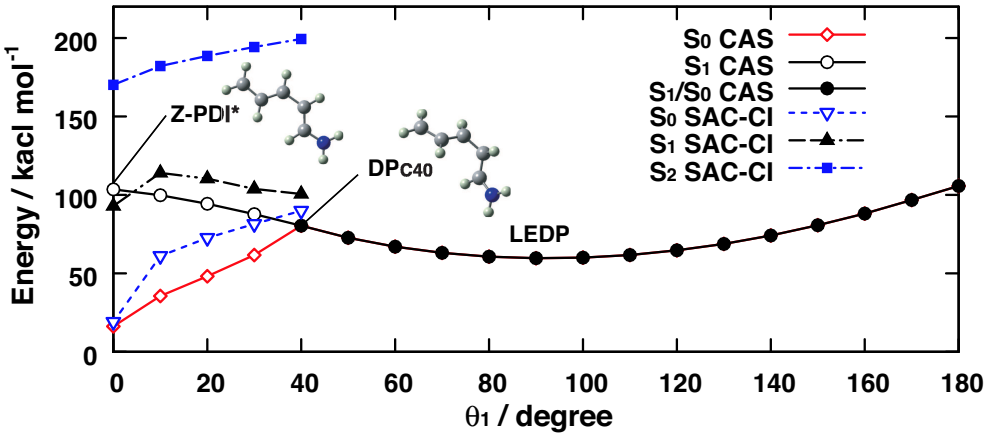

Figure 4.14: Relaxed S_1 PES including the S_1/S_0 DS as a function of θ_1 through CAS/6-31G* and SAC-CI//CAS/6-31G*

According to Fig. 4.15 , Z-PDI* can reach the S_1/S_0 DS at $\theta_1 = 40°$ (DP_{C40} in Fig. 4.15) without barrier in CASSCF/6-31G* level. At DP_{C40}, the value of θ_2 is 127.6°. Therefore, there are evidently DPs where S_1 excited Z-PDI can reach mainly by the A_2 HOOP (θ_2 distortion) on the S_1 PES. Figure 4.19 shows the gradient difference and derivative coupling vectors calculated by CAS/6-31G* at DP_{C40}. These vectors evidently include the A_2 HOOP motion and induce the rotation around C2=C3 and the bond alternation. Therefore, the conical intersection whose apex is DP_{C40} is related to the Z to E photoisomerization.

In SAC-CI//CAS/6-31G* level, the barrier lies at $\theta_1 = 10°$ about 20 kcal mol^{-1} above planar Z-PDI* and 15 kcal mol^{-1} above the S_1 vertical excited state of Z-PDI

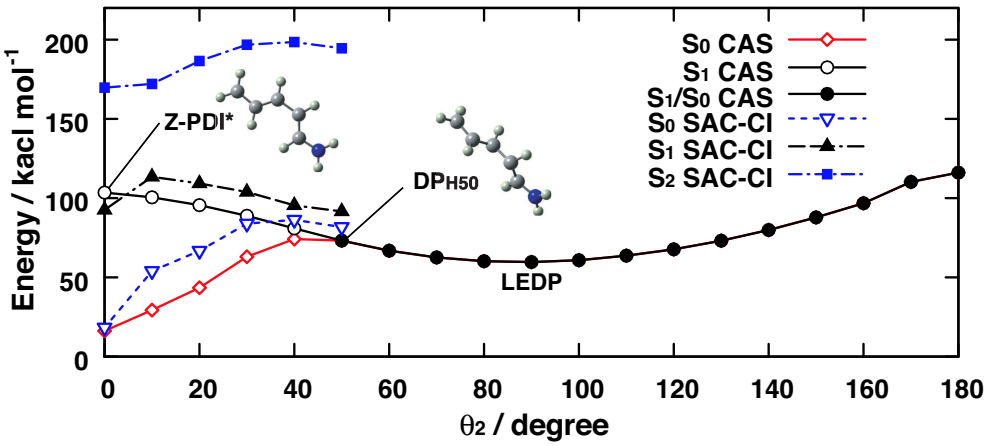

Figure 4.15: Relaxed S_1 PES including the S_1/S_0 DS as a function of θ_2 through CAS/6-31G* and SAC-CI//CAS/6-31G*

(see the Table 4.7 additionally). It may be impossible for S_1 exited planar Z-PDI to overcome the barrier because the barrier lies energetically higher than the S_1 vertical excited energy. The existence of the barrier should lower the quantum yield of Z to E photoisomerization of PDI. However, if the ground state structure of Z-PDI is twisted about the reactive C1–C2–C3–C4 dihedral angle, Z-PDI can reach the S_1/S_0 DS without barrier by the A_2 HOOP motion. Considering the fact the central C10–C11–C12–C13 dihedral angle of the 11-cis RPSB in rhodopsin is distorted by approximately 8° ,[31] what the 11-cis RPSB is distorted in rhodopsin has also an important "catalytic" effect on the photoisomerization. We will revisit the issue on this barrier later.

In order to see the effect of the HOOP motion more specifically, we calculated the S_1 PES including the S_1/S_0 DS as a function of θ_2. In contrast to that of θ_1, this PES may be produced when the HOOP motion (i.e. θ_2 distortion) is constrained due to some effect but θ_1 is free. As shown in Fig. 4.17, when $\theta_2 = 50°$ and $\theta_1 = 128.6°$ (DP_{H50}), S_1 Z-PDI can reach the S_1/S_0 DS. Figure 4.19 shows the derivative coupling and gradient difference vector that have the A_2 HOOP motion as the component. Hence DP_{H50} is also expected to be related to the Z → E photoisomerization.

Similarly to Fig. 4.14, the result by CAS/6-31G* exhibited the path without barrier up to the S_1/S_0 DS, whereas SAC-CI//CAS/6-31G* show the barrier lying about 20 kcal mol^{-1} above Z-PDI*. Therefore, Z-PDI* in SAC-CI seems to be stable

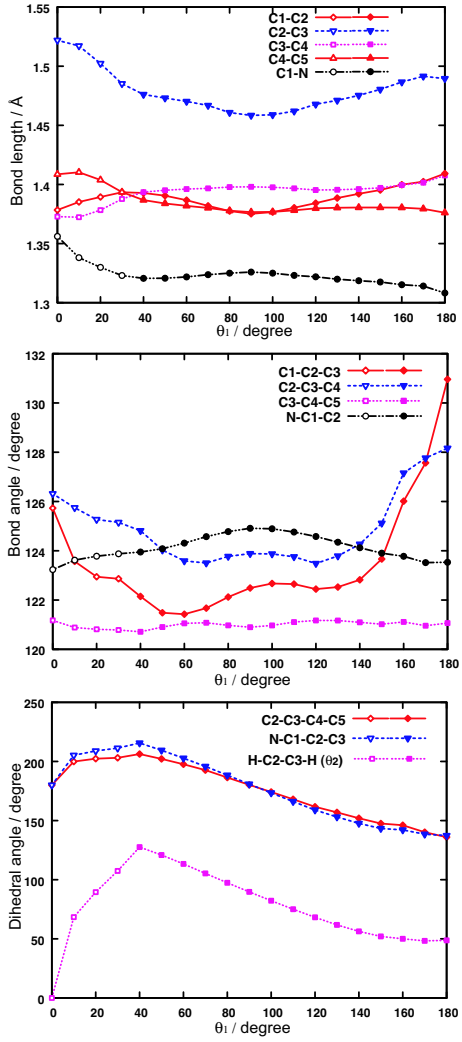

Figure 4.16: Skeletal geometric changes along relaxed S_1 PES including the S_1/S_0 DS as a function of θ_1 shown in Fig. 4.14

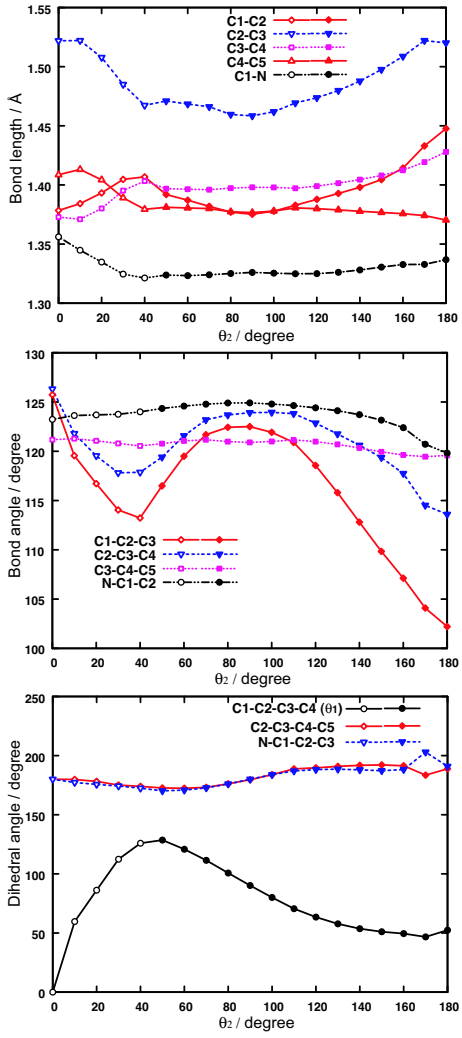

Figure 4.17: Skeletal geometric changes along relaxed S_1 PES including the S_1/S_0 DS as a function of θ_2 shown in Fig. 4.15

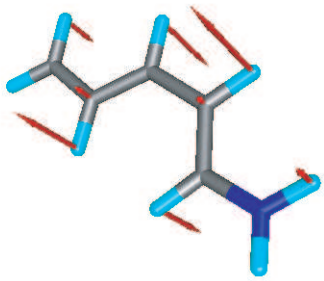

Figure 4.18: Normal mode of vibration of Z-PDI* which have an imaginary frequency (312i cm^{-1}). Clearly, the main component is the A_2 HOOP motion.

for the rotation about the reactive C2–C3. This result is similar to the recent result by CC2 (Ref.61) rather than the previously reported result by CASSCF or CASPT2 calculation.[8,26,36,55–57] We will elucidate whether this barrier is true or not.

As shown in Figs. 4.14 and 4.15, S_1 excited Z-PDI can also reach the S_1/S_0 DS related to Z to E isomerization by large distortion of H–C2–C3–H or C1–C2–C3–C4 dihedral angle. Since a carbon atom is much heavier than a hydrogen atom, it may be more time consuming process to reach the S_1/S_0 DS by large distortion of C1–C2–C3–C4 than by large distortion of H–C2–C3–H. Consequently, the A_2 HOOP motion in S_1 state would play a primary role to accelerate S_1 excited Z-PDI to transit to S_0 state. Thus, the control of the HOOP motion may be possibly used as a tool to tune photochemical reactivity and its efficiency as well as a substituent controls.[62]

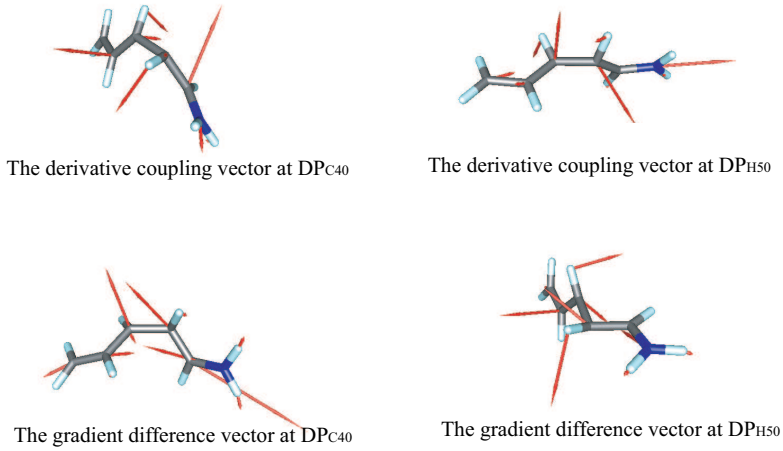

Figure 4.19: Derivative coupling and gradient difference vectors at DP_{C40} (left) and DP_{H50} (right) calculated by CAS/6-31G*

Origin of the barrier on the S_1 PES

It is necessary to ascertain whether the existence of barriers at $\theta_1 = 10°$ and $\theta_2 = 10°$ are true or not because the existence of these barriers are possibly due to the incompleteness of geometry optimization. Hence, we checked these barriers by geometry optimization and vibrational analysis using SAC-CI/6-31G*. It is too expensive to carry out geometry optimization at all points. Thus, we carried out the geometry optimization at Z-PDI*, $\theta_1 = 10°$, and $\theta_2 = 10°$. These results are summarized in Table 4.7 and main geometric parameters are given in Table 4.8. As shown in Table 4.7, each point is stabilized by 1-2 kcal mol^{-1} but the relaxed structures at $\theta_1 = 10°$ and $\theta_1 = 10°$ are still energetically higher than Z-PDI*. Therefore, Z-PDI* is evidently stable for the rotation around C2=C3 on the SAC-CI/6-31G* level. Moreover, the vibrational analysis by SAC-CI/6-31G* shows that Z-PDI* does not have imaginary frequencies. That is, Z-PDI* is the real minimum structure on the S_1 PES which traps the S_1 excited Z-PDI.

What is the origin of this barrier? We considered the following possibilities: (i)

Table 4.7: Result of geometry optimization on Z-PDI*, $\theta_1 = 10°$, and $\theta_2 = 10°$ by SAC-CI/6-31G*

Species	State	$E_{\mathrm{SAC-CI}}$[a]	$E_{\mathrm{SAC-CI}}$[b]
Z-PDI*	S_0	−248.73462(18.3)	−248.74621(11.0)
	S_1	−248.61622(92.6)	−248.61693(92.1)
	S_2	−248.49327(169.7)	−248.49136(167.2)
RS at $\theta_1 = 10°$[c]	S_0	−248.66644(61.0)	−248.68486(49.5)
	S_1	−248.58203(114.0)	−248.58491(112.2)
	S_2	−238.47351(118.1)	−248.48256(176.4)
RS at $\theta_2 = 10°$[d]	S_0	−248.67776(54.0)	−248.68255(50.9)
	S_1	−248.58296(113.4)	−248.58381(112.9)
	S_2	−248.48957(172.1)	−248.47923(178.5)

a) SAC-CI//CAS/6-31G* energy (geometry optimized by CAS/6-31G*) in atomic unit. The value of parentheses is relative energy for Z-PDI (planar) in kcal mol^{-1}.

b) SAC-CI/6-31G* energy (geometry optimized by SAC-CI/6-31G*) in atomic unit. The value of parentheses is relative energy for Z-PDI (planar) in kcal mol^{-1}.

c) The relaxed structure at $\theta_1 = 10°$

d) The relaxed structure at $\theta_2 = 10°$

Table 4.8: Geometric parameters of Z-PDI*, relaxed structure (RS) at $\theta_1 = 10°$ and $\theta_2 = 10°$ optimized by CAS/6-31G* or SAC-CI/6-31G*

	Z-PDI*		RS at $\theta_1 = 10°$		RS at $\theta_2 = 10°$	
	CAS	SAC-CI	CAS	SAC-CI	CAS	SAC-CI
Bond lengths (Å)						
C1–C2	1.3784	1.3906	1.383	1.3812	1.3842	1.3864
C1–N	1.3561	1.3419	1.3326	1.3343	1.3448	1.3357
C2–C3	1.5219	1.4817	1.5137	1.5081	1.5221	1.5104
C3–C4	1.3728	1.3892	1.3698	1.3738	1.3710	1.3719
C4–C5	1.4086	1.3901	1.4004	1.3951	1.4131	1.4014
Bond angles (°)						
C2–C1–N	123.236	122.691	123.147	123.299	123.626	123.830
C1–C2–C3	125.732	125.800	124.008	124.076	119.570	119.928
C2–C3–C4	126.320	125.470	125.833	124.684	121.800	122.187
C3–C4–C5	121.172	121.242	120.908	120.009	121.277	121.291
Dihedral angles (°)						
N–C1–C2–C3	180.0	180.0	−159.82	160.38	177.29	177.77
C1–C2–C3–C4	0.0	0.0	10.0	10.0	59.66	57.87
C2–C3–C4–C5	180.0	180.0	−162.67	162.60	−179.79	−178.80
H–C2–C3–H	0.0	0.0	57.62	52.53	10.0	10.0

The barrier is induced by the interaction between the S_1 and the second excited state (S_2). Namely, three-state is involved in the photoisomerization as suggested in the all-trans to 12-cis photoisomerization in bacteriorhodopsin.[63] (ii) In SAC-CI/6-31G*, the double bond of C2=C3 does not become so weak that the rotation around C2=C3 is possible by S_0 to S_1 excitation.

The reason (i) is immediately ruled out because S_2 and S_1 is sufficiently separated energetically as shown in Table 4.7. Its energetic difference is larger than 60 kcal mol^{-1}. On the other hand, the reason (ii) seems plausible. Since CASSCF method is known to emphasize the character of the originally unoccupied orbitals,[25] the result of CASSCF in Z-PDI* is possibly an artifact. As shown in Table 4.8, C2=C3 bond length of Z-PDI* by SAC-CI/6-31G* is 1.482 Å which is shorter than that by CASSCF/6-31G* (1.522 Å). Therefore, we suggest that this barrier is due to the breaking of the π-bond between C2–C3. This barrier may be involved in the multi-exponential decays on S_1 state in 11-cis RPSB.[64]

Bypass from DP_{C40} neighborhood to E-PDI on S_0 PES

A bypass from DP_{C40} to E-PDI on the S_0 PES which seems to be geometrically connected to these appeared in the S_1 relaxed scan is found. Here, the "bypass" means the reaction path where Z $\leftrightarrow$ E isomerization transition states (TSs) on the S_0 PES are not involved.

Two TSs on the S_0 PES were located in the direction of the positive and negative derivative coupling vector at the LEDP. The moiety of C3–C4–C5 is positively charged in the one and the moiety of N–C1–C2 (N-tail) positively charged in the other. The imaginary frequencies in TS_1 and TS_2 are 907i and 537i cm^{-1} respectively (single-state CASSCF calculation). These frequencies correspond to rotation around C2–C3. Two TSs on the S_0 PES were located in the direction of the positive. TS_1 and TS_2 are located 60 kcal mol^{-1} in SAC-CI (50 kcal mol^{-1} in CASSCF) higher than Z-PDI on the S_0 PES. TS_1 and TS_2 are enough for separating Z- from E-PDI. The single-state CASSCF calculation indicates that TS_2 is more stable than TS_1 by 0.21 kcal mol^{-1}. S_1/S_0 state-averaged energy is needed for comparison with other species. In the S_1/S_0 state-averaged calculation, relative position is reversed on S_0 PES between TS_1 and TS_2; TS_2 is more unstable than TS_1 by 1.48 kcal mol^{-1}. Moreover, electronic structure is also reversed. In the single-state calculation, a pos-

itive charge in TS_1 is located on the N-tail (0.843) and the positive charge in TS_2 is located on the C-tail (0.776). On the other hand, in the state-averaged calculation, these electronic structures are completely alternated. In TS_1, C-tail carries the positive charge of 0.9315 while N-tail carries the positive charge of 0.9832 in TS_2. Moreover, in SAC-CI, the C-tail at both TS_1 and TS_2 is positively charged. Similar situation was seen in other model systems.[65] More detailed exploration is necessary about TS_1 and TS_2. However, this issue is left for future works.

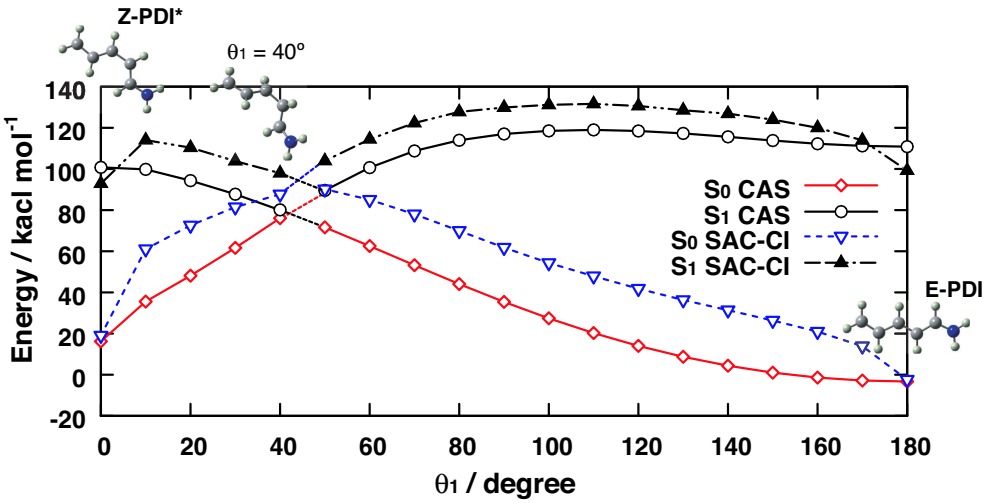

Figure 4.20: Relaxed S_1 and S_0 PES as a function of θ_1 by CAS/6-31G* and SAC-CI//CAS/6-31G*

In Fig. 4.20, we show the result of the relaxed scan calculation as a function of θ_1 from Z-PDI* to S_0 E-PDI. The geometrical change corresponding to Fig. 4.20 is shown in Fig. 4.21. This relaxed scan suggests the existence of a bypass since TS_1 and TS_2 are not involved. The S_1 relaxed structure at $\theta_1 = 40°$ seems to be geometrically connected with the S_0 relaxed structure at $\theta_1 = 50°$ though the relaxed structure at $\theta_1 = 40°$ is not connected geometrically with the DP at $\theta_1 = 50°$. As shown in Fig. 4.21 geometrical anomaly can be seen at $\theta_1 = 50°$ mainly in C2–C3–C4. This anomaly may be due to the conical intersection. That is to say, the derivative coupling and gradient difference vector strongly influence the geometry optimization around $\theta_1 = 50°$. The abnormal geometric change means the abnormal change in the electronic structure of the molecule. In Fig. 4.22, we plot the summarized Mulliken charge population of N-tail and C-tail along the S_1/S_0 relaxed

PES of Fig. 4.20. Clearly, The electronic structure at $\theta_1 = 50°$ is strange. More detailed exploration around $\theta_1 = 50°$ is necessary for detailed discussion. However, except for the S_0 relaxed structure at $\theta_1 = 50°$, the electronic structure seems to continuously change as a function of θ_1. Therefore, we believe that this relaxed scan result is informative.

According to Fig. 4.21, the correlation between θ_1 and θ_2 can be seen. Namely, θ_2 is changed from 0° to 180° inducing the distortion of θ_1. The distortion of θ_2 reaches the ceiling after switching the state for geometry optimization from the S_1 to S_0 state. The distortion of C1–C2–C3–C4 mainly occurs on S_0 state. Therefore, the result of relaxed scan along θ_1 is plausible as the reaction path way where the fast decay is mediated by the A_2 HOOP motion that strongly coupled with skeletal structure of PDI. In other words, the result of this relaxed scan along θ_1 is compatible with the suggested mechanism by Kukura et al. As shown in Fig .4.20, there is no barrier in the area between $\theta_1 = 50°$ and 180° in both CAS/6-31G* and SAC-CI//CAS/6-31G*. There are no barriers that interrupt the isomerization except for the barrier on the S_1 state around $\theta_1 = 10°$. Therefore, after S_1 to S_0 deactivation around DP_{C40}, absorbed photon energy can be used as the energy of molecular vibration, which possibly induces another reaction or conformational change of the protein. We have estimated that this excess energy available as the vibrational energy in the S_0 state. As mentioned above, it may be difficult for planar Z-PDI on the S_0 state. Hence, we have located the S_0 relaxed structure at $\theta_1 = 10°$ [Z-PDI (twist) in Table 4.6]. We regarded the S_1 vertical excited energy from Z-PDI (twist) as the photon energy. The S_1 vertical excitation energy from Z-PDI (twist) is 98.7 kcal mol^{-1} in SAC-CI result while DP_{C40} lies about 14.3 kcal mol^{-1} below the S_1 excitation energy of Z-PDI (twist). Therefore, no less than 85.5% of the absorbed energy can be used ideally as the vibration energy in S_0 state. This is higher than that of the energy stored in bathorhodopsin (about 60%).[21,31,44] On the other hand, when S_1 to S_0 transition occurs at LEDP, at least 54.1% of the absorbed photo energy can be used as the vibrational energy in S_0 state. Another system anticipated to undergo cis $\leftrightarrow$ trans photoisomerization initiated by the fast HOOP motion is maleic and fumaric anion radical system.[66] In this system, 48.8% photon energy can be used as the molecular vibration energy due to the A_2 HOOP motion on the first excited state.

4.3.4 Summary

We have found the barriers on the S_1 PES that may appear in the initial part of reaction pathway of Z-PDI through SAC-CI//CAS/6-31G*. The existence of barrier may prevent Z-PDI from isomerizing to E-PDI when Z-PDI is planar in the ground state. However, if Z-PDI is slightly twisted around the reactive C2=C3, it is possible for the S_1 excited Z-PDI to reach the S_1/S_0 DS by the A_2 H–C2–C3–H HOOP motion that is related to the Z $\leftrightarrow$ E photoisomerization. On the other hand, it is also possible for the S_1 exited Z-PDI to reach the S_1/S_0 DS by C1–C2–C3–C4 distortion. However, the S_1 excited PDI can reach the S_1/S_0 DS by H–C2–C3–H HOOP motion faster than by C1–C2–C3–C4 distortion because carbon atom is much heavier than a hydrogen atom. Consequently, the HOOP mode in the S_1 state plays a role to accelerate the S_1 to S_0 transition. Moreover, this HOOP motion is strongly coupled with the skeletal change of Z-PDI. Therefore, our calculation is compatible with the suggestion by Kukura et al. Finally, we have summarized the 11-cis to all-trans photoisomerization of RPSB in Fig. 4.23, which is imagined through our calculation on PDI.

It is necessary for the 11-cis RPSB in S_0 state to be twisted around the reactive C=C. Otherwise, quantum yield of the 11-cis to all-trans photoisomerization may be low. Even if the 11-cis RPSB in S_0 state is twisted, a few S_1 excited 11-cis RPSBs go back to the S_1 planar 11-cis RPSB inducing the fluorescence. Because the quantum yields of the fluorescence is very small (0.9×10^{-6}),[67] the S_1 FC point may lie in the side of S_1/S_0 conical intersections. After the excitation to the S_1 state, bond alternation occurs leading to the S_1 TS. From the S_1 TS, the rotation around the reactive C=C is started. Most S_1 excited 11-cis RPSB can reach the S_1/S_0 conical intersection by the A_2 HOOP motion but a few S_1 excited 11-cis RPSB goes back to the S_1 planar 11-cis RPSB inducing the fluorescence. After the S_1 to S_0 decay, the change of the skeletal structure of RPSB occurs on the S_0 state.

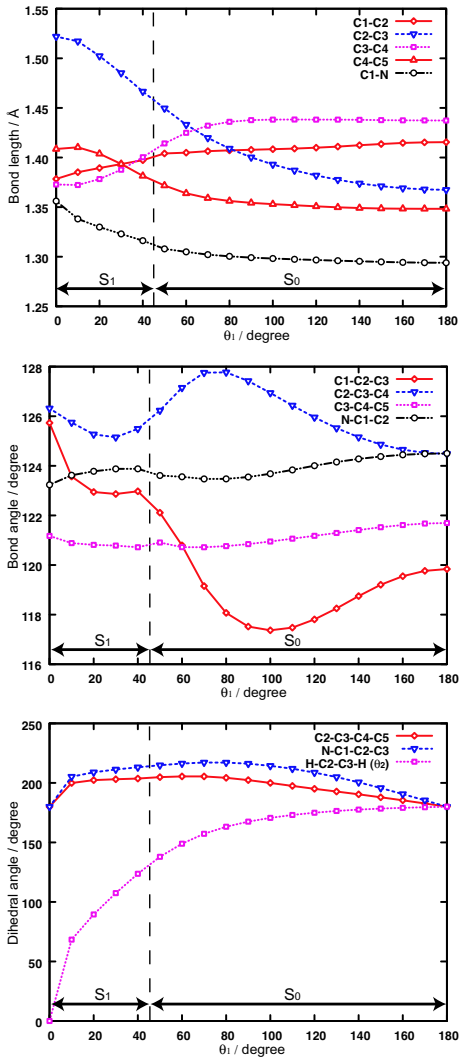

Figure 4.21: Skeletal geometric changes along relaxed S_1 and S_0 PES as a function of θ_1 shown in Fig. 4.20.

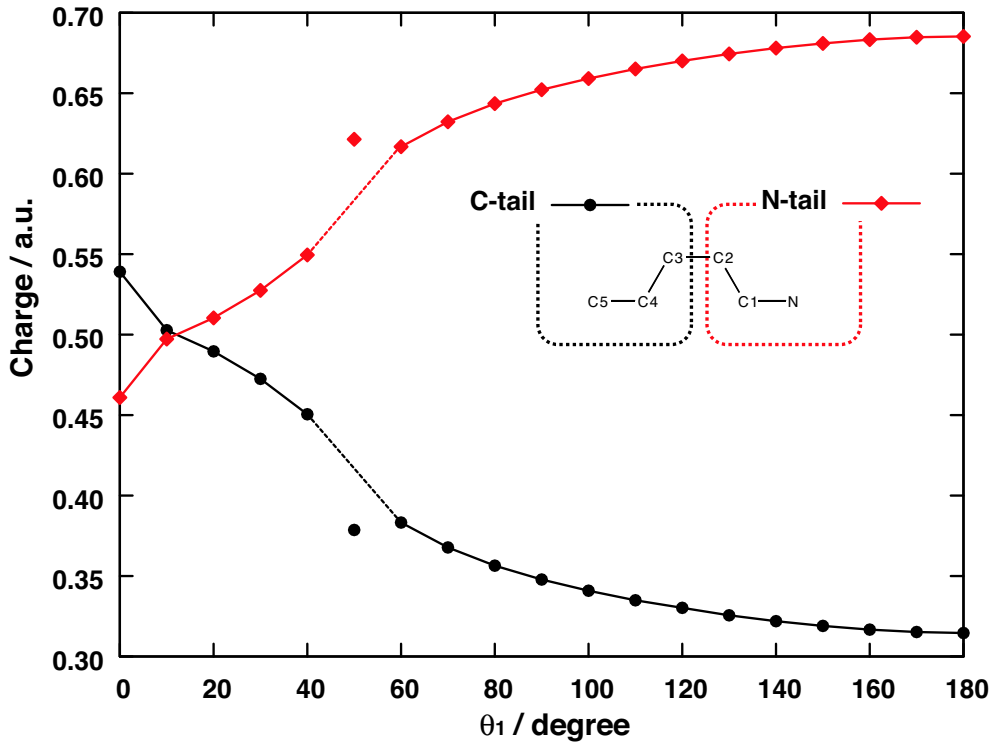

Figure 4.22: Summarized Mulliken charge population on the N-tail and C-tail along the S_1/S_0 relaxed PES (Fig. 4.20).

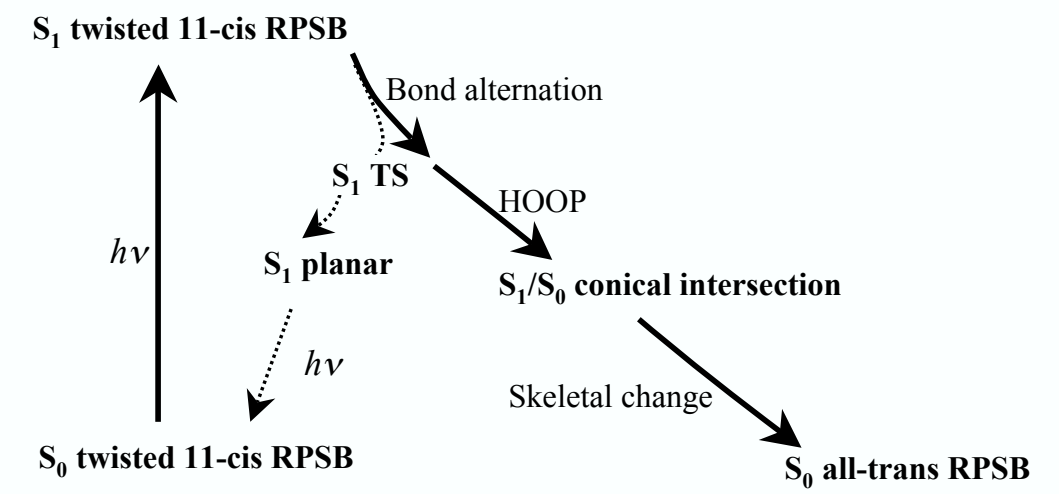

Figure 4.23: Schematic energy diagram for the 11-cis to all-trans photoisomerization of RPSB. It is necessary for effective photoisomerization that 11-cis RPSB is twisted around the reactive C=C bond.

References

[1] A. Migani, M. Olivucci, *Conical Intersection and Organic Reaction mechanisms. In Conical Intersections: Electronic Structure, Dynamics & Spectroscopy; Advance Series in Physical Chemistry Vol. 15*; W, Domcke, D. R. Yarkony, H. Köppel (Eds.); World Scientific: Singapore, 2004; p 271.

[2] L. Blancafort, D. Gonzalez, M. Olivucci, M. A. Robb, *J. Am Chem. Soc.* **124**, 6398(2002).

[3] D. R. Yarkony, *Conical Intersection: Their Description and Consequences. In Conical Intersections: Electronic Structure, Dynamics & Spectroscopy; Advance Series in Physical Chemistry Vol. 15*; W. Domcke, D. R. Yarkony, H. Köppel (Eds.); World Scientific: Singapore, 2004; p 41.

[4] F. Bernardi, M. Olivucci, M. A. Robb, *Chem. Soc. Rev.* **25**, 321(1996).

[5] I. N. Ragazos, M. A. Robb, F. Bernardi, M. Olivucci, *Chem. Phys. Lett.* **197**, 217(1997).

[6] M. J. Bearpark, M. A. Robb, H. B. Schlegel, *Chem. Phys. Lett.* **223**, 269 (1994).

[7] M. Dallos, H. Lischka, R. Shepard, D. R. Yarkony, P. G. Szalay, *J. Chem. Phys.* **120**, 7330(2004).

[8] A. Migani, M. A. Robb, M. Olivucci, *J. Am. Chem. Soc.* **125**, 2804(2003).

[9] A. Venturini, T. Vreven, F. Bernardi, M. Olivucci, M. A. Robb, *Organometallics*, **14**, 4953(1995).

[10] O. Takahashi, M. Sumita, *J. Chem. Phys.* **121**, 7030(2004).

[11] O. Takahashi, M. Sumita, *J. Mol. Struct.: Theochem*, **731**, 173(2005).

[12] (a) M. Ben-Nun, T. J. Martinez, *Chem. Phys.* **259**, 237(2000). (b) D. S. Ruiz, A. Cenbran, M. Garavelli, M. Olivucci, W. Fuβ, *Photochem Photobiol.* **76**, 622(2002). P. A. Hunt, M. A. Robb, *J. Am. Chem. Soc.* **127**, 5720(2005).

[13] A. Torikai, T. Suzuki,T. Miyazaki,K. Fueki, Z. Kuri, *J. Phys. Chem.* **75**, 482 (1971). A. Torikai, F. Nakano, K. Fueki, Z. Kuri, *Bull. Chem. Soc. Jpn.* **48**, 339 (1975).

[14] E. Hayon, M. Simic, *J. Am. Chem. Soc.* **95**, 2433 (1073).

[15] T. Shida, W. H. Hamill, *J. Chem. Phys.* **44**, 4372 (1966).

[16] S. F. Nelsen, *Tetrahedron Lett.* **39**, 3795 (1967).

[17] A. P. Doherty, K. J. Scott, *Electoanal. Chem.* **442**, 35 (1998).

[18] B. O. Roos, P. R. Taylor, P. E. M. Siegbahn, *Chem. Phys.* **48**, 157(1980). B. O. Roos, *The Multiconfigurational Self-Consistent Field Theory. In Lecture Notes in Quantum Chemistry (European Summer School in Quantum Chemistry*, B. O. Roos, Ed: Springer-Verlag Berlin Heidelberg 1992, p 177.

[19] O. Takahashi, O. Kikuchi, *J. Chem. Phys.* **100**, 1350 (1994).

[20] D. R. Yarkony, *Acc. Chem. Res.* **31**, 511 (1998).

[21] P. Kukura, D.W. McCamant, S. Yoon, D. B. Wandschneider, R. A. Mathies, *Science*, **310**, 1006 (2005).

[22] M. A. Matos, M. S. Miranda, V. M. F. Morais, J. F. Liebman, *Org. Biomol. Chem.* **1**, 2930 (2003). E. M. S. Macoas, R. Fausto, J. Lundell, M. Pettersson, L. Khriachtchev, M. Rasanen, *J. Phys. Chem. A*, **105**, 3922 (2001). W. O. George, A. J. Porter, *J. Chem. Soc., Perkin II*, 954(1973). D. A. C. Compton, W. O. George, A. J. Porter, *J. Chem. Soc., Perkin II*, 400 (1075). H. G. Buge, P. Peich, E. J. Steger, *J. Mol. Struct.* **35**, 175(1976).

[23] H. I. Elson, T. J. Kemp, D. Greatorex, H. D. B. J. Jenkins, *J. Chem. Soc., Faraday Trans.* **69**, 1402(1973). S. F. Nelsen, J. P. Gillespie, *J. Org. Chem.* **40**, 2391(1975).

[24] M. J. Frisch, G. W. Trucks, H. B. Schlegel, G. E. Scuseria, M. A. Robb, J. R. Cheeseman, V. G. Zakrzewski, J. A. Montgomery, Jr., R. E. Stratmann, J. C. Burant, S. Dapprich, J. M. Millam, A. D. Daniels, K. N. Kudin, M. C. Strain, O. Farkas, J. Tomasi, V. Barone, M. Cossi, R. Cammi, B. Mennucci, C. Pomelli, C. Adamo, S. Clifford, J. Ochterski, G. A. Petersson, P. Y. Ayala, Q. Cui, K. Morokuma, N. Rega, P. Salvador, J. J. Dannenberg, D. K. Malick, A. D. Rabuck, K. Raghavachari, J. B. Foresman, J. Cioslowski, J. V. Ortiz, A. G. Baboul, B. B. Stefanov, G. Liu, A. Liashenko, P. Piskorz, I. Komaromi, R. Gomperts, R. L. Martin, D. J. Fox, T. Keith, M. A. Al-Laham, C. Y. Peng, A. Nanayakkara, M. Challacombe, P. M. W. Gill, B. Johnson, W. Chen, M. W. Wong, J. L. Andres, C. Gonzalez, M. Head-Gordon, E. S. Replogle, and J. A. Pople, Gaussian 98, Revision A.11.3, Gaussian, Inc., Pittsburgh PA, 2002.

[25] K. Andresson, B. O. Roos, *Multiconfigurational second-order perturbation theory. In Modern Electronicl Structure Theory Part I*; Advance Series in Physical Chemistry Vol. 2; D. R. Yarkony, Ed.; World Scientific: Singapore, 1995; p 55.

[26] (a)M. Garavelli, P. Celani, F. Bernardi, M. A. Robb, M. Olivucci, *J. Am. Chem. Soc.* **119**, 6891(1997). (b)M. Garavelli, T. Vreven, P. Celani, F. Bernardi, M. A. Robb, *J. Am. Chem. Soc.* **120**, 1285(1998).

[27] O. Takahashi, O. Kikuchi, *J. Mol. Struct.: Theochem*, **313**, 207(1994). T. Oshiyama, O. Takahashi, K. Morihashi, O. Kikuchi, K. Tokumaru, *Bull. Chem. Soc. Jpn.* **66**, 1622(1993). O. Kikuchi, T. Oshiyama, O. Takahashi, K. Tokumaru, *Bull. Chem. Soc. Jpn.* **65**, 2267(1992).

[28] G. J. Bischof, S. S. Xantheas, K. Ruedenberg, *J. Chem. Phys.* **95**, 1862(1991).

[29] H. Hettema, D. R. Yarkony, *J. Chem. Phys.* **102**, 8431(1995).

[30] R. W. Schoenlein, L. A. Peteanu, R. A. Mathies, *Science*, **412**, 254 (1991)

[31] J. Lugtenburg, R. Mathies, in: D. G. Stavenga, W. J. Grip, E. N. Pugh (Eds.), *Handbook of Biological Physics*, vol. 3, Elsevier, Amsterdam, 2000, p. 55.

[32] T. Andruniów, N. Ferré, M. Olivucci, *Proc. Natl. Acad. Sci. USA*, **101**, 17908(2004).

[33] R. S. H. Liu, A. E. Asato, *Proc. Natl. Acad. Sci. USA*, **82**, 259(1985) .

[34] M. Garavelli, F. Bernardi, M.A. Robb, M. Olivucci, *J. Mol. Struct.: Theochem*, **463**, 59(1999).

[35] M. Garavelli, F. Bernardi, P. Celani, M.A. Robb, M. Olivucci, *J. Photochem. Photobiol. A*, **114**, 109(1998).

[36] O. Weingart, A. Migani, M. Olivucci, M.A. Robb, V. Buss, P. Hunt, *J. Phys. Chem. A*, **108**, 4695(2004).

[37] O. Wilsey, K. H. Houk, *Photochem. Photobiol.* **76**, 616(2002).

[38] M. Ben-Nun, T. J. Martinez, *Chem. Phys.* **259**, 237(2000).

[39] P. Celani, M. Garavelli, S. Ottani, F. Bernardi, M. A. Robb, M. Olivucci, *J. Am. Chem. Soc.* **117**, 11584(1995).

[40] J. R. Ackerman, S. A. Forman, M. Hossain, B. Kohler, *J. Chem. Phys.* **80**, 39(1984).

[41] D. S. Ruiz, A. Cembran, M. Garavelli, M. Olivucci, W. Fuβ, *Photochem. Photobiol.* **76**, 622(2002).

[42] W. Fuβ, C. Kosmidis, W.E. Schmid, S.A. Trushin, *Angew. Chem. Int. Ed.* **43**, 4178(2004).

[43] R. Needlman, In *CRC Handbook of Organic Photochemistry and Photobiology*; W. M. Horpool, P. S. Song, Eds.; CRC press: Boca Raton, Fl, 1995, p 1508.

[44] H. Kandori,Y. Shichida, T. Yoshizawa, *Biochemistry (Moscow)*, **66**, 1483 (2001).

[45] (a) R. S. Becker, K. Freedman, *J. Am. Chem. Soc.* **107**, 1477(1985). (b) Y. Koyama, K. Kubo, M. Komori, H. Yasuda, Y. Mukai, *Photochem. Photobiol.* **54**, 433(1991).

[46] K. Palczewski, T. Kumasaka, T. Hori, C. A. Behnke, H. Motoshima, B.A. Fox, I. L. Trong, D. C. Teller, T. Okada, R. E. Stenkamp, M. Yamamoto, M. Miyano, *Science*, **289**, 739(2000).

[47] (a) S. O. Smith, I. Palings, M. E. Miley, J. Courtin, H. de Groot, J. Lugtenburg, R. A. Mathies, R. G. Griffin, *Biochem.* **29**, 8158 (1990). (b) S. O. Smith, J. Courtin, H. de. Groot, R. Gebhard, J. Lugtenburg, *Biochem.* **30**, 7409(1991).

[48] N. Ferré, M. Olivucci, *J. Am. Chem. Soc.* **125**, 6868 (2003).

[49] A. Cembran, R. González-Luque, P. Altoè, M. Merchán, F. Bernardi, M. Olivucci, M. Gravelli, *J. Phys. Chem. A*, **109**, 6597(2005).

[50] R. Mathies, R. B. Freedman, L. Stryer, *J. Mol. Biol.* **109**, 367(1977).

[51] S. W. Lin, M. Groesbeek, I. van der Hoef, P. Verdegem, J. Lugtenbureg, R. A. Mathies, *J. Phys. Chem. B*, **102**, 2787(1998).

[52] T. Kakitani, R. Akiyama, Y. Hatano, Y. Imamoto, Y. Shichida, P. Verdegem, J. Lugtenburg, *J. Phys. Chem. B*, **102**, 1334(1998).

[53] L. M. Frutos, T. Andruniów, F. Santoro, N. Ferré, M. Olivucci, *Proc. Natl. Acad. Sci. USA*, **104**, 7764(2007).

[54] (a) H. Nakatsuji, M. Ehara, *J. Chem. Phys.* **98**, 7179(1993). (b) H. Nkatsuji, K. Hirao, *J. Chem. Phys.* **68**, 2053(1978).

[55] M. Garavelli, F. Bernardi, M. Olivucci, T. Vreven, K. Stephane, P. Celani, M. A. Robb, *Faraday Discuss*, **110**, 51(1998).

[56] S. Fantacci, A. Migani, M. Olivucci, *J. Phys. Chem. A*, **108**, 1208(2004).

[57] (a) R. González-Luque, M. Gravelli, F. Bernardi, M. Merchan, M. A. Robb, M. Olivucci, *Proc. Natl. Acad. Sci. USA*, **97**, 9379(2000). (b) A. Cembran, R. González-Luque, L. Serrano-Andrés, M. Merchán, M. Garavelli, *Theor. Chem. Acc.* **118**, 173(2007).

[58] A. Cembran, F. Bernardi, M. Olivucci, M. Garavelli, *Proc. Natl. Acad. Sci. USA*, **102**, 6255(2005).

[59] M. J. Frisch, G. W. Trucks, H. B. Schlegel, G. E. Scuseria, M. A. Robb, J. R. Cheeseman, J. A. Montgomery, Jr., T. Vreven, K. N. Kudin, J. C. Burant, J. M. Millam, S. S. Iyengar, J. Tomasi, V. Barone, B. Mennucci, M. Cossi,

G. Scalmani, N. Rega, G. A. Petersson, H. Nakatsuji, M. Hada, M. Ehara, K. Toyota, R. Fukuda, J. Hasegawa, M. Ishida, T. Nakajima, Y. Honda, O. Kitao, H. Nakai, M. Klene, X. Li, J. E. Knox, H. P. Hratchian, J. B. Cross, V. Bakken, C. Adamo, J. Jaramillo, R. Gomperts, R. E. Stratmann, O. Yazyev, A. J. Austin, R. Cammi, C. Pomelli, J. W. Ochterski, P. Y. Ayala, K. Morokuma, G. A. Voth, P. Salvador, J. J. Dannenberg, V. G. Zakrzewski, S. Dapprich, A. D. Daniels, M. C. Strain, O. Farkas, D. K. Malick, A. D. Rabuck, K. Raghavachari, J. B. Foresman, J. V. Ortiz, Q. Cui, A. G. Baboul, S. Clifford, J. Cioslowski, B. B. Stefanov, G. Liu, A. Liashenko, P. Piskorz, I. Komaromi, R. L. Martin, D. J. Fox, T. Keith, M. A. Al-Laham, C. Y. Peng, A. Nanayakkara, M. Challacombe, P. M. W. Gill, B. Johnson, W. Chen, M. W. Wong, C. Gonzalez, and J. A. Pople, Gaussian, Inc., Wallingford CT, 2004. Gaussian 03, Revision D.02.

[60] (a) M. Sumita, K. Saito, *Chem. Phys. Lett.* **424**, 374(2006). (b) M. Sumita, K. Saito, *J. Chem. Theory Comput.* **4**, 42(2008).

[61] R. Send, D. Sundholm, *J. Phys. Chem A*, **111**, 8766(2007).

[62] I. Conti, M. Garavelli, *J. Photochem. Photobiolo. A*, **190**, 258(2007).

[63] K. C. Hasson, F. Gai, P. A. Anfinrud, *Proc. Natl. Acad. Sci. USA*, **93**, 15124(1996).

[64] (a) M. Yan, L. Rothberg, R. Callender, *J. Phys. Chem. B*, **105**, 856(2001). (b) H. Kandori, Y. Furutani, S. Nishimura, Y. Shichida, H. Chosrowjan, Y. Shibata, N. Mataga, *Chem. Phys. Lett.* **334**, 271(2001). (c) M. Olivucci, A. Lami. F. Santoro, *Angew. Chem. Int. Ed.* **44**, 5118(2005). (d) F. Santoro, A. Lami, M. Olivucci, *Theor. Chem. Acc.* **117**, 1061(2007).

[65] L. D. Vico, C. S. Page, M. Garavelli, F. Bernardi, R. Basosi, M. Olivucci, *J. Am. Chem. Soc.* **124**, 4124(2002).

[66] M. Sumita, K. Saito *J, Phys. Chem. A*, **110**, 12276(2006).

[67] (a) A. G. Doukas, M. R. Junnarker, R. R. Alfano, R. H. Callender, T. Kakitani, B. Honig, *Proc. Natl. Acad. Sci. USA*, **81**, 4790(1984). (b) G. G. Kochendoerfer, R. A. Mathies, *J. Phys. Chem.* **100**, 14526(1996).

Chapter 5

Gross Conclusion

The motivation of this work lies on the question, i.e., how will the interpreation of chemical reaction process change by taking degeneracy space into account? Degeneracy point is crucial for discussion in chemical reaction where non-adiabatic phenomena occur but it is not isolated point.

We progressed our work step by step. First of all, we proposed the computational strategy to characterize the degeneracy space. This strategy is to locate the degneracy point with geometric constraint by two step using the projected gradient method. By virtue of this strategy, it becomes possible to calculate the degeneracy space as a function of a variable. Additionally, we estimated how well energy is minimized in the intersection adapted coordinate, which is the complement space to derivative coupling and gradient difference vector. In the next step, we attempted to elucidate the influence of degeneracy space on the photochemical reaction. To this end, we selected fulvene, maleic/fumaric acid anion radical, and penta-2,4-dieniminium (PDI) as the target for research.

In fulvene, three degeneracy points between the first and ground state have been found. At the first degeneracy points, DP_{planar}, fulvene has the planar structure with C_{2v}. At the next degeneracy point, DP_{63}, the exocyclic methylene of fulvene is rotated by 63°. At the fianl degeneracy point, DP_{perp} the exocyclic methylene of fulvene is rotated by 90° with C_{2v}. DP_{planar} and DP_{63} is related to the photophisics of fulvene. On the other hand, DP_{perp} is related to 180° rotation of the exocyclic methylene. We have shown that these degeneracy points lie on the same degeneracy space. Namely, the photochemically different degeneracy points of fulvene lie in the

same degeneracy space.

In maleic/fumaric acid anion radical and Z/E-PDI, the importance of their hydrogen out-of-plane motion on the first excited state is shown. The decay from the first excited state to the ground state is mediated by their hydrogen out-of-plane motion without large skeletal arrangement. Consequently, cis-trans isomerization occurs in the ground state. In addition to the hydrogen out-of-plane motion, we have also explored the possibility of hula-twist motion of PDI. According to our calculation result, both motions play roles to accelerate the transtion from the first excited state to the ground state.

In Z/E-PDI, we also carried out the symmetry adapted cluster/configuration interaction (SAC-CI) on the optimized structure by the complete active space self-consistent field (CASSCF). Qualitative shap of the potential energy surface of SAC-CI is more reliable than that of CASSCF, because CASSCF does not consider dynamical electronic correlation. According to the SAC-CI calculation, the barrier, which prevents the first excited PDI from reaching degeneracy space related to Z $\rightarrow$ E isomerization, was found. Due to the existance of the barrier, the photoisomerization seems not to occur. However, the barrier may be circumvented by deforming the structure of PDI on the ground state. Therefore, what we can imagine from the calculation of PDI as the model system of retinal protonated Schiff base is the deformed structure in rhodopsin has a very important "catalytic" effect.

As mentionsed above, interpretation of photoreaction processes is certainly changed by considering a degeneracy space instead of a degeneracy point. We believe that more research about the degeneracy space will be needed to unvail the influence of the degneracy space to the chemical reactions The nature of "degeneracy" between the electronic states will be clarified by exploring the invariance of the molecular electronic structure in the degeneracy space. The elucidation of the nature will be useful to see the qualitative shape of potential energy surfaces without computation because the degeneracy space is the hump in the PES of the ground state.

List of published papers concerning this thesis

(1) M. Sumita, Mikhail N. Ryazantsev, and K. Saito "Acceleration of the *Z* to *E* photoisomerization of penta-2,4-dieniminium by hydrogen out-of-plane motion: Theoretical study on a model system of Retinal protonated Schiff base" *Physical Chemistry Chemical Physics*, **11**, 6406-6414, 2009.

(2) M. Sumita and K. Saito "Revisiting the S_1/S_0 degeneracy space along the exocyclic methylene twist motion of fulvene through a two-step procedure" *Journal of Chemical Theory and Computation*, **4**, 42-48, 2008.

(3) M. Sumita and K. Saito "Ab initio study on one-way photoisomerization of maleic acid and fumaric acid anion radical system as a model system of their esters" *The Journal of Physical Chemistry A*, **110**, 12276-12281, 2006.

(4) M. Sumita and K. Saito "Theoretical study on hula-twist motion of penta-2,4-dieniminium on the S_1 surface under isolated condition by the complete active space self-consistent field theory" *Chemical Physics Letters*, **424**, 374-378, 2006.

(5) O. Takahashi and M. Sumita "A note on geometric constraints in conical intersection optimizations" *Journal of Molecular Structure (Theochem)*, **731**, 173-175, 2005.

(6) O. Takahashi and M. Sumita "Characterization of the hyperline of D_1/D_0 conical intersections between the maleic acid and fumaric acid anion radicals" *The Journal of Chemical Physics*, **121** (14), 7030-7031, 2004.

Appendix A

Supporting Information

A.1 Supporting Information for Chap. 3

The Cartesian coordinates of DPs in S_1/S_0 degeneracy space by CASSCF/cc-pVDZ are tabulated. Values are given in Å.

Species DP_{planar}

C	0.000000	0.000000	0.000000
C	0.000000	0.000000	1.578236
C	1.106325	0.000000	2.389046
C	-1.106325	0.000000	2.389046
C	0.659882	0.000000	3.853343
C	-0.659882	0.000000	3.853343
H	-0.934250	0.000000	-0.537374
H	0.934250	0.000000	-0.537374
H	2.138729	0.000000	2.066918
H	-2.138729	0.000000	2.066918
H	1.331175	0.000000	4.698098
H	-1.331175	0.000000	4.698098

Species DP_5

C	0.000000	0.000000	0.000000
C	0.000000	0.000000	1.577289
C	1.106469	0.000000	2.388297
C	-1.106469	0.000000	2.388297
C	0.659987	-0.001212	3.852198
C	-0.659987	0.001212	3.852198
H	-0.930613	0.081418	-0.537555
H	0.930613	-0.081418	-0.537555
H	2.138851	0.002941	2.066149
H	-2.138851	-0.002941	2.066149
H	1.331150	-0.003925	4.697052
H	-1.331150	0.003925	4.697052

Species DP_{10}

C	0.000000	0.000000	0.000000
C	0.000000	0.000000	1.574431
C	1.106904	0.000000	2.386038
C	-1.106904	0.000000	2.386038
C	0.660307	-0.002381	3.848722
C	-0.660307	0.002381	3.848722
H	-0.919733	0.162174	-0.538098
H	0.919733	-0.162174	-0.538098
H	2.139220	0.005789	2.063829
H	-2.139220	-0.005789	2.063829
H	1.331069	-0.007698	4.693881
H	-1.331069	0.007698	4.693881

Species DP_{15}

C	0.000000	0.000000	0.000000
C	0.000000	0.000000	1.569732
C	1.107642	0.000000	2.382343
C	-1.107642	0.000000	2.382343
C	0.660854	-0.003462	3.842966
C	-0.660854	0.003462	3.842966
H	-0.901713	0.241613	-0.538985
H	0.901713	-0.241613	-0.538985
H	2.139847	0.008442	2.060032
H	-2.139847	-0.008442	2.060032
H	1.330942	-0.011204	4.688641
H	-1.330942	0.011204	4.688641

Species DP_{20}

C	0.000000	0.000000	0.000000
C	0.000000	0.000000	1.563325
C	1.108697	0.000000	2.377355
C	-1.108697	0.000000	2.377355
C	0.661656	-0.004399	3.835018
C	-0.661656	0.004399	3.835018
H	-0.876724	0.319101	-0.540185
H	0.876724	-0.319101	-0.540185
H	2.140748	0.010775	2.054889
H	-2.140748	-0.010775	2.054889
H	1.330779	-0.014299	4.681433
H	-1.330779	0.014299	4.681433

Species DP_{25}

C	0.000000	0.000000	0.000000
C	0.000000	0.000000	1.555356
C	1.110079	0.000000	2.371226
C	-1.110079	0.000000	2.371226
C	0.662742	-0.005138	3.824987
C	-0.662742	0.005138	3.824987
H	-0.844992	0.394026	-0.541667
H	0.844992	-0.394026	-0.541667
H	2.141932	0.012738	2.048546
H	-2.141932	-0.012738	2.048546
H	1.330602	-0.016772	4.672375
H	-1.330602	0.016772	4.672375

Species DP_{30}

C	0.000000	0.000000	0.000000
C	0.000000	0.000000	1.546151
C	1.111819	0.000000	2.364281
C	-1.111819	0.000000	2.364281
C	0.664169	-0.005607	3.813106
C	-0.664169	0.005607	3.813106
H	-0.806817	0.465816	-0.543358
H	0.806817	-0.465816	-0.543358
H	2.143427	0.014116	2.041309
H	-2.143427	-0.014116	2.041309
H	1.330439	-0.018508	4.661724
H	-1.330439	0.018508	4.661724

Species DP_{35}

C	0.000000	0.000000	0.000000
C	0.000000	0.000000	1.535831
C	1.113902	0.000000	2.356624
C	-1.113902	0.000000	2.356624
C	0.665972	-0.005779	3.799484
C	-0.665972	0.005779	3.799484
H	-0.762509	0.533914	-0.545257
H	0.762509	-0.533914	-0.545257
H	2.145229	0.014961	2.033299
H	-2.145229	-0.014961	2.033299
H	1.330367	-0.018885	4.649566
H	-1.330367	0.018885	4.649566

Species DP_{40}

C	0.000000	0.000000	0.000000
C	0.000000	0.000000	1.524957
C	1.116377	0.000000	2.348773
C	-1.116377	0.000000	2.348773
C	0.668222	-0.005550	3.784528
C	-0.668222	0.005550	3.784528
H	-0.712479	0.597841	-0.547244
H	0.712479	-0.597841	-0.547244
H	2.147372	0.014899	2.024971
H	-2.147372	-0.014899	2.024971
H	1.330387	-0.018300	4.636350
H	-1.330387	0.018300	4.636350

Species DP_{45}

C	0.000000	0.000000	0.000000
C	0.000000	0.000000	1.513934
C	1.119211	0.000000	2.341093
C	-1.119211	0.000000	2.341093
C	0.670991	-0.004897	3.768654
C	-0.670991	0.004897	3.768654
H	-0.657132	0.657132	-0.549266
H	0.657132	-0.657132	-0.549266
H	2.149827	0.013569	2.016673
H	-2.149827	-0.013569	2.016673
H	1.330613	-0.016399	4.622459
H	-1.330613	0.016399	4.622459

Species DP_{50}

C	0.000000	0.000000	0.000000
C	0.000000	0.000000	1.503271
C	1.122393	0.000000	2.333982
C	-1.122393	0.000000	2.333982
C	0.674311	-0.003782	3.752310
C	-0.674311	0.003782	3.752310
H	-0.596921	0.711383	-0.551238
H	0.596921	-0.711383	-0.551238
H	2.152563	0.012252	2.008775
H	-2.152563	-0.012252	2.008775
H	1.331092	-0.012855	4.608326
H	-1.331092	0.012855	4.608326

Species DP_{55}

C	0.000000	0.000000	0.000000
C	0.000000	0.000000	1.493509
C	1.125860	0.000000	2.327842
C	-1.125860	0.000000	2.327842
C	0.678215	-0.002273	3.736089
C	-0.678215	0.002273	3.736089
H	-0.532313	0.760221	-0.553080
H	0.532313	-0.760221	-0.553080
H	2.155524	0.010197	2.001666
H	-2.155524	-0.010197	2.001666
H	1.331928	-0.007710	4.594475
H	-1.331928	0.007710	4.594475

Species DP_{60}

C	0.000000	0.000000	0.000000
C	0.000000	0.000000	1.485220
C	1.129504	0.000000	2.323078
C	-1.129504	0.000000	2.323078
C	0.682679	-0.000449	3.720684
C	-0.682679	0.000449	3.720684
H	-0.463799	0.803323	-0.554695
H	0.463799	-0.803323	-0.554695
H	2.158582	0.008277	1.995674
H	-2.158582	-0.008277	1.995674
H	1.333134	-0.001015	4.581552
H	-1.333134	0.001015	4.581552

Species DP_{63}

C	0.000000	0.000000	0.000000
C	0.000000	0.000000	1.481038
C	1.131837	0.000000	2.320944
C	-1.131837	0.000000	2.320944
C	0.685736	0.000753	3.711763
C	-0.685736	-0.000753	3.711763
H	-0.418976	0.827349	-0.555538
H	0.418976	-0.827349	-0.555538
H	2.160519	0.006921	1.992676
H	-2.160519	-0.006921	1.992676
H	1.334117	0.003541	4.574186
H	-1.334117	-0.003541	4.574186

Species DP_{65}

C	0.000000	0.000000	0.000000
C	0.000000	0.000000	1.479010
C	1.133215	0.000000	2.320033
C	-1.133215	0.000000	2.320033
C	0.687620	0.001450	3.706867
C	-0.687620	-0.001450	3.706867
H	-0.391892	0.840415	-0.555958
H	0.391892	-0.840415	-0.555958
H	2.161653	0.006187	1.991215
H	-2.161653	-0.006187	1.991215
H	1.334777	0.006255	4.570198
H	-1.334777	-0.006255	4.570198

Species DP_{70}

C	0.000000	0.000000	0.000000
C	0.000000	0.000000	1.475332
C	1.136803	0.000000	2.318875
C	-1.136803	0.000000	2.318875
C	0.692859	0.003060	3.695457
C	-0.692859	-0.003060	3.695457
H	-0.317112	0.871259	-0.556763
H	0.317112	-0.871259	-0.556763
H	2.164557	0.004320	1.988436
H	-2.164557	-0.004320	1.988436
H	1.336861	0.012820	4.561098
H	-1.336861	-0.012820	4.561098

Species DP_{75}

C	0.000000	0.000000	0.000000
C	0.000000	0.000000	1.474348
C	1.140039	0.000000	2.319561
C	-1.140039	0.000000	2.319561
C	0.698049	0.004010	3.687167
C	-0.698049	-0.004010	3.687167
H	-0.239986	0.895639	-0.557044
H	0.239986	-0.895639	-0.557044
H	2.167093	0.003540	1.987427
H	-2.167093	-0.003540	1.987427
H	1.339218	0.016622	4.554858
H	-1.339218	-0.016622	4.554858

Species DP_{80}

C	0.000000	0.000000	0.000000
C	0.000000	0.000000	1.475559
C	1.142636	0.000000	2.321586
C	-1.142636	0.000000	2.321586
C	0.702469	0.003802	3.682077
C	-0.702469	-0.003802	3.682077
H	-0.161050	0.913357	-0.556863
H	0.161050	-0.913357	-0.556863
H	2.169122	0.002913	1.988014
H	-2.169122	-0.002913	1.988014
H	1.341410	0.015870	4.551418
H	-1.341410	-0.015870	4.551418

Species DP_{85}

C	0.000000	0.000000	0.000000
C	0.000000	0.000000	1.477181
C	1.144307	0.000000	2.323435
C	-1.144307	0.000000	2.323435
C	0.705576	0.002303	3.679544
C	-0.705576	-0.002303	3.679544
H	-0.080849	0.924107	-0.556596
H	0.080849	-0.924107	-0.556596
H	2.170388	0.001410	1.988766
H	-2.170388	-0.001410	1.988766
H	1.343163	0.010008	4.549934
H	-1.343163	-0.010008	4.549934

Species DP_{perp}

C	0.000000	0.000000	0.000000
C	0.000000	0.000000	1.478002
C	1.144879	0.000000	2.324275
C	-1.144879	0.000000	2.324275
C	0.706678	-0.000001	3.678872
C	-0.706678	0.000001	3.678872
H	0.000000	0.927723	-0.556449
H	0.000000	-0.927723	-0.556449
H	2.170814	-0.000010	1.989221
H	-2.170814	0.000010	1.989221
H	1.343793	-0.000004	4.549641
H	-1.343793	0.000004	4.549641

A.2 Supporting Information for Sec. 4.1

The Cartesian coordinates of the stationary points in the D_1 and D_0 states and the D_1/D_0 degeneracy points which discussed in the text by CASSCF/cc-pVDZ are tabulated. Values are given in Å.

Species: D_0 $MA^{-\bullet}$

C	0.000000	0.000000	0.000000
C	0.000000	0.000000	1.409655
C	1.064701	0.000000	-0.946554
C	1.064701	0.000000	2.356208
O	2.269197	0.000000	-0.809799
O	2.269197	0.000000	2.219454
O	0.584002	0.000000	-2.247012
O	0.584002	0.000000	3.656667
H	-0.978378	0.000000	-0.464330
H	-0.978378	0.000000	1.873985
H	1.365387	0.000000	-2.780881
H	1.365387	0.000000	4.190536

Species: D_0 $FA^{-\bullet}$

C	0.000000	0.000000	0.000000
C	0.000000	0.000000	1.402949
C	1.193099	0.000000	-0.768352
C	-1.193099	0.000000	2.171300
O	2.351694	0.000000	-0.389020
O	-2.351694	0.000000	1.791969
O	0.973943	0.000000	-2.127172
O	-0.973943	0.000000	3.530121
H	-0.936326	0.000000	-0.538555
H	0.936326	0.000000	1.941504
H	1.841255	0.000000	-2.506540
H	-1.841255	0.000000	3.909488

Species: D_1 $MA^{-\bullet}$

C	0.000000	0.000000	0.000000
C	0.000000	0.000000	1.544365
C	1.036037	0.000000	-0.920151
C	1.036037	0.000000	2.464516
O	2.264977	0.000000	-0.755813
O	2.264977	0.000000	2.300179
O	0.594994	0.000000	-2.245538
O	0.594994	0.000000	3.789903
H	-0.992362	0.000000	-0.430240
H	-0.992362	0.000000	1.974605
H	1.395392	0.000000	-2.748979
H	1.395392	0.000000	4.293344

Species D_1 $FA^{-\bullet}$

C	0.000000	0.000000	0.000000
C	0.000000	0.000000	1.535886
C	1.185095	0.000000	-0.706848
C	-1.185095	0.000000	2.242734
O	2.337556	0.000000	-0.227781
O	-2.337556	0.000000	1.763667
O	1.081585	0.000000	-2.088366
O	-1.081585	0.000000	3.624252
H	-0.945814	0.000000	-0.515801
H	0.945814	0.000000	2.051687
H	1.978261	0.000000	-2.389195
H	-1.978261	0.000000	3.925081

LEDP

C	0.000000	0.000000	0.000000
C	0.000000	0.000000	1.448526
C	1.186198	0.000000	-0.784957
C	-0.025400	1.185926	2.233483
O	2.349318	-0.007886	-0.428798
O	-0.058190	2.348611	1.877324
O	0.942787	-0.005523	-2.141163
O	-0.025709	0.942453	3.589689
H	-0.926392	-0.015827	-0.569162
H	0.004013	-0.926519	2.017688
H	1.803187	0.004131	-2.535781
H	-0.034481	1.802862	3.984308

D_0 TS

C	-0.037783	-0.017497	-0.055896
C	-0.029730	-0.001683	1.410089
C	1.147264	0.011547	-0.771927
C	-0.026078	1.207510	2.232240
O	2.313741	0.038834	-0.375584
O	-0.093795	2.353083	1.873951
O	0.979742	-0.022929	-2.149836
O	0.042719	0.937161	3.568540
H	-0.981801	-0.055285	-0.585229
H	-0.017050	-0.908863	2.015789
H	1.868576	0.006746	-2.473104
H	0.049527	1.779605	4.002124

$DMM^{-\bullet}$ (a)

C	-1.098153	0.000000	-0.704277
C	-1.098153	0.000000	0.704277
C	-0.036634	0.000000	-1.652251
C	-0.036634	0.000000	1.652251
O	1.188617	0.000000	-1.531158
O	1.188617	0.000000	1.531158
O	-0.593941	0.000000	-2.971607
O	-0.593941	0.000000	2.971607
H	-2.083427	0.000000	-1.165735
H	-2.083427	0.000000	1.165735
C	0.375630	0.000000	3.993274
H	-0.175060	0.000000	4.942077
H	1.028010	-0.883374	3.948998
H	1.028010	0.883374	3.948998
C	0.375630	0.000000	-3.993274
H	1.028010	-0.883374	-3.948998
H	-0.175060	0.000000	-4.942077
H	1.028010	0.883374	-3.948998

$DMF^{-\bullet}$ (a)

C	-0.051031	0.000000	-0.698568
C	0.051031	0.000000	0.698568
C	1.080227	0.000000	-1.554621
C	-1.080227	0.000000	1.554621
O	2.286363	0.000000	-1.266748
O	-2.286363	0.000000	1.266748
O	0.695460	0.000000	-2.918611
O	-0.695460	0.000000	2.918611
H	-1.034927	0.000000	-1.156707
H	1.034927	0.000000	1.156707
C	-1.780310	0.000000	3.819895
H	-1.344436	0.000000	4.825995
H	-2.420978	0.884067	3.697860
H	-2.420978	-0.884067	3.697860
C	1.780310	0.000000	-3.819895
H	2.420978	-0.884067	-3.697860
H	1.344436	0.000000	-4.825995
H	2.420978	0.884067	-3.697860

DMM$^{-\bullet}$ (b)

C	-0.697839	-0.101138	-0.698233
C	-0.697839	0.101138	0.698233
C	0.391467	-0.456795	-1.552412
C	0.391467	0.456795	1.552412
O	1.517650	-0.842956	-1.268728
O	1.517650	0.842956	1.268728
O	0.119857	-0.427483	-2.961811
O	0.119857	0.427483	2.961811
H	-1.684775	-0.100856	-1.156154
H	-1.684775	0.100856	1.156154
C	-0.966112	-0.317030	3.453940
H	-0.790580	-0.471463	4.527715
H	-1.933896	0.203555	3.343959
H	-1.055900	-1.296279	2.961907
C	-0.966112	0.317030	-3.453940
H	-1.055900	1.296279	-2.961907
H	-0.790580	0.471463	-4.527715
H	-1.933896	-0.203555	-3.343959

DMF$^{-\bullet}$ (b)

C	-0.169741	0.000000	-0.680909
C	0.169741	0.000000	0.680909
C	0.826879	0.000000	-1.698814
C	-0.826879	0.000000	1.698814
O	2.052568	0.000000	-1.546987
O	-2.052568	0.000000	1.546987
O	0.409141	0.000000	-3.054910
O	-0.409141	0.000000	3.054910
H	-1.224666	0.000000	-0.925891
H	1.224666	0.000000	0.925891
C	0.965084	0.000000	3.363264
H	1.039855	0.000000	4.457822
H	1.484450	-0.889814	2.975872
H	1.484450	0.889814	2.975872
C	-0.965084	0.000000	-3.363264
H	-1.484450	0.889814	-2.975872
H	-1.039855	0.000000	-4.457822
H	-1.484450	-0.889814	-2.975872

DMM$^{-\bullet}$ (c)

C	-0.880677	0.165409	-0.631145
C	-0.885775	0.194498	0.778489
C	0.176752	-0.084843	-1.552244
C	0.205021	0.308439	1.692724
O	1.350794	-0.414894	-1.392644
O	1.383102	0.573859	1.489500
O	-0.319741	0.067840	-2.884675
O	-0.121945	0.147107	3.084455
H	-1.850164	0.291365	-1.109499
H	-1.880640	0.225151	1.216528
C	-1.315130	-0.490149	3.463063
H	-1.207138	-0.775159	4.519071
H	-2.201612	0.163540	3.381595
H	-1.512301	-1.394633	2.868765
C	0.640831	-0.205500	-3.879848
H	1.011515	-1.238976	-3.828165
H	0.141423	-0.044693	-4.843165
H	1.515106	0.454982	-3.804440

DMF$^{-\bullet}$ (c)

C	-0.365436	0.000000	-0.635221
C	-0.171637	0.000000	0.753513
C	0.717406	0.000000	-1.552386
C	-1.260591	0.000000	1.671043
O	1.937064	0.000000	-1.325648
O	-2.466400	0.000000	1.407793
O	0.263466	0.000000	-2.892165
O	-0.970251	0.000000	3.063247
H	-1.375211	0.000000	-1.031623
H	0.853600	0.000000	1.104175
C	0.367416	0.000000	3.500377
H	0.339397	0.000000	4.597446
H	0.922234	-0.889780	3.164637
H	0.922234	0.889780	3.164637
C	1.300072	0.000000	-3.849486
H	1.945836	-0.884184	-3.760585
H	0.811666	0.000000	-4.830959
H	1.945836	0.884183	-3.760585

DMM$^{-\bullet}$ (d)

C	-1.555318	-0.128124	-0.693634
C	-1.555318	0.128124	0.693634
C	-0.564265	-0.145265	-1.718229
C	-0.564265	0.145265	1.718229
O	-0.757964	-0.494730	-2.897382
O	-0.757964	0.494730	2.897382
O	0.695261	0.320514	-1.345314
O	0.695261	-0.320514	1.345314
H	-2.539703	-0.304709	-1.125770
H	-2.539703	0.304709	1.125770
C	1.661229	-0.268083	2.372446
H	2.591536	-0.643066	1.931179
H	1.815563	0.754078	2.743421
H	1.384352	-0.889834	3.234793
C	1.661229	0.268083	-2.372446
H	1.384352	0.889834	-3.234793
H	2.591536	0.643066	-1.931179
H	1.815563	-0.754078	-2.743421

DMF$^{-\bullet}$ (d)

C	-0.087648	0.000000	-0.696259
C	0.087648	0.000000	0.696259
C	0.941404	0.000000	-1.674373
C	-0.941404	0.000000	1.674373
O	0.812635	0.000000	-2.910110
O	-0.812635	0.000000	2.910110
O	2.239070	0.000000	-1.119815
O	-2.239070	0.000000	1.119815
H	-1.091604	0.000000	-1.107458
H	1.091604	0.000000	1.107458
C	-3.275334	0.000000	2.076701
H	-4.214250	0.000000	1.510957
H	-3.238401	-0.884332	2.727193
H	-3.238401	0.884332	2.727193
C	3.275334	0.000000	-2.076701
H	3.238401	0.884332	-2.727193
H	4.214250	0.000000	-1.510957
H	3.238401	-0.884332	-2.727193

DMM$^{-\bullet}$ (e)

C	-1.370295	-0.158542	-0.687377
C	-1.370295	0.158542	0.687377
C	-0.373783	-0.491360	-1.659466
C	-0.373783	0.491360	1.659466
O	-0.575694	-0.524155	-2.880498
O	-0.575694	0.524155	2.880498
O	0.939808	-0.780432	-1.232749
O	0.939808	0.780432	1.232749
H	-2.358754	-0.167972	-1.146404
H	-2.358754	0.167972	1.146404
C	1.081082	1.845053	0.310142
H	2.112278	1.816229	-0.056587
H	0.405311	1.757289	-0.545370
H	0.906229	2.815545	0.805284
C	1.081082	-1.845053	-0.310142
H	0.906229	-2.815545	-0.805284
H	2.112278	-1.816229	0.056587
H	0.405311	-1.757289	0.545370

DMF$^{-\bullet}$ (e)

C	0.229290	-0.000095	-0.663265
C	-0.229290	-0.000095	0.663265
C	1.584910	-0.000054	-1.085226
C	-1.584910	-0.000054	1.085226
O	2.015995	0.000191	-2.250496
O	-2.015995	0.000191	2.250496
O	2.503031	-0.000351	-0.013942
O	-2.503031	-0.000351	0.013942
H	-0.489483	-0.000041	-1.475964
H	0.489483	-0.000041	1.475964
C	-3.855887	0.000198	0.413778
H	-4.447314	0.000059	-0.509167
H	-4.110585	-0.883909	1.013754
H	-4.110071	0.884876	1.013134
C	3.855887	0.000198	-0.413778
H	4.110071	0.884876	-1.013134
H	4.447314	0.000059	0.509167
H	4.110585	-0.883909	-1.013754

DMM$^{-\bullet}$ (f)

C	-1.404340	0.241673	-0.912800
C	-1.469003	0.145725	0.493453
C	-0.365424	0.163935	-1.897391
C	-0.497766	0.232289	1.532548
O	-0.462379	0.636415	-3.037440
O	-0.722799	0.131816	2.751693
O	0.846449	-0.488419	-1.610280
O	0.803969	0.488159	1.093926
H	-2.355038	0.476367	-1.392429
H	-2.473452	0.102433	0.912313
C	1.760240	0.587529	2.128623
H	2.719431	0.774826	1.634640
H	1.532939	1.409019	2.820959
H	1.822698	-0.333694	2.723043
C	0.764648	-1.751138	-0.980623
H	0.258386	-2.486490	-1.628695
H	1.796251	-2.085971	-0.817619
H	0.246732	-1.720335	-0.018267

DMF$^{-\bullet}$ (f)

C	0.029683	-0.133276	-0.688356
C	-0.029629	0.133419	0.688433
C	1.200201	-0.411455	-1.442220
C	-1.200167	0.411542	1.442256
O	1.279361	-0.650126	-2.658969
O	-1.279399	0.650376	2.658932
O	2.378635	-0.402061	-0.666760
O	-2.378637	0.401876	0.666742
H	-0.885643	-0.136900	-1.270838
H	0.885665	0.137158	1.270977
C	-3.553292	0.676227	1.398306
H	-4.378323	0.636330	0.677651
H	-3.725827	-0.059285	2.195655
H	-3.525092	1.667636	1.870316
C	3.553263	-0.676459	-1.398336
H	3.725893	0.059122	-2.195614
H	4.378273	-0.636748	-0.677661
H	3.525018	-1.667834	-1.870539

$DMM^{-\bullet}$ (g)

C	-1.330710	0.000000	-0.410012
C	-1.279736	0.000000	0.999410
C	-0.332163	0.000000	-1.424939
C	-0.241459	0.000000	1.976787
O	0.900404	0.000000	-1.397796
O	-0.422951	0.000000	3.209019
O	-0.981634	0.000000	-2.703475
O	1.051844	0.000000	1.474218
H	-2.338197	0.000000	-0.821150
H	-2.252149	0.000000	1.488527
C	2.063554	0.000000	2.457580
H	3.012183	0.000000	1.910598
H	2.009671	0.884641	3.106823
H	2.009671	-0.884641	3.106823
C	-0.087655	0.000000	-3.791908
H	0.565959	-0.883620	-3.795127
H	-0.705380	0.000000	-4.698595
H	0.565959	0.883620	-3.795127

$DMF^{-\bullet}$ (g)

C	0.144197	0.000000	-0.453481
C	0.285528	0.000000	0.941654
C	1.257396	0.000000	-1.333922
C	-0.760989	0.000000	1.899895
O	2.469368	0.000000	-1.074489
O	-0.658706	0.000000	3.137868
O	0.840836	0.000000	-2.689452
O	-2.047485	0.000000	1.317633
H	-0.844239	0.000000	-0.899733
H	1.287157	0.000000	1.360796
C	-3.103118	0.000000	2.253286
H	-4.030252	0.000000	1.668240
H	-3.079508	-0.884335	2.904387
H	-3.079508	0.884335	2.904387
C	1.905348	0.000000	-3.614938
H	2.548596	-0.884078	-3.507240
H	1.446878	0.000000	-4.611042
H	2.548596	0.884078	-3.507240

DMM$^{-\bullet}$ (h)

C	-1.135932	0.072624	-0.537326
C	-1.140078	0.067447	0.873893
C	-0.089410	0.383164	-1.458087
C	-0.109026	-0.004065	1.857477
O	1.010678	0.892099	-1.271453
O	-0.281759	0.096080	3.085575
O	-0.375175	0.121429	-2.842788
O	1.161219	-0.250982	1.358135
H	-2.118903	-0.078285	-0.978645
H	-2.122661	0.066906	1.343466
C	2.183099	-0.263884	2.331611
H	3.116718	-0.429986	1.784317
H	2.240529	0.685916	2.879315
H	2.039029	-1.062198	3.072912
C	-1.409382	-0.760708	-3.198054
H	-2.411719	-0.301028	-3.138512
H	-1.238289	-1.052848	-4.243822
H	-1.420034	-1.664953	-2.571875

DMF$^{-\bullet}$ (h)

C	0.396994	0.000000	-0.511719
C	0.571613	0.000000	0.881297
C	1.506175	0.000000	-1.405824
C	-0.460521	0.000000	1.855626
O	2.706060	0.000000	-1.119379
O	-0.341170	0.000000	3.091270
O	1.244190	0.000000	-2.804908
O	-1.756401	0.000000	1.291887
H	-0.615594	0.000000	-0.894096
H	1.581066	0.000000	1.279555
C	-2.798357	0.000000	2.243322
H	-3.734134	0.000000	1.672227
H	-2.764681	-0.884359	2.893710
H	-2.764681	0.884359	2.893710
C	-0.082907	0.000000	-3.271344
H	-0.645273	0.890058	-2.948318
H	-0.030850	0.000000	-4.367580
H	-0.645273	-0.890058	-2.948318

DMM$^{-\bullet}$ (i)

C	-1.257111	0.022484	-0.236852
C	-1.192712	0.077348	1.171338
C	-0.265925	0.210649	-1.239086
C	-0.144707	0.167458	2.144489
O	0.946070	0.444169	-1.169728
O	-0.334218	0.503372	3.321703
O	-0.865794	0.098770	-2.527861
O	1.180390	-0.107212	1.780246
H	-2.257958	-0.099169	-0.646559
H	-2.163823	0.114515	1.663831
C	1.431272	-1.352822	1.159975
H	2.429636	-1.296254	0.715342
H	1.417192	-2.167356	1.906451
H	0.715682	-1.584634	0.367796
C	0.036582	0.291255	-3.594429
H	0.849238	-0.448150	-3.589360
H	-0.549241	0.184637	-4.515314
H	0.503290	1.285380	-3.569683

DMF$^{-\bullet}$ (i)

C	0.240392	-0.060313	-0.405646
C	0.073013	0.164009	0.968316
C	1.518349	-0.124182	-1.019666
C	-1.157570	0.243890	1.670291
O	2.644085	-0.005810	-0.514579
O	-1.329195	0.441306	2.884586
O	1.407654	-0.360240	-2.413498
O	-2.284655	0.070738	0.837152
H	-0.626118	-0.193173	-1.044196
H	0.958022	0.293578	1.583926
C	-3.519377	0.146226	1.515104
H	-3.612715	-0.623985	2.292648
H	-3.665594	1.119825	2.002219
H	-4.295152	-0.003790	0.755171
C	2.647974	-0.434545	-3.081272
H	3.276912	-1.250030	-2.698578
H	2.417838	-0.614958	-4.138103
H	3.227010	0.494076	-2.985137

DMM$^{-\bullet}$ (j)

C	0.605538	-0.85919	0.188838
C	-0.765896	-1.20496	0.218081
C	1.252249	0.230961	-0.453714
C	-2.006620	-0.542807	-0.095309
O	0.764403	1.13671	-1.135840
O	-3.019970	-1.161293	-0.440654
O	2.673872	0.31816	-0.329140
O	-2.162351	0.832998	0.020528
H	1.251411	-1.633859	0.593128
H	-0.959858	-2.255275	0.435651
C	-1.377249	1.559569	0.956237
H	-0.446318	1.905011	0.503265
H	-1.985514	2.422284	1.260492
H	-1.154421	0.953785	1.844258
C	3.373171	-0.536746	0.539011
H	3.390415	-1.583042	0.190746
H	4.408805	-0.173620	0.574564
H	2.960694	-0.528940	1.559892

DMF$^{-\bullet}$ (j)

C	-0.642749	-0.080645	-0.000568
C	0.466163	-0.941414	0.000233
C	-1.977848	-0.577935	-0.000500
C	1.830724	-0.550856	0.000168
O	-2.344223	-1.755892	-0.000178
O	2.832399	-1.284015	0.001057
O	-3.046768	0.361613	-0.000864
O	2.007196	0.851402	-0.000807
H	-0.455454	0.985379	-0.001182
H	0.294049	-2.012884	0.000862
C	3.357404	1.261540	-0.000351
H	3.898834	0.901147	0.884650
H	3.899923	0.899626	-0.883965
H	3.344230	2.357745	-0.001312
C	-2.770354	1.740895	0.001286
H	-2.205855	2.060920	-0.888521
H	-3.739510	2.255802	0.002525
H	-2.205088	2.057892	0.891665

A.3 Supporting Information for Sec. 4.2

The Cartesian coordinates of the stationary points in the S_1 and S_0 states and the S_1/S_0 degeneracy points which discussed in the text by CASSCF/6-31G* are tabulated. Values are given in Å.

Species: S_0 tZt-PDI

C	0.000000	0.000000	0.000000
C	0.000000	0.000000	1.418160
C	1.141120	0.000000	2.176530
C	2.516407	0.000000	1.744382
C	3.524528	0.000000	2.639623
N	-1.077806	0.000000	-0.714819
H	0.919440	0.000000	-0.552972
H	-0.953463	0.000000	1.915337
H	0.990584	0.000000	3.241813
H	2.749897	0.000000	0.695342
H	4.549827	0.000000	2.323628
H	3.341875	0.000000	3.698613
H	-1.043823	0.000000	-1.715586
H	-1.990158	0.000000	-0.298484

Species: S_0 tZt-PDI*

C	0.000000	0.000000	0.000000
C	0.000000	0.000000	1.378442
C	1.235426	0.000000	2.267220
C	2.541376	0.000000	1.844085
C	3.606483	0.000000	2.765832
N	-1.134246	0.000000	-0.743228
H	0.906592	0.000000	-0.572109
H	-0.937490	0.000000	1.902298
H	1.032346	0.000000	3.322197
H	2.785543	0.000000	0.798216
H	4.626912	0.000000	2.434685
H	3.426054	0.000000	3.824359
H	-1.096151	0.000000	-1.738257
H	-2.040040	0.000000	-0.326354

Species: DP40

C	0.000000	0.000000	0.000000
C	0.000000	0.000000	1.399803
C	1.231833	0.000000	2.187351
C	2.406258	0.720345	1.919271
C	3.635063	0.125431	2.123217
N	-0.935981	0.557931	-0.731146
H	0.804256	-0.452236	-0.552109
H	-0.645950	0.802516	1.747632
H	1.444839	-0.960167	2.634577
H	2.367052	1.622623	1.333972
H	4.520113	0.547705	1.688579
H	3.736536	-0.796218	2.663937
H	-0.858199	0.585427	-1.726288
H	-1.727402	1.016138	-0.326178

Species: DP60

C	0.000000	0.000000	0.000000
C	0.000000	0.000000	1.381742
C	1.256976	0.000000	2.122867
C	2.252082	1.008446	2.033696
C	3.501676	0.648476	1.614437
N	-1.057133	0.269364	-0.746953
H	0.895620	-0.230297	-0.547213
H	-0.868686	0.407709	1.876779
H	1.640299	-0.976256	2.386734
H	1.944391	2.034066	1.923261
H	4.178767	1.386966	1.229606
H	3.841838	-0.370448	1.640398
H	-1.000797	0.257360	-1.742465
H	-1.955525	0.450226	-0.349811

Species: LEDP

C	0.000000	0.000000	0.000000
C	0.000000	0.000000	1.375236
C	1.229226	0.000000	2.159740
C	1.862711	1.159620	2.616045
C	3.010692	1.087163	3.372216
N	-1.087050	-0.014695	-0.759015
H	0.928933	0.016763	-0.539921
H	-0.930641	-0.030333	1.919957
H	1.662214	-0.948944	2.438245
H	1.443158	2.117186	2.366768
H	3.504777	1.973522	3.721067
H	3.448156	0.142413	3.637251
H	-1.020651	-0.012663	-1.753518
H	-2.005871	-0.036447	-0.369423

Species: tEt-PDI

C	0.000000	0.000000	0.000000
C	0.000000	0.000000	1.415516
C	1.186154	0.000000	2.095926
C	1.302473	0.000000	3.528526
C	2.503237	0.000000	4.141752
N	-1.066363	0.000000	-0.732891
H	0.933476	0.000000	-0.533206
H	-0.939410	0.000000	1.939437
H	2.104337	0.000000	1.531885
H	0.396080	0.000000	4.107361
H	2.581713	0.000000	5.211746
H	3.424139	0.000000	3.587297
H	-1.015005	0.000000	-1.732655
H	-1.985388	0.000000	-0.332520

A.4 Supporting Information for Sec. 4.3

The Cartesian coordinates of the stationary points in the S_1 and S_0 states and the S_1/S_0 degeneracy points which discussed in the text by CASSCF/6-31G* and SAC-CI/6-31G* are tabulated. Values are given in Å.

A.4.1 Results of CAS/6-31G*

Species: S_0 Z-PDI (planar)

C	0.000000	0.000000	0.000000
C	0.000000	0.000000	1.418160
C	1.141120	0.000000	2.176530
C	2.516407	0.000000	1.744381
C	3.524528	0.000000	2.639622
N	-1.077806	0.000000	-0.714819
H	0.919440	0.000000	-0.552972
H	-0.953463	0.000000	1.915337
H	0.990584	0.000000	3.241813
H	2.749896	0.000000	0.695341
H	4.549827	0.000000	2.323627
H	3.341876	0.000000	3.698612
H	-1.043823	0.000000	-1.715586
H	-1.990158	0.000000	-0.298484

Species: S_0 Z-PDI (twist)

C	0.000000	0.000000	0.000000
C	0.000000	0.000000	1.418046
C	1.143252	0.000000	2.173193
C	2.506945	0.195171	1.747414
C	3.521005	0.171507	2.635787
N	-1.073029	-0.103412	-0.714497
H	0.917263	0.063697	-0.553206
H	-0.949827	-0.091522	1.913846
H	0.997503	-0.105111	3.234033
H	2.725824	0.366596	0.709146
H	4.537014	0.320823	2.325115
H	3.352253	0.005572	3.684041
H	-1.039049	-0.102662	-1.715249
H	-1.981467	-0.186838	-0.298020

Species: TS_1

C	0.001432	-0.005796	-0.037636
C	-0.004545	-0.011174	1.380869
C	1.245348	-0.037113	2.168044
C	1.872553	1.116280	2.619757
C	3.032116	1.113713	3.391944
N	-1.082186	0.001618	-0.751746
H	0.932478	-0.004427	-0.574635
H	-0.960407	-0.016306	1.880519
H	1.626498	-1.008838	2.433457
H	1.441768	2.069350	2.360115
H	3.481137	2.031969	3.714419
H	3.504167	0.195675	3.687751
H	-1.049239	0.008146	-1.754499
H	-1.995430	0.000524	-0.333790

Species: TS_2

C	-0.003491	-0.025093	0.004718
C	0.007419	0.035698	1.350967
C	1.240290	0.040684	2.146871
C	1.865329	1.194252	2.617790
C	2.996483	1.073107	3.379364
N	-1.106021	-0.163623	-0.776502
H	0.921921	-0.010899	-0.543789
H	-0.895206	-0.029248	1.940383
H	1.685891	-0.903661	2.426008
H	1.458536	2.158412	2.375086
H	3.515279	1.935547	3.755979
H	3.406061	0.110287	3.626533
H	-1.036314	0.074968	-1.739585
H	-2.010490	-0.036811	-0.379258

Species: S_1 Z-PDI*

C	0.000000	0.000000	0.000000
C	0.000000	0.000000	1.378417
C	1.235440	0.000000	2.267232
C	2.541391	0.000000	1.844213
C	3.606425	0.000000	2.766115
N	-1.134231	0.000000	-0.743239
H	0.906599	0.000000	-0.572101
H	-0.937489	0.000000	1.902274
H	1.032281	0.000000	3.322195
H	2.785680	0.000000	0.798372
H	4.626896	0.000000	2.435101
H	3.425849	0.000000	3.824616
H	-1.096124	0.000000	-1.738270
H	-2.040033	0.000000	-0.326376

Species: Relaxed Structure at $\theta_1 = 40°$(RS_{40})

C	0.000000	0.000000	0.000000
C	0.000000	0.000000	1.397286
C	1.230284	0.000000	2.195417
C	2.387691	0.732853	1.905203
C	3.617424	0.331050	2.389851
N	-0.915433	0.596753	-0.733743
H	0.777087	-0.495013	-0.554315
H	-0.638947	0.813437	1.734367
H	1.440687	-0.929498	2.703949
H	2.330644	1.591439	1.259714
H	4.520966	0.793269	2.042416
H	3.711474	-0.494297	3.070145
H	-0.864001	0.582936	-1.730216
H	-1.699694	1.065882	-0.328839

Species: DP_{C40}

C	0.000000	0.000000	0.000000
C	0.000000	0.000000	1.392799
C	1.249807	0.000000	2.178229
C	2.389726	0.735370	1.859530
C	3.643972	0.312630	2.273516
N	-0.890591	0.637847	-0.737486
H	0.759907	-0.522709	-0.552106
H	-0.612843	0.832390	1.726789
H	1.483041	-0.943282	2.649108
H	2.307877	1.608467	1.236904
H	4.532866	0.774872	1.890292
H	3.764574	-0.530336	2.927414
H	-0.836065	0.625608	-1.733320
H	-1.655886	1.137511	-0.334202

Species: DP_{C50}

C	0.000000	0.000000	0.000000
C	0.000000	0.000000	1.390452
C	1.256252	0.000000	2.159809
C	2.310191	0.885699	1.933778
C	3.597015	0.577547	2.339288
N	-0.952279	0.538214	-0.740104
H	0.804723	-0.452874	-0.550048
H	-0.724179	0.697473	1.794874
H	1.548562	-0.943320	2.595675
H	2.131367	1.797651	1.392570
H	4.428892	1.189890	2.049675
H	3.808138	-0.308191	2.908503
H	-0.903140	0.518778	-1.736386
H	-1.760199	0.966386	-0.337130

Species: DP_{C60}

C	0.000000	0.000000	0.000000
C	0.000000	0.000000	1.386744
C	1.254565	0.000000	2.153282
C	2.216812	1.007194	2.059758
C	3.509330	0.801645	2.503296
N	-1.006620	0.422728	-0.745072
H	0.848596	-0.368000	-0.547205
H	-0.814522	0.542633	1.847197
H	1.591690	-0.941897	2.558220
H	1.957579	1.943453	1.598781
H	4.274604	1.536266	2.342878
H	3.795149	-0.111551	2.990960
H	-0.957578	0.396006	-1.741249
H	-1.856233	0.764093	-0.344888

Species: DP_{C70}

C	0.000000	0.000000	0.000000
C	0.000000	0.000000	1.381941
C	1.248360	0.000000	2.152084
C	2.113646	1.094405	2.217866
C	3.387014	0.965769	2.734220
N	-1.048595	0.297257	-0.751142
H	0.886730	-0.268839	-0.544253
H	-0.879602	0.374302	1.884613
H	1.619331	-0.941770	2.526487
H	1.788781	2.044434	1.833454
H	4.076860	1.787522	2.725662
H	3.732966	0.035412	3.144677
H	-0.994557	0.267792	-1.746728
H	-1.933261	0.539121	-0.355089

Species: DP_{C80}

C	0.000000	0.000000	0.000000
C	0.000000	0.000000	1.377523
C	1.237208	0.000000	2.154279
C	2.002545	1.144282	2.396542
C	3.226098	1.059177	3.024287
N	-1.076624	0.159056	-0.755783
H	0.916517	-0.145117	-0.541893
H	-0.917407	0.198584	1.909721
H	1.633735	-0.945307	2.492089
H	1.633369	2.099878	2.071073
H	3.834817	1.929265	3.178490
H	3.612956	0.119098	3.371505
H	-1.014762	0.139624	-1.750723
H	-1.986108	0.285765	-0.363446

Species: DP_{C90}

C	0.000000	0.000000	0.000000
C	0.000000	0.000000	1.375249
C	1.230137	0.000000	2.158564
C	1.887553	1.160560	2.577188
C	3.049669	1.088860	3.311659
N	-1.087185	0.016234	-0.758861
H	0.928874	-0.012352	-0.540140
H	-0.931084	0.010804	1.919893
H	1.656539	-0.948487	2.448377
H	1.476834	2.118200	2.313850
H	3.565253	1.975686	3.626568
H	3.477852	0.144210	3.591742
H	-1.020874	0.013962	-1.753379
H	-2.006181	0.021095	-0.369080

Species: DP_{C100}

C	0.000000	0.000000	0.000000
C	0.000000	0.000000	1.376588
C	1.228022	0.000000	2.164126
C	1.774939	1.142786	2.754248
C	2.870814	1.056689	3.583289
N	-1.079617	-0.124691	-0.757956
H	0.921450	0.120090	-0.539655
H	-0.918936	-0.176336	1.914147
H	1.683150	-0.950024	2.401230
H	1.324396	2.098555	2.557555
H	3.285357	1.929163	4.050531
H	3.341964	0.114251	3.793084
H	-1.015617	-0.108075	-1.752638
H	-1.991306	-0.240658	-0.367888

Species: DP_{C110}

C	0.000000	0.000000	0.000000
C	0.000000	0.000000	1.380291
C	1.231005	0.000000	2.169014
C	1.670224	1.091234	2.922136
C	2.696393	0.961067	3.832687
N	-1.055230	-0.260841	-0.754346
H	0.895584	0.246512	-0.540316
H	-0.883167	-0.348958	1.894901
H	1.708217	-0.950906	2.355189
H	1.186525	2.042497	2.793329
H	3.010721	1.788909	4.438552
H	3.205885	0.025716	3.972918
H	-0.998701	-0.229351	-1.749534
H	-1.944128	-0.492018	-0.361947

Species: DP_{C120}

C	0.000000	0.000000	0.000000
C	0.000000	0.000000	1.384242
C	1.238693	0.000000	2.171697
C	1.576141	1.007813	3.075700
C	2.531101	0.802631	4.050275
N	-1.015693	-0.390967	-0.750218
H	0.853277	0.365086	-0.541839
H	-0.827214	-0.503865	1.865500
H	1.731308	-0.952094	2.308905
H	1.067880	1.953404	3.017512
H	2.751911	1.558023	4.779449
H	3.071198	-0.123395	4.119783
H	-0.969356	-0.348207	-1.745816
H	-1.868047	-0.730553	-0.354858

Species: DP_{C130}

C	0.000000	0.000000	0.000000
C	0.000000	0.000000	1.388501
C	1.240367	0.000000	2.179500
C	1.493858	0.888469	3.225360
C	2.403245	0.582909	4.217740
N	-0.971603	-0.493474	-0.744692
H	0.810537	0.449214	-0.544450
H	-0.749732	-0.646883	1.827999
H	1.736642	-0.957237	2.261277
H	0.955393	1.818345	3.265207
H	2.548248	1.235683	5.056653
H	2.975682	-0.325783	4.193961
H	-0.934712	-0.445352	-1.740701
H	-1.784229	-0.916778	-0.345810

Species: DP_{C140}

C	0.000000	0.000000	0.000000
C	0.000000	0.000000	1.392097
C	1.239817	0.000000	2.191764
C	1.421372	0.741588	3.360542
C	2.289430	0.317294	4.346547
N	-0.922052	-0.584275	-0.739686
H	0.762831	0.523110	-0.547642
H	-0.658131	-0.770160	1.782256
H	1.736768	-0.961014	2.212668
H	0.861992	1.649346	3.500680
H	2.373200	0.848079	5.275019
H	2.885619	-0.568299	4.227512
H	-0.895644	-0.530068	-1.735830
H	-1.690845	-1.080566	-0.337735

Species: DP_{C150}

C	0.000000	0.000000	0.000000
C	0.000000	0.000000	1.395334
C	1.232138	0.000000	2.215964
C	1.352464	0.571380	3.485171
C	2.192614	0.024971	4.434594
N	-0.877064	-0.653089	-0.734883
H	0.719742	0.577758	-0.551328
H	-0.559104	-0.871284	1.730506
H	1.728229	-0.961558	2.170907
H	0.773344	1.443930	3.730667
H	2.229966	0.421162	5.430755
H	2.810953	-0.825876	4.216637
H	-0.861547	-0.592528	-1.730993
H	-1.606528	-1.203903	-0.330307

Species: DP_{C160}

C	0.000000	0.000000	0.000000
C	0.000000	0.000000	1.399806
C	1.202526	0.000000	2.273894
C	1.270006	0.381493	3.618727
C	2.131161	-0.246517	4.495923
N	-0.862861	-0.671227	-0.731156
H	0.713755	0.582681	-0.554153
H	-0.464039	-0.946786	1.678762
H	1.703448	-0.953145	2.155535
H	0.642256	1.178008	3.977775
H	2.138903	0.011578	5.536959
H	2.796335	-1.025786	4.173615
H	-0.850699	-0.607848	-1.727526
H	-1.583979	-1.233210	-0.325872

Species: DP_{C170}

C	0.000000	0.000000	0.000000
C	0.000000	0.000000	1.402354
C	1.182297	0.000000	2.311630
C	1.197380	0.192400	3.699764
C	2.028007	-0.553031	4.510433
N	-0.820259	-0.726277	-0.725659
H	0.660403	0.639146	-0.558968
H	-0.365991	-1.006905	1.623815
H	1.703306	-0.932145	2.121232
H	0.566030	0.942035	4.144185
H	2.007745	-0.429856	5.575694
H	2.702143	-1.286490	4.108893
H	-0.826119	-0.650932	-1.721389
H	-1.500980	-1.335115	-0.317435

Species: DP_{C180}

C	0.000000	0.000000	0.000000
C	0.000000	0.000000	1.409231
C	1.124857	0.000000	2.385655
C	1.056168	0.000000	3.791594
C	1.868110	-0.819157	4.542224
N	-0.801852	-0.739047	-0.722703
H	0.643335	0.656511	-0.560244
H	-0.265165	-1.053405	1.564771
H	1.706311	-0.878864	2.127309
H	0.384163	0.673042	4.295406
H	1.801665	-0.821128	5.612584
H	2.581989	-1.481347	4.088695
H	-0.805412	-0.663511	-1.719116
H	-1.475489	-1.358151	-0.315670

Species: DP_{H50}

```
C     0.000000   0.000000   0.000000
C     0.000000   0.000000   1.391905
C     1.316516   0.000000   2.048036
C     1.591746   0.951183   3.033190
C     2.756097   0.885690   3.773030
N    -1.077028  -0.186029  -0.746853
H     0.879560   0.297562  -0.542849
H    -0.729567  -0.693799   1.782199
H     1.851155  -0.926029   2.209436
H     0.937572   1.797399   3.144582
H     3.011512   1.652333   4.479133
H     3.457168   0.081832   3.642919
H    -1.052142  -0.059774  -1.735411
H    -1.964360  -0.411027  -0.348171
```

Species: DP_{H60}

```
C    0.000000    0.000000    0.000000
C    0.000000    0.000000    1.387122
C    1.278127    0.000000    2.110116
C    1.614396    1.021628    3.000621
C    2.744024    0.935424    3.789493
N   -1.075487   -0.173576   -0.751167
H    0.892562    0.258309   -0.540406
H   -0.801761   -0.563553    1.840277
H    1.778584   -0.940993    2.288521
H    1.023346    1.919583    3.013077
H    3.039701    1.744773    4.428870
H    3.373973    0.065252    3.772015
H   -1.038968   -0.063812   -1.741635
H   -1.969395   -0.380829   -0.356927
```

Species: DP_{H70}

C	0.000000	0.000000	0.000000
C	0.000000	0.000000	1.381895
C	1.247638	0.000000	2.151886
C	1.673570	1.087327	2.916771
C	2.780738	0.994773	3.735355
N	-1.078730	-0.137423	-0.755201
H	0.908548	0.196590	-0.539030
H	-0.867098	-0.401714	1.883913
H	1.719563	-0.949883	2.355829
H	1.155305	2.024428	2.824007
H	3.136812	1.842655	4.288061
H	3.327936	0.075692	3.835397
H	-1.029022	-0.052226	-1.747517
H	-1.982718	-0.302719	-0.364171

Species: DP_{H80}

C	0.000000	0.000000	0.000000
C	0.000000	0.000000	1.377010
C	1.231925	0.000000	2.159748
C	1.770258	1.142469	2.757676
C	2.894277	1.065364	3.549903
N	-1.084230	-0.075289	-0.758130
H	0.923743	0.103172	-0.539203
H	-0.915177	-0.200897	1.912116
H	1.683148	-0.949470	2.406505
H	1.308348	2.095201	2.573069
H	3.325101	1.943026	3.992005
H	3.377865	0.126341	3.746292
H	-1.022279	-0.031636	-1.752104
H	-1.998898	-0.166313	-0.368453

Species: DP_{H90}

C	0.000000	0.000000	0.000000
C	0.000000	0.000000	1.375222
C	1.229943	0.000000	2.158903
C	1.886031	1.160142	2.580855
C	3.041488	1.087671	3.325602
N	-1.087312	0.000283	-0.758892
H	0.928930	-0.004395	-0.540173
H	-0.931084	0.010450	1.919854
H	1.658572	-0.948824	2.444263
H	1.475452	2.118046	2.318256
H	3.550447	1.974194	3.651943
H	3.469544	0.142708	3.604825
H	-1.020954	-0.008335	-1.753369
H	-2.006295	-0.004549	-0.369087

Species: DP_{H100}

C	0.000000	0.000000	0.000000
C	0.000000	0.000000	1.377750
C	1.240775	0.000000	2.150815
C	2.009325	1.142153	2.393510
C	3.211043	1.059781	3.062658
N	-1.085953	0.074137	-0.756321
H	0.921457	-0.110108	-0.541766
H	-0.914323	0.215742	1.907793
H	1.648615	-0.948894	2.463805
H	1.638725	2.099688	2.075473
H	3.793080	1.936380	3.272886
H	3.599970	0.117294	3.400994
H	-1.026802	0.011705	-1.749622
H	-2.000784	0.153630	-0.364118

Species: DP_{H110}

C	0.000000	0.000000	0.000000
C	0.000000	0.000000	1.382788
C	1.260775	0.000000	2.137207
C	2.126563	1.094542	2.204776
C	3.377584	0.981282	2.777573
N	-1.081875	0.132926	-0.753076
H	0.905320	-0.200052	-0.543224
H	-0.869702	0.400993	1.879238
H	1.652601	-0.951139	2.462429
H	1.788533	2.052278	1.852380
H	4.023738	1.831970	2.877992
H	3.738747	0.041286	3.151550
H	-1.036794	0.026436	-1.743745
H	-1.986838	0.284585	-0.358345

Species: DP_{H120}

C	0.000000	0.000000	0.000000
C	0.000000	0.000000	1.387802
C	1.294336	0.000000	2.092396
C	2.212223	1.051182	1.993892
C	3.488425	0.930039	2.504582
N	-1.081986	0.155909	-0.748798
H	0.891824	-0.249108	-0.545836
H	-0.817307	0.539192	1.840418
H	1.706539	-0.948460	2.399346
H	1.891819	1.993446	1.587071
H	4.170943	1.758071	2.501731
H	3.831400	0.010501	2.941561
H	-1.051674	0.015575	-1.735718
H	-1.978872	0.341291	-0.350240

Species: DP_{H130}

C	0.000000	0.000000	0.000000
C	0.000000	0.000000	1.392780
C	1.332283	0.000000	2.036840
C	2.273225	1.007740	1.785277
C	3.577216	0.876253	2.213818
N	-1.085761	0.162890	-0.743777
H	0.878141	-0.289077	-0.549082
H	-0.759723	0.653334	1.792272
H	1.772367	-0.945619	2.312411
H	1.951051	1.936446	1.349566
H	4.279725	1.681973	2.118288
H	3.923365	-0.024918	2.685587
H	-1.071802	-0.014359	-1.724808
H	-1.974918	0.373201	-0.340966

Species: DP_{H140}

C	0.000000	0.000000	0.000000
C	0.000000	0.000000	1.397977
C	1.371422	0.000000	1.974745
C	2.308471	0.973418	1.591360
C	3.635831	0.834351	1.933361
N	-1.094057	0.153185	-0.737186
H	0.865599	-0.319245	-0.553226
H	-0.706236	0.741325	1.737658
H	1.845277	-0.942049	2.203138
H	1.971275	1.892582	1.146989
H	4.342051	1.624700	1.763419
H	3.999680	-0.053501	2.417352
H	-1.097677	-0.067070	-1.709132
H	-1.976960	0.377216	-0.328994

Species: DP_{H150}

C	0.000000	0.000000	0.000000
C	0.000000	0.000000	1.404536
C	1.408751	0.000000	1.912843
C	2.320005	0.954210	1.421465
C	3.665068	0.817592	1.681392
N	-1.104979	0.140286	-0.727755
H	0.850610	-0.351020	-0.558196
H	-0.663943	0.804107	1.681085
H	1.919266	-0.936361	2.077563
H	1.958132	1.866931	0.983468
H	4.360484	1.604420	1.457715
H	4.057366	-0.061310	2.159881
H	-1.130971	-0.133557	-1.685286
H	-1.980191	0.379380	-0.312402

Species: DP_{H160}

C	0.000000	0.000000	0.000000
C	0.000000	0.000000	1.414234
C	1.441805	0.000000	1.858362
C	2.309176	0.950462	1.275947
C	3.666937	0.839464	1.467812
N	-1.113735	0.160609	-0.714073
H	0.821298	-0.407809	-0.564091
H	-0.634938	0.845938	1.627527
H	1.989249	-0.925910	1.945753
H	1.912375	1.851888	0.844713
H	4.336431	1.636527	1.204106
H	4.098632	-0.025557	1.937906
H	-1.179509	-0.178050	-1.648704
H	-1.970627	0.444456	-0.288888

Species: DP_{H170}

C	0.000000	0.000000	0.000000
C	0.000000	0.000000	1.432953
C	1.476261	0.000000	1.803561
C	2.263158	0.939741	1.087869
C	3.621796	0.976304	1.289845
N	-1.055152	0.446945	-0.680680
H	0.656874	-0.630138	-0.574590
H	-0.635931	0.860864	1.571122
H	2.071158	-0.899846	1.813446
H	1.794595	1.752023	0.560991
H	4.215798	1.803527	0.949392
H	4.127178	0.212729	1.853022
H	-1.293821	0.058292	-1.567731
H	-1.775199	0.974708	-0.232746

Species: DP_{H180}

C	0.000000	0.000000	0.000000
C	0.000000	0.000000	1.447562
C	1.485727	0.000000	1.768998
C	2.213194	1.036980	1.109979
C	3.582372	1.042376	1.164528
N	-1.138835	0.219728	-0.664688
H	0.752761	-0.501036	-0.582877
H	-0.668154	0.840731	1.560424
H	2.084526	-0.885988	1.627274
H	1.704508	1.920150	0.765629
H	4.149521	1.912861	0.893157
H	4.134064	0.202285	1.546340
H	-1.346267	-0.300543	-1.490430
H	-1.932199	0.613598	-0.203065

Species: LEDP

```
C     0.000000   0.000000   0.000000
C     0.000000   0.000000   1.375239
C     1.229234   0.000000   2.159732
C     1.862711   1.159625   2.616034
C     3.010697   1.087184   3.372198
N    -1.087047  -0.014715  -0.759014
H     0.928935   0.016775  -0.539917
H    -0.930640  -0.030344   1.919962
H     1.662226  -0.948944   2.438233
H     1.443145   2.117185   2.366754
H     3.504769   1.973551   3.721049
H     3.448174   0.142441   3.637235
H    -1.020648  -0.012670  -1.753517
H    -2.005868  -0.036468  -0.369422
```

Species: E-PDI

```
C     0.000000   0.000000   0.000000
C     0.000000   0.000000   1.415516
C     1.186167   0.000000   2.095903
C     1.302540   0.000000   3.528499
C     2.503336   0.002581   4.141658
N    -1.066352  -0.000735  -0.732907
H     0.933483   0.000558  -0.533193
H    -0.939404  -0.000569   1.939447
H     2.104334   0.000615   1.531836
H     0.396177  -0.001460   4.107379
H     2.581879   0.003024   5.211646
H     3.424201   0.004224   3.587145
H    -1.014971  -0.000632  -1.732670
H    -1.985385  -0.001431  -0.332557
```

A.4.2 Results of SAC-CI/6-31G*

Species: Z-PDI* optimized by SAC-CI/6-31G*

C	0.021740	0.000000	0.007052
C	0.011555	0.000000	1.397569
C	1.206951	0.000000	2.273091
C	2.525834	0.000000	1.836642
C	3.583688	0.000000	2.738443
N	-1.102218	0.000000	-0.725935
H	0.936136	0.000000	-0.560860
H	-0.939037	-0.000001	1.906002
H	1.007737	0.000000	3.332122
H	2.759748	-0.000001	0.784457
H	4.606548	0.000000	2.398853
H	3.412199	0.000002	3.803373
H	-1.064054	-0.000001	-1.730035
H	-2.014145	0.000001	-0.302226

Species: relaxed structure at $\theta_1 = 10°$ optimized by SAC-CI/6-31G*

C	0.023155	0.054905	-0.004633
C	0.022400	0.057516	1.376516
C	1.270172	0.011142	2.222260
C	2.547923	0.157453	1.739176
C	3.651251	-0.246016	2.491531
N	-1.011779	0.468107	-0.738548
H	0.870185	-0.309941	-0.563221
H	-0.838189	0.499175	1.868453
H	1.146986	-0.445583	3.195742
H	2.719843	0.556150	0.750714
H	4.648063	-0.209181	2.084223
H	3.534817	-0.638174	3.489552
H	-0.990215	0.402003	-1.742569
H	-1.852696	0.829707	-0.319904

Species: relaxed structure at $\theta_2 = 10^\circ$ optimized by SAC-CI/6-31G*

```
C     0.001916   0.008503   0.001193
C     0.008459  -0.010921   1.387445
C     1.320774   0.001663   2.135047
C     2.243898   1.003717   1.974170
C     3.457696   0.994474   2.674513
N    -1.110029  -0.043891  -0.737057
H     0.916243   0.143317  -0.556808
H    -0.839171  -0.481673   1.868046
H     1.380751  -0.602673   3.029867
H     2.074780   1.782818   1.245103
H     4.195632   1.764354   2.522387
H     3.700514   0.196861   3.359085
H    -1.068200   0.041323  -1.738681
H    -2.025701  -0.094109  -0.320238
```